Harnessing high sensitivity NMR for organic and inorganic substrates

Thomas Price

MSc by Research

University of York

Chemistry

December 2014

Abstract

This thesis describes the use of SABRE as a hyperpolarisation technique in NMR spectroscopy. Hyperpolarisation is a technique to increase the observed signal during NMR and MRI experiments. The primary aim of this research project was to develop SABRE towards a specific application – either for the study of reaction mechanisms around a metal centre or for medical imaging.

In this dissertation the use SABRE hyperpolarisation on a number new of substrates, both organic and inorganic, is described. The pyridine derivatives, 3-aminopyridine, (4-phenyl)pyridine, 3-hydroxypyridine, 4-hydroxypyridine, 3-methoxypyridine, 4-methoxypyridine and 2-fluoro-3hydroxypyridine, have been shown to undergo SABRE polarisation for the first time. Two ferrocene derivatives, ferroceneacetonitrile and (4-pyridyl)ferrocene, have been polarised as has [tris(bipyrazyl)ruthenium(II)]$^{2+}$. This is the first time that SABRE hyperpolarisation of a substrate containing a metal centre has been reported.

Chapters 4 and 5 detail the effects of pH on SABRE hyperpolarisation with a view to applying SABRE hyperpolarised substrates as pH probes for MRI imaging. The results of this study suggest that tracking the chemical shift of a carbon environment within a substrate will be a viable method for applying SABRE to the production of a hyperpolarised pH probe. The addition of acetic acid to the sample inhibited SABRE polarisation of 3-hydroxypyridine. The addition of caesium carbonate also reduced the SABRE polarisation of 3-hydroxypyridine, in contrast it increased the SABRE polarisation of 4-hydroxypyridine. The dissociation rate constant for both of these substrates increased in the samples containing caesium carbonate when compared to the native samples. SABRE polarisation of 3-methoxypyridine and 4-methoxypyridine was hindered by the addition of caesium carbonate and deuteration of these substrates proceeded much more rapidly in the presence of the base. These effects were seen for both proton and carbon resonances. Additionally, the tertiary carbon resonances of 3-hydroxypyridine and 4-hydroxypyridine were shown to change by 4 ppm across the pH ranges tested. This result has the potential to be further developed into a pH sensitive, SABRE hyperpolarised, probe for medical application.

Table of Contents

Table of Figures

List of Tables

List of Equations

Acknowledgements

Firstly, I would like to thank my supervisor, Prof. Simon Duckett, for giving me the opportunity to learn invaluable skills in a research environment and for his help during my time as a student.

Secondly, thanks must go to the entire Duckett research group for your support and help throughout my project. Particular thanks must go to Marianna and Alexandra for your guidance and assistance. Thanks must go to Ryan for acting as my mentor this year and to my fellow students, Amy, Chris, Kate and Sarah, for making this year so enjoyable.

Finally I would like to thank my family and friends for all of their support. Mum and Dad – thank you for all of your encouragement throughout this year.

Declaration

I hereby declare that all the work presented within this thesis is original to the best of my knowledge, except where stated, and has not been submitted or published for other degrees.

Thomas Price

1. Introduction

1.1 Introduction

Nuclear Magnetic Resonance (NMR) has become a very popular spectroscopic technique for chemical and medical applications. In chemistry it has become ubiquitous for the characterisation of compounds and has found use in the study of reaction kinetics [1-4] and mechanisms.[5, 6] Magnetic Resonance Imaging (MRI) uses the same principles as NMR but provides spatial information rather than chemical information – this has become a standard technique in medicine and research for the imaging of soft tissue and brain function.[7] However, both techniques suffer from a sensitivity limitation; recent developments in the field of hyperpolarisation aim to resolve this issue.

Signal Amplification By Reversible Exchange (SABRE)[8] is a non-hydrogenative hyperpolarisation technique that transfers polarisation from a *para*hydrogen (pH$_2$) source to a target substrate through interaction with a metal catalyst. Whilst SABRE polarisation has been shown to apply to a variety of nuclei and substrates[8-11] it has not yet found a specific application. None the less it has been shown to improve the signal received in NMR by almost 4 orders of magnitude,[12] and it has been shown to be capable of detecting analytes at <1 μM concentration.[13] Developments in the field have focussed on using SABRE to produce a contrast agent for MRI,[14] but hydrogenative techniques that use pH$_2$ as a polarisation source have found use in the investigation of reaction mechanisms.[15, 16] In this study I will investigate the potential application of SABRE to these two areas.

1.2 Nuclear Magnetic Resonance

NMR can be used for single (1D) and multiple dimension (XD) spectroscopic experiments on a wide variety of nuclei. 1D spectroscopy gives information about the nuclear environments being probed; multiple dimension spectroscopy gives information about relationships between these environments.

The most commonly studied nucleus is the proton (^{1}H) – it is the most sensitive to magnetic fields and is almost 100 % naturally abundant. 1D ^{1}H NMR has become the workhorse of chemical characterisation and identification allowing rapid confirmation of a product's identity. The signal received for proton nuclei is quantitative, the frequency observed depends on the proton's environment, and the splitting patterns seen can be highly indicative of individual environments and neighbouring nuclei.

In addition to the study of ^1H environments within a compound, NMR is regularly used to study other spin ½ nuclei. The heteronuclei commonly studied are ^{13}C, ^{15}N, ^{19}F and ^{31}P. Heteronuclear NMR is less sensitive than ^1H NMR – for example the carbon nucleus has a much lower sensitivity to magnetic fields and the NMR active isotope is naturally only 1.1 % abundant. These factors make ^{13}C NMR almost 400 times less sensitive than ^1H NMR.

An example of where multidimensional, multinuclear, NMR techniques have been used to maximum effect is in the structural determination of proteins in solution without the need for a crystal structure. This is achieved by combining ^1H, ^{13}C and ^{15}N chemical shifts and through space interactions to build up the protein structure in solution.[17]

1.3 The Sensitivity Issue

In a normal NMR experiment the magnetic nuclei within the system are allowed to come to a thermal equilibrium that is dependent on the magnetic field. This population distribution follows a Boltzmann distribution as described in Equation 1.

$$\frac{n_{upper}}{n_{lower}} = e^{\frac{-\Delta E}{kT}} \qquad \text{(Equation 1)}$$

Equation 1: Boltzmann population distribution. n is the population of an energy level, ΔE is the difference between energy levels, k is the Boltzmann constant, T is the temperature of the system.

The energy levels probed by NMR correspond to the nuclear energy levels. In a magnetic field, B, they align along a number of specific directions. The number of possible orientations that a nucleus can take is determined by its spin quantum number, I. This quantum number gives the number of energy levels according to Equation 2.

$$Number\ of\ nuclear\ energy\ levels\ = 2I + 1 \qquad \text{(Equation 2)}$$

Equation 2: Number of nuclear energy levels. I is the spin quantum number.

A typical nucleus that would be studied by NMR, such as a proton, will have $I = 1/2$. This results in 2 possible alignments –with the z component of the nuclear spin parallel or anti-parallel to the field. The difference in energy between these two levels depends on the magnetic field and the gyromagnetic ratio of the nucleus being measured as described in Equation 3.

$$\Delta E = \hbar\gamma B \qquad \text{(Equation 3)}$$

Equation 3: Nuclear energy level separation. ħ is the reduced Planck constant, γ is the gyromagnetic ratio of the nucleus being investigated, B is the magnetic field.

For a proton ($\gamma = 26.75 \times 10^{7}\ T^{-1}\ s^{-1}$) in a magnetic field of 9.4 T (typical for an NMR experiment) this gives a difference in energy corresponding to a radio wave of frequency $\nu = 400$ MHz.

As NMR spectroscopy depends on transitions between two energy levels, the population difference between the energy levels is very important. Using the Equation 3 for the energy difference gives a Boltzmann population difference at 298 K of:

$$\frac{n_{upper}}{n_{lower}} = 0.99993$$

This corresponds to an effective difference of 1 in 31,000 molecules.

As both excitation and relaxation transitions are seen during an NMR experiment (absorbance and emission respectively) the received signals will almost cancel each other out. The small population difference is responsible for the entire observed signal. This is exacerbated for nuclei with a smaller gyromagnetic ratio or in which the abundance of magnetic nuclei is less than 100 % (e.g. ^{13}C, 1.1 % natural abundance, $\gamma = 6.73 \times 10^{7}\ T^{-1}\ s^{-1}$) requiring a long experiment time with a high number of scans to get a high resolution spectrum.

The low sensitivity of this technique limits the applications of NMR – to distinguish signal from noise a high concentration or large number of scans is needed. This prohibits the study of reaction intermediates formed *in situ*, may limit the study of reaction kinetics and mechanisms and generally makes the technique more expensive in both material and time costs

There are a number of ways to improve the signal received in NMR. Increasing the energy gap by increasing the magnetic field is one possibility – however this is limited and very expensive as NMR magnets need to be stable and homogenous. The strongest NMR magnet currently in operation is 23.5 T (with a proton frequency of 1 GHz) in Lyon. Using the previous example of a proton at 298 K, this would result in a population difference of 1 in 12,400. An alternative would be to cool the sample – as the temperature decreases the population difference increases - but this has a small effect and is limited by the solvent being used. For example, methanol freezes at 175.6 K. Using this temperature, and a 9.4 T magnet, would result in a ^{1}H population difference of 1 in 18,300. This also may not be practical for studies of reaction intermediates or rates as it could significantly change the reaction pathway and will result in much slower rates due to the lower temperature. This is also highly impractical for medical imaging.

Another alternative method of increasing the received signal is to force the population away from the Boltzmann distribution. The field studying this in NMR is referred to as “hyperpolarisation”.

1.4 Hyperpolarisation

1.4.1 Dynamic Nuclear Polarisation

A popular hyperpolarisation technique is Dynamic Nuclear Polarisation (DNP).[18] The polarisation source for DNP is free radicals. These unpaired electrons are very sensitive to magnetic fields ($\gamma = 2802 \times 10^{7}$ T^{-1} s^{-1}, approximately 100 times more sensitive to magnetic fields than protons) and as such deliver a much larger population difference than is seen for protons in a magnetic field. Both the radical source and the target molecule are contained in a glassy mixture within a high magnetic field. Transfer of polarisation from the radicals to the nuclei is caused by microwave stimulation at 1.2 K. After irradiation the sample must be warmed to return it to the liquid state without losing the polarisation before the molecule that is cross-polarised is studied by NMR.

DNP has had some significant success in the polarisation of pyruvate for molecular imaging purposes.[19] As the hyperpolarised pyruvate is converted in the body the products can also be seen as hyperpolarised signals allowing for rapid study of the metabolism using this technique (Figure 1).

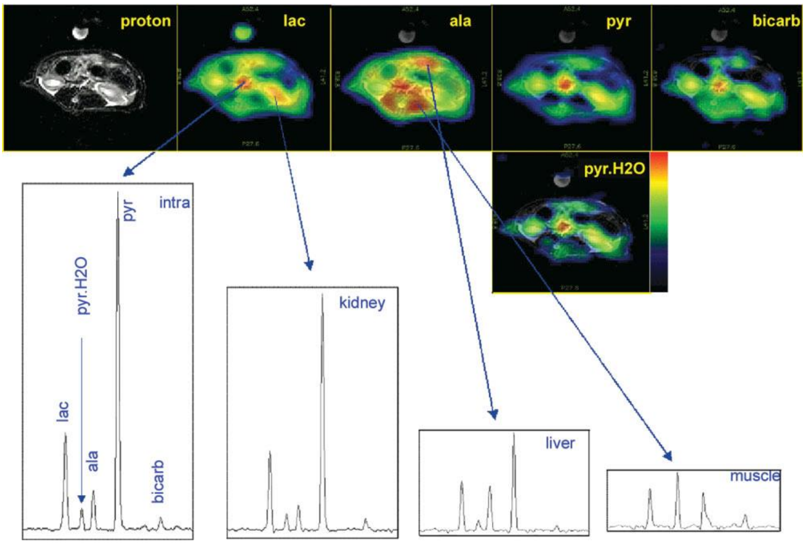

Figure 1: Chemical shift imaging derived maps, collected after injection of DNP polarised pyruvate, detailing rat metabolism. Hyperpolarised signals can be seen for pyruvate metabolites in different proportions in different organs. Image taken from Kohler *et al.*[19]

1.4.2 Optical Pumping

Optical pumping is a technique for hyperpolarising noble gases *via* polarisation of a metal center.[20, 21]

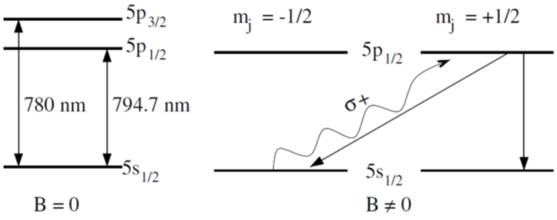

Figure 2: Excitation of rubidium from the electronic ground state to an excited state by circularly polarised light (σ+). Scheme taken from Leawoods *et al.* [22]

An example of optical pumping is the hyperpolarisation of NMR active helium, ^{3}He, using vaporised rubidium. This process is shown in Figure 2. The rubidium is polarised using circularly polarised light of wavelength 794.7 nm. The only electronic transition allowed is from $5s_{1/2}$ $m_j = -1/2$ to $5p_{1/2}$ $m_j = +1/2$ due to the selection rule $\Delta m_j = +1$ imposed by the circular polarisation of the light.

Relaxation of electrons from $5p_{1/2}$ occurs randomly to $5s_{1/2}$ $m_j = +1/2$ and $m_j = -1/2$, with an equal likelihood of relaxing to either of the two. The electrons in $5s_{1/2}$ $m_j = +1/2$ cannot be excited by the polarised light as they have no energy level to be excited to under the imposed selection rules; however those that have relaxed to $5s_{1/2}$ $m_j = -1/2$ can be re-excited to $5p_{1/2}$ $m_j = +1/2$. Continuous excitation leads to a population imbalance with $5s_{1/2}$ $m_j = +1/2$ being highly populated in comparison to $5s_{1/2}$ $m_j = -1/2$.

This source of polarisation is then transferred to the noble gas through collision induced spin exchange. This approach has found use in the imaging of airways – in particular the mouth[20] and lungs (Figure 3).[21]

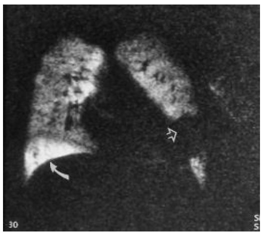

Figure 3: MRI acquisition of lungs using hyperpolarised ^{3}He completed in 28 s. Bright regions indicated the presence of hyperpolarised gas. The dark region on the right of the image, indicated by an unfilled arrow, is due to the presence of a tumour. Image taken from Kauczor *et al*.[21]

1.4.3 *Para*Hydrogen Induced Polarisation

*Para*Hydrogen Induced Polarisation (PHIP) uses *para*hydrogen (pH$_2$) as a source of polarisation. This polarisation can be exploited in a number of different ways, both hydrogenative and non-hydrogenative. The resulting polarisation depends strongly on the magnetic field where the observable polarisation is first created. This concept will be explored further in section 1.5.

1.5 PHIP

1.5.1 *Para*Hydrogen

Nuclei can take on 2*I*+1 nuclear spin states. As a spin, *I* = ½ nucleus, ^1H nuclei can take on 2 spin states. These have their z axis aligned parallel (α) and aligned antiparallel (β) to the applied magnetic field as shown in Figure 4. However, α ≠ -β.

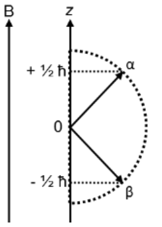

Figure 4: Schematic of the two spin angular momentum states in the presence of a magnetic field, B. The two spins states, α and β, have an overall magnitude of √(3/2) ħ and a z component $I_z = \pm \frac{1}{2}\hbar$.

In a molecule of hydrogen (H_2), the two ^1H nuclei have 4 potential spin energy pairings when in a magnetic field: αα, αβ, βα and ββ. As the spin energy levels must be either symmetric or antisymmetric with respect to nucleus interconversion a linear combination of αβ and βα is needed.[23] This gives the allowed states as:

$$\alpha\alpha, \qquad \frac{\alpha\beta + \beta\alpha}{\sqrt{2}}, \qquad \beta\beta \quad and \quad \frac{\alpha\beta - \beta\alpha}{\sqrt{2}}$$

The first three of these states are symmetric with respect to nucleus interconversion, and form a triplet, and known as *ortho*hydrogen (*o*H_2). The remaining state,$\frac{\alpha\beta - \beta\alpha}{\sqrt{2}}$, is antisymmetric with respect to nucleus interconversion. This state is restricted to a single term, in other words, a singlet state known as *para*hydrogen (*p*H_2).

Due to Pauli's exclusion principle, the overall wavefunction of fermions, such as protons, must be antisymmetric with respect to the interchange of the nuclei. The overall molecular wavefunction is made up of translational, rotational, vibrational, electronic and nuclear wavefunctions. For hydrogen the majority of these are symmetrical with respect to nuclear interchange; however the rotational and nuclear wave functions can be either symmetrical or antisymmetrical. As such the antisymmetric *para*hydrogen state is restricted to molecules with symmetric rotational energy levels with rotational quantum numbers, J, = 0, 2, 4 etc. to give an overall antisymmetric molecular wavefunction. The symmetric *ortho*hydrogen states arise from molecules with antisymmetric rotational energy levels, J = 1, 3, 5 etc. This results in $p\text{H}_2$ being lower in energy than $o\text{H}_2$.[24]

Direct conversion between $o\text{H}_2$ and $p\text{H}_2$ is spin forbidden.[24] The interaction of hydrogen with a catalytic surface breaks the symmetry of the molecule and allows conversion between *ortho*- and *para*hydrogen. Examples of spin conversion catalysts are activated charcoal and iron chloride.[24] At low temperatures the population of the hydrogen sample can be biased to be predominantly $p\text{H}_2$. Once the hydrogen gas is removed from the catalyst bed it can no longer interconvert between states – this gives a highly stable source of polarisation that can be produced on demand or stored.

The nuclear wavefunction of *para*hydrogen, $\psi = \frac{\alpha\beta - \beta\alpha}{\sqrt{2}}$, has a total nuclear spin of 0 and is therefore “NMR silent”.[25] To transfer the polarisation from the $p\text{H}_2$ to the molecule of interest the symmetry of the hydrogen nuclei must be broken and some interaction between the hydrogen and the target must take place. Incorporation of the hydrogen directly into a species is used in PASADENA and ALTADENA to polarise unsaturated organic molecules and to study reactions at metal centres. SABRE uses a polarisation transfer catalyst to bind the hydrogen – this allows transfer of the polarisation to a substrate that is also bound to the catalyst, without the need to incorporate the hydrogen into the substrate. This substrate can then dissociate, making the hyperpolarisation process non-hydrogenative with respect to the substrate.

1.5.2 PASADENA and ALTADENA

Parahydrogen And Synthesis Allow Dramatically Enhanced Nuclear Alignment (PASADENA) and Adiabatic Longitudinal Transfer After Dissociation Engenders Nuclear Alignment (ALTADENA) are two hydrogenative techniques for *Para*Hydrogen Induced Polarisation (PHIP).

When the PASADENA technique is applied, reaction and polarisation transfer occurs at a high field – typically inside the NMR magnet – and results in antiphase signals for the PHIP enhanced peaks.[26] This can be understood if the symmetry of the pH_2 is broken as it reacts. This process leads to the pure *para*hydrogen state becoming evenly distributed over both αβ and βα product states as shown in Figure 5. These two states can both undergo absorption to form the ββ state or emission to the αα state. Both absorption and emission effects are equally likely. The observed NMR peak corresponding to the protons is therefore antiphase, with strong absorption and emission characteristics that are separated by the coupling between the two proton environments (J_{HH}).

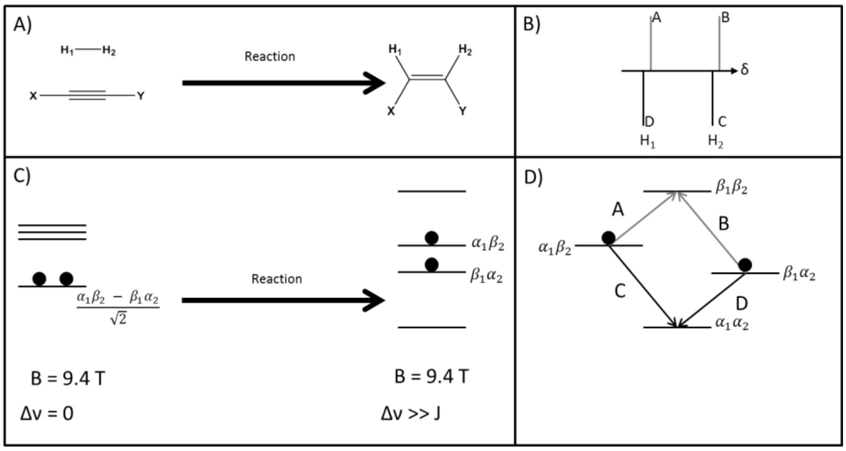

Figure 5: A) Schematic of the PASADENA process. B) Schematic of hyperpolarised PHIP NMR spectrum expected from the product in this system under PASADENA conditions. The peaks have been labelled according to their transition source. C) Schematic of energy levels occupied by protons during the PASADENA process. Note that as the symmetry of the hydrogen is broken in a weak coupling regime the $\alpha_1\beta_2$ and $\beta_1\alpha_2$ states are equally populated. D) Schematic representation of observed transitions. Transitions A and B are due to absorption, transitions C and D are due to emission.

The antiphase nature of PASADENA PHIP signals can reduce the net signal gain due to destructive interference between the emission and absorption peaks if J_{HH} is small. In contrast, ALTADENA (Figure 6) involves polarisation transfer at a lower field before the sample is transferred to high field for NMR measurement.[27] This results in inphase signals for the PHIP enhanced peaks, but only one component of each resonance is detected.

In this case, the reaction of hydrogen and substrate occurs at low field and the strong coupling regime is in effect. Hence the coupling between the two protons, J_{HH}, is greater than the difference in their chemical shift, Δν. This leads to the retention of the pure pH$_2$ state during reaction as shown in Figure 6. Transport to the high field for measurement leads to the selective population of the lowest energy αβ or βα term. The resulting NMR spectrum shows a single in-phase PHIP enhanced peak for each environment.

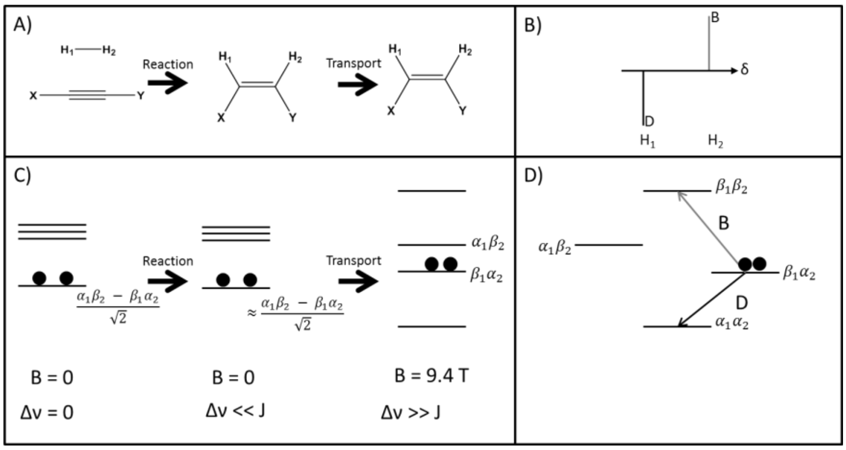

Figure 6: A) Schematic of the ALTADENA process. B) Schematic of hyperpolarised PHIP NMR spectrum expected from the product in this system under ALTADENA conditions. The peaks have been labelled according to their transition source. C) Schematic of energy levels occupied by protons during the ALTADENA process. Note that the singlet state is the only state occupied after the reaction, and upon transport into the high field only one state is occupied. D) Schematic representation of observed transitions. Transition B is due to absorption, transition D is due to emission. Transitions A and C are not seen.

These two techniques have found widespread use in the characterisation of reaction intermediates [28, 29] and for the determination of reaction mechanisms,[30] particularly around metal centres. Recently PASADENA has been used in conjunction with *in situ* laser photolysis as a means of developing time resolved NMR. [31]

1.6 SABRE

1.6.1 Signal Amplification By Reversible Exchange

SABRE[8] is a PHIP technique that does not incorporate hydrogen into the target molecule. Instead, a polarisation transfer catalyst reversibly binds both hydrogen and the substrate to be polarised. When $p\mathrm{H}_2$ is used, the polarisation is transferred from the hydrogen to the substrate whilst bound to the metal catalyst and the continuous exchange the system undergoes allows the polarisation to build up in solution without chemically changing the substrate.

1.6.2 SABRE polarisation transfer catalysts

SABRE was first discovered using Crabtree's catalyst and analogous iridium complexes for the polarisation of pyridine. Catalysts of the type [Ir(PR_3)(cod)(**Py**)]Cl (PR_3 = phosphine ligand, cod = 1,5-cyclooctadiene, **Py** = pyridine) were used to polarise pyridine with a proton signal enhancement of 550 fold reported using Crabtree's catalyst, in which PR_3 = PCy_3 (Cy = cyclohexyl).[8] The phosphine species was varied[32] and shown to play a significant role in the polarisation process, with the most efficient ligand for polarisation transfer being PCy_2Ph (Cy = cyclohexyl, Ph = phenyl) – the most sterically bulky and electron donating phosphine tested in this study. This catalyst is shown in Figure 7.

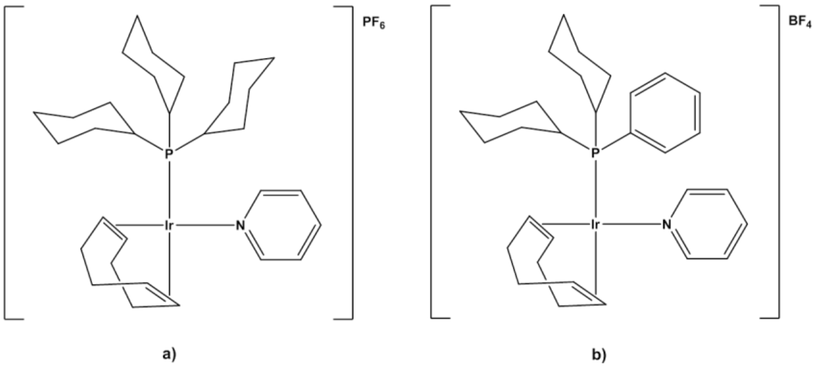

Figure 7: Schematic of a) Crabtree's catalyst and b) the optimised SABRE polarisation transfer catalyst of this type, [Ir(PCy_2Ph)(cod)(**Py**)]BF_4.

This modest polarisation was significantly improved upon by replacing the phosphine ligand with an N-Heterocyclic Carbene (NHC) ligand. Similar changes have been shown to affect the hydrogenative ability of the iridium catalysts due to the greater electron donation of the NHC ligand rather than the phosphine.[33-35] A polarisation level of 8100 fold was reported for pyridine when the catalyst [Ir(IMes)(cod)Cl] (**1-cod-Cl**) (IMes = 1,3-bis(2,4,6-trimethylphenyl)imidazole-2-ylidene) [12] was employed (shown in Figure 8). This is currently the standard catalyst employed for SABRE polarisation.

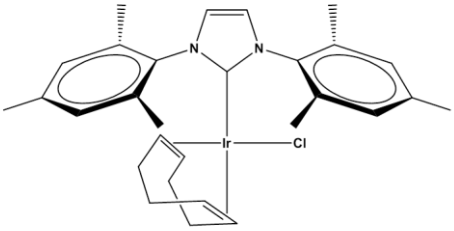

Figure 8: Schematic of [Ir(IMes)(cod)Cl] (**1-cod-Cl**)

A variety of iridium-NHC complexes have been tested for SABRE activity; the identity of the NHC ligand has been shown to have a significant effect on the level of polarisation seen. [36, 37] A report by van Weerdenburg *et al.* concluded that the electronic differences between the NHC ligands had little effect on the polarisation, and that it was the buried volume that had the greatest effect on the observed polarisation due to its effect on the substrate dissociation rate. They also noted that the NHCs with aromatic groups showed an interaction with the pyridine ligands used – this may further affect the dissociation rate of the substrate.

1.6.3 Activation of the polarisation transfer catalyst

The active polarisation transfer catalyst is formed *in situ* from the square planar catalyst by addition of hydrogen and a suitable substrate (**L**). The key steps in this activation are:

- The substrate displaces the chlorine from **1-cod-Cl** to form [Ir(IMes)(cod)(**L**)]Cl (**1-cod-L**)[12]
- Hydrogen binds to the iridium centre
- The cod ligand is hydrogenated to form cyclooctane, the bound hydrogen forms two hydrides *via* an oxidative addition[38]
- Two further substrate ligands are bound to the iridium

This process, summarised in Figure 9, results in the formation of the catalyst [Ir(IMes)(H)$_2$(**L**)$_3$]Cl (**1-L**)[12] in which the substituents *cis* to the NHC are labile.

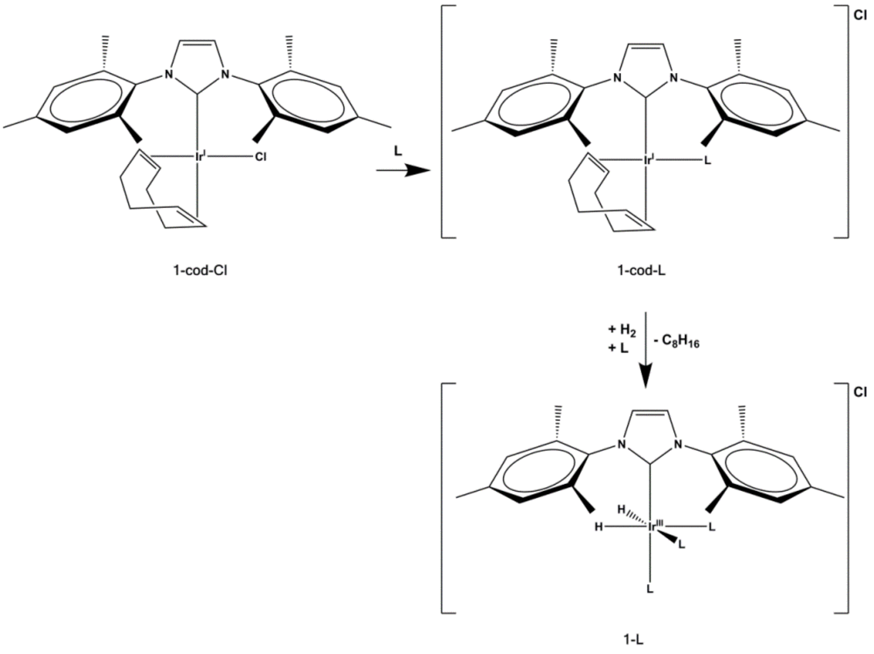

Figure 9: Schematic of key steps in the activation of **1-cod-Cl** by addition of **L** (where **L** is a 2 electron donor) and hydrogen to give **1-L**

1.6.4 Exchange and polarisation transfer mechanism

Exchange of both substrate and hydrogen are crucial when considering the SABRE polarisation transfer mechanism. Experimental evidence suggests that the substrate exchange for pyridine (**Py**) and [Ir(IMes)(H)$_2$(**Py**)$_3$]$^+$ (**1-Py**) proceeds via a dissociative mechanism.[12] This results in a 16 electron intermediate which can bind free substrate from solution, be trapped by the solvent,[36] or go on to undergo hydrogen exchange.

The proposed process of exchange for the hydride species is shown in Figure 10. Following dissociation of **Py**, a dihydrogen molecule can bind to the complex. Whilst both the dihydrogen and the two hydrides are bound to the iridium they can interconvert. This is the route which enables polarisation transfer from fresh *para*hydrogen in solution. Subsequent dissociation of a dihydrogen ligand returns the species to the 16 electron intermediate. This route has been mapped out using kinetic data and Density Functional Theory (DFT).[12]

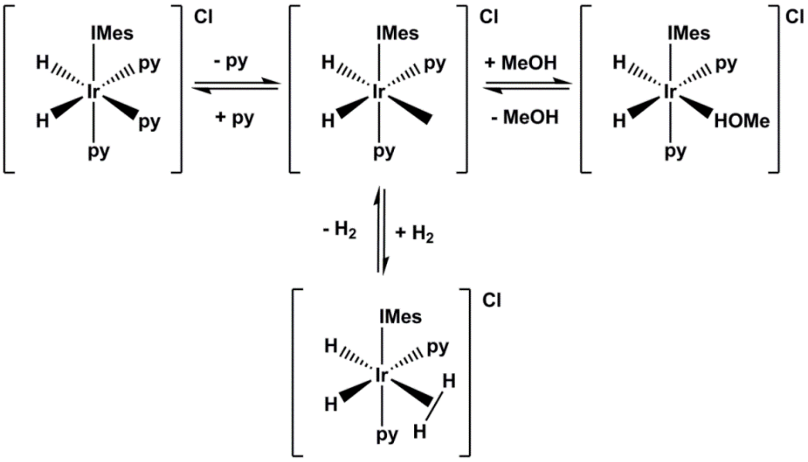

Figure 10: Schematic of hydrogen and ligand exchange for **1-Py** in methanol, and formation of the solvent-bound complex. Reproduced from Lloyd *et al*.[36]

1.6.5 Increasing SABRE polarisation transfer efficiency

1.6.5.1 Optimisation of NHC ligand

A number of different iridium-NHC complexes were tested for their polarisation properties with regards to their kinetic, steric and electronic parameters with the aim of understanding the requirements of the polarisation transfer method and optimising the polarisation observed.[36, 37] The complex **1-Py** described above was found to be superior to the other systems studied at room temperature.

The polarisation transfer catalysts [Ir(ICy)(H)$_2$(**Py**)$_3$]Cl (ICy = 1,3-bis(cyclohexyl)-imidazole) and [Ir(SIPr)(H)$_2$(**Py**)$_3$]Cl (SIPr = 1,3-bis(2,6-diisopropyl)-4,5-dihydroimidazol-2-ylidene) were used to exemplify the dependence of polarisation on the lifetime of the octahedral complex. [Ir(ICy)(H)$_2$(**Py**)$_3$]Cl has a long lifetime compared to **1-Py** at room temperature. At higher temperatures this lifetime decreased and the observed polarisation due to [Ir(ICy)(H)$_2$(**Py**)$_3$]Cl increased as shown in Figure 11. At room temperature, [Ir(SIPr)(H)$_2$(**Py**)$_3$]Cl was found to have a much shorter lifetime than **1-Py**; cooling the sample containing [Ir(SIPr)(H)$_2$(**Py**)$_3$]Cl improved the polarisation observed.[36] These results suggest that there is an optimum lifetime of the octahedral species for maximum polarisation transfer. An ideal pyridine dissociation rate of 0.5 – 0.08 s^{-1} was determined for maximising SABRE.[36]

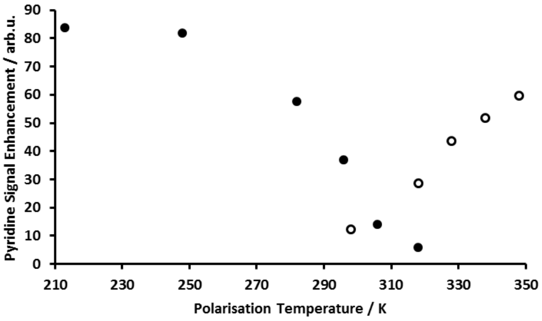

Figure 11: The effect of temperature on polarisation of **Py** by two polarisation transfer catalysts. ● Polarisation of **Py** by [Ir(SIPr)(H)$_2$(**Py**)$_3$]Cl ○ Polarisation of **Py** by [Ir(ICy)(H)$_2$(**Py**)$_3$]Cl. Reproduced from Lloyd *et al.*[36]

1.6.5.2 Concentration of polarisation

Another approach to optimising the SABRE polarisation is to reduce the number of polarisable protons. This is achievable by reducing the number of exchangeable sites or by reducing the number of polarisable protons on the target substrate.

Fekete *et al.* reported a system, shown in Figure 12, in which both a phosphine and NHC ligand were bound to the iridium.[39] This reduced the number of bound substrates from 3 to 2, focusing the polarisation transfer onto fewer protons which should result in a greater polarisation. This system was shown to undergo SABRE polarisation – although the desired improvement in polarisation was not seen. This is likely due to the phosphine ligand occupying the site *trans* to the NHC; this site does not undergo rapid exchange and so the change in polarisable protons was minimal.

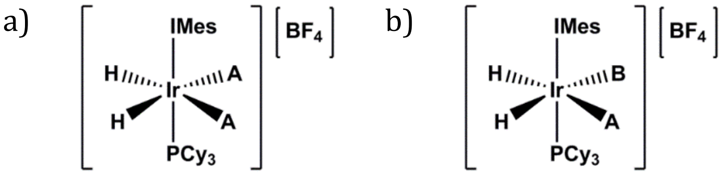

Figure 12: a) [Ir(IMes)(PCy$_3$)(H)$_2$(**Py**)$_2$]BF$_4$ b) [Ir(IMes)(PCy$_3$)(H)$_2$(**Py**)(**MeCN**)]BF$_4$ Iridium-NHC-phosphine species tested for SABRE activity by Fekete *et al.*[39]

The number of polarisable protons was reduced further by using acetonitrile (**MeCN**) as a substrate instead of pyridine – this reduces the number of polarisable protons from 5 per substrate site to 3 per site. The polarisation of **MeCN** as a substrate has been investigated,[40] but is not directly comparable to the polarisation of **Py**.

The mixed ligand complex, [Ir(IMes)(PCy$_3$)(H)$_2$(**Py**)(**MeCN**)]BF$_4$, (Figure 12) was found to be as effective as **1-Py** for polarisation transfer to **Py**, despite having a ligand dissociation constant that was only half that recorded for **1-Py**. The use of *d$_5$*-pyridine led to an increase in polarisation of **MeCN** by [Ir(IMes)(PCy$_3$)(H)$_2$(***d$_5$*-Py**)(**MeCN**)]BF$_4$. This confirms that reducing the number of polarisable protons will increase the polarisation seen.[39]

Another development in this area is the use of a "PNP-pincer" ligand to reduce the number of sites available for substrate binding.[41] This system is shown in Figure 13. This tridentate ligand permanently occupies one of the labile sites in the plane of the hydrides limiting the number of substrate molecules that can bind to the catalyst. This system was shown to polarise **Py** and also the pyridine functionality in the PNP-pincer that was bound to the iridium. By using a deuterated form of the PNP-pincer ligand, a 35% increase in the polarisation transfer efficiency was achieved. This further confirms that reducing the number of polarisable protons will increase the polarisation seen.

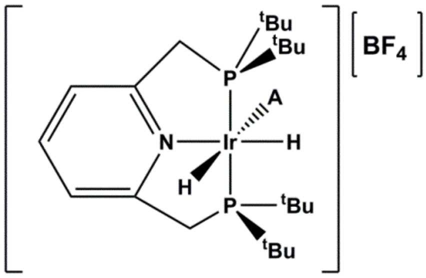

Figure 13: Iridium PNP-pincer complex used as a SABRE catalyst by Holmes *et al*.[41]

1.6.5.3 Development of polarisation transfer method

Whilst initial studies into SABRE used manual agitation of an NMR tube followed by rapid insertion into the NMR magnet, development of a flow probe system[12] which automates polarisation and transfer of the sample into the NMR magnet improved the reliability of measurements and offered a controlled, variable, polarisation field. This has improved understanding into the role that the polarisation transfer field plays in the SABRE effect.[10] Through repeated polarisation and injection cycles, SABRE has been applied to rapid acquisition of 2D COrrelated SpectroscopY (COSY) and ^1H-^{13}C Heteronuclear Multiple Bond Correlation (HMBC) spectra.[42]

1.6.6 Towards biocompatible SABRE

1.6.6.1 Physiological considerations

One of the major targets in the development of SABRE is its application to *in vivo* studies. A key part of achieving this target will be ensuring that the system can produce a non-toxic probe. As a result, each component of the polarisation system must either be non-toxic or completely removed from the system prior to measurement. The key components to consider are:

- Substrate
- Catalyst
- Solvent

A number of approaches to resolving these issues have been published and are briefly outlined below.

1.6.6.2 Biologically relevant substrates

A number of biologically relevant substrates have been polarised using SABRE. These include nicotine, nicotinamide and drug fragments,[8] amino acids and small peptides,[9] many pyrazole derivatives,[10] and the tuberculosis drugs pyrazinamide and isoniazid.[43] Of these, nicotinamide has seen the most development due to its substantial polarisation and low toxicity.[14, 38]

1.6.6.3 Removal of the catalytic species

Shi *et al*. used a polymer bound polarisation transfer catalyst to demonstrate that SABRE polarisation could be performed by a readily removable catalyst.[44] By taking advantage of the non-labile substrate site *trans* to the NHC, a polymer bound pyridine derivative was attached to $[Ir(IMes)(cod)PF_6]$ to yield [Ir(IMes)(cod)(**Py**-polymer)]PF_6. This catalyst was then used to promote SABRE activity. Upon removal of the polymer beads (and therefore the SABRE catalyst) prior to polarisation, no residual polarisation was seen. This shows that the polymer supported catalyst is capable of SABRE polarisation and that the polarisation seen is not due to “leeched” homogeneous catalyst.

This approach will reduce the amount of catalyst present in the sample and would allow for the re-use of the same catalyst for hyperpolarisation of multiple samples. These properties are highly desirable when considering applications of SABRE as they increase the viability of the technique and can reduce the costs of its use.

1.6.6.4 Reduction of solvent toxicity

The methanol solvent used for polarisation transfer is a significant hurdle for biocompatible SABRE contrast agents. The ideal solvent would be water or saline. The use of a water-ethanol mixture for SABRE polarisation has shown some success[14] – the ethanol providing the solubility parameters needed, whilst the high water content makes the mixture non-toxic by dilution. Whilst polarisation has been achieved under these conditions it has not yet achieved the levels of polarisation seen in methanol.

An alternative method of preparing the active catalyst in methanol, replacing the methanol with water and then carrying out the polarisation process has shown some success. Zeng *et al*. first reported this technique;[45] addition of water was carried out prior to removal of methanol under vacuum. The remaining solution contained 10 % methanol in water and showed limited polarisation ability. The mixture also led to significant foaming – a problem for repeated experimentation and for any medical applications. Completely drying the activated complex **1-Py** prior to dissolution into deuterated water resulted in retention of polarisation activity – the polarisation of nicotinamide reported by Truong *et al*.[38] was approximately 1/3 of the value reported in ethanol in the same report.

1.7 Aims of this Project

This project aims to develop the SABRE methodology towards application in catalysis and medical imaging.

One of the areas in which I will develop SABRE will be the polarisation of new substrates – both organic and inorganic. A greater variety of organic substrates that have been proven to undergo efficient SABRE polarisation will allow for greater understanding of the polarisation process and further opportunities for future development. Polarisation of inorganic substrates will be a key step towards the polarisation of catalytic species – this will allow application of SABRE to study reaction mechanisms.

A key medical use of SABRE would be for molecular imaging. In this project I will explore the effect of pH on SABRE polarisation and on potential substrates to investigate the application of SABRE polarised substrates as pH probes for the purpose of molecular imaging. Developing a specific medical application of SABRE will drive development of the technique to meet the associated requirements.

2. SABRE Polarisation of 3-aminopyridine

2.1 3-aminopyridine

The catalyst $[Ir(IMes)(H)_2(\mathbf{L})_3]^+$, **(1-L)**, has been shown to be very efficient at polarising substrates **(L)** based on a pyridine **(Py)** motif through SABRE.[12] There is a reported precedent that the efficiency of **1-L** as a polarisation transfer catalyst depends critically on the identity of the substrate.[43] In order to explore this dependency, and to expand the pool of substrates polarised through SABRE, the functionalised pyridine, 3-aminopyridine **(3AmPy)** was selected for this study. This substrate was selected because:

- It has a pyridine nitrogen with a pK_{aH} of 6.07[46] – it is therefore more basic than pyridine ($pK_{aH} = 5.23$)[46] and as such should bind readily to the iridium catalyst through the lone pair of the aromatic nitrogen.
- It contains exchangeable NH protons that might polarise or impact dramatically on the SABRE process.
- The additional amine functional group could provide an alternative binding mode and mechanism of polarisation transfer. This may also lead to a bridged complex with multiple iridium centers; the effect of this on SABRE polarisation could then be explored.

It is common for NR_2H or NH_3 ligands to bind to metal centers through their lone pair.[47, 48] A comparison of this binding to that of the pyridine nitrogen would increase understanding of the SABRE mechanism and potentially open up a new class of substrates that do not rely on the pyridine motif for SABRE polarisation.

Although the oxidative addition of an N-H bond to a metal centre is relatively uncommon,[49] there are a number of examples in which this addition occurs over an iridium centre.[50-52] Many of these examples use pincer systems as ligands[51, 52], and one example forms a pincer system through the oxidative addition of an N-H bond to iridium.[50] If this type of N-H bonding is seen for **3AmPy** and **1-3AmPy** it could lead to introduction of *para*hydrogen (*p*H_2) into the substrate. This would be a very different and distinctive method of polarising the substrate in comparison to the approach typically used in SABRE. It will therefore be very important to detail the binding interactions with iridium.

C, shown in Figure 14, was characterised using standard 1D and 2D NMR techniques. The four aromatic proton peaks of **C** were readily identified in its ^{1}H NMR spectrum (Figure 15). At 243 K the multiplet at δ 7.10 can be resolved into two peaks – a doublet of doublets at δ 7.17 and a doublet of doublets of doublets at δ 7.10.

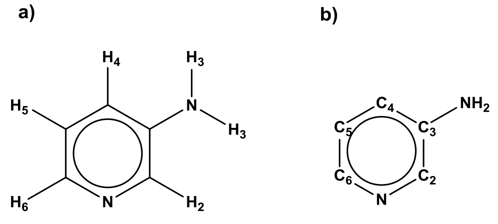

3AmPy

Figure 14: Schematic of **3AmPy** showing a) ^{1}H notation and b) ^{13}C notation.

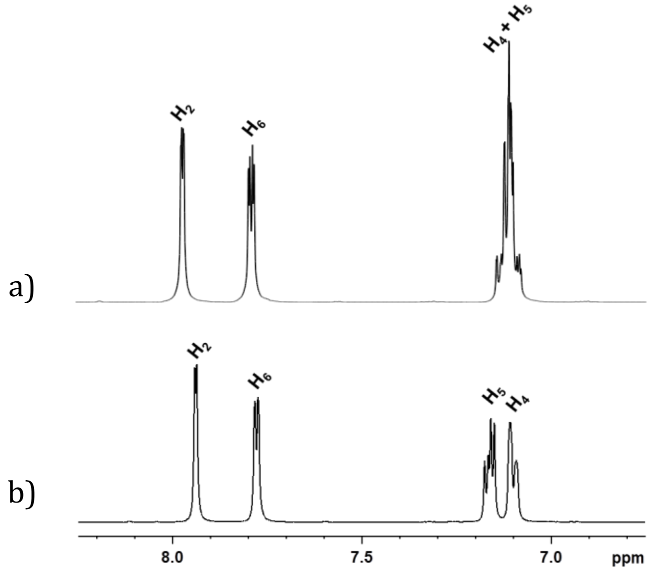

Figure 15: ^{1}H NMR spectrum of **3AmPy** in *d₄*-methanol at a) 298 K and b) 243 K. The peaks corresponding to H_4 and H_5 have separated sufficiently to be individually resolved. The peaks corresponding to H_2 and H_6 have also shifted with temperature indicating an increase in shielding at lower temperatures.

A ^{1}H-^{15}N Heteronuclear Multiple Quantum Correlation(HMQC) spectrum, collected at 298 K, revealed the ring nitrogen atom appears at δ 297.7, and couples to the two ^{1}H resonances at δ 7.94 and 7.79. This suggests that these resonances correspond to protons H_2 and H_6 of **C** as they will couple most strongly to the aromatic nitrogen.

A 1D selective excitation nuclear Overhauser effect (nOe) experiment was carried out on each of these peaks at 243 K (Figure 16) to assign them more specifically and also to identify H_4 and H_5. The strong nOe between δ 7.78 and 7.17 suggests that these peaks correspond to H_6 and H_5 respectively. The weak nOe between both δ7.94 and 7.78 and the remaining peak at δ 7.10 support the assignment of this peak arising from H_4. Both H_2 and H_6 are a similar distance in space away from this environment and exhibit a similar nOe effect to it.

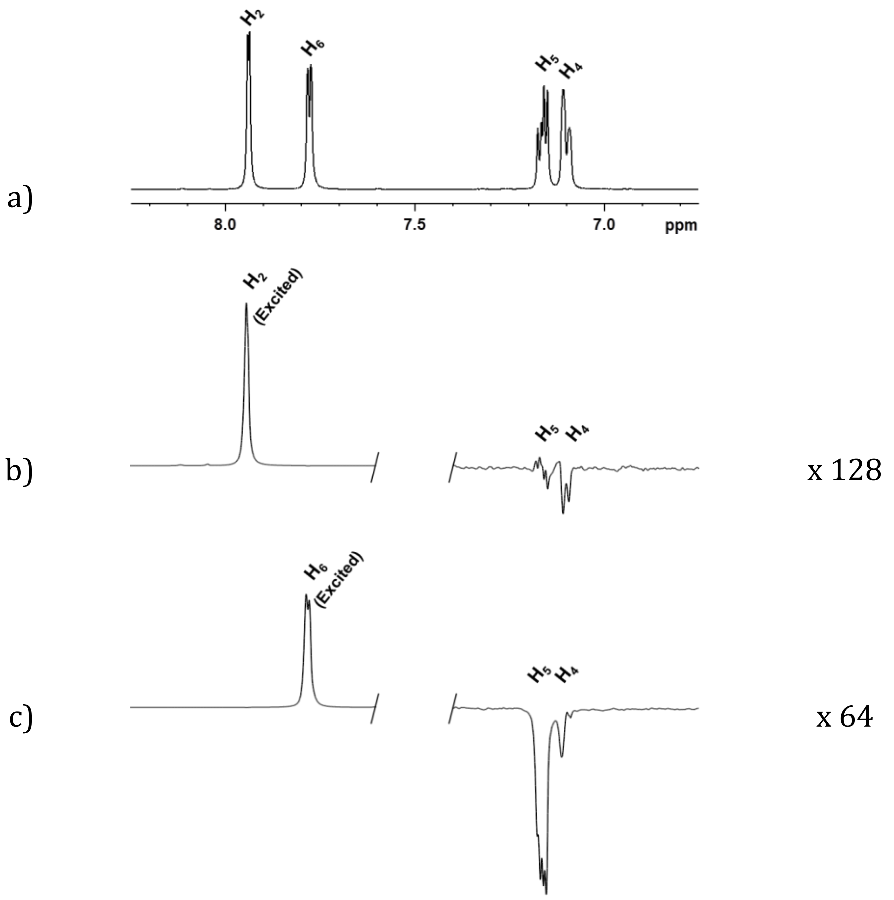

Figure 16: a) ^{1}H spectrum of **3AmPy** in d_4-methanol at 243 K b) Selective nOe experiment with excitation of the peak at δ 7.94, due to H_2, showing through space interaction to H_4 and very weakly to H_5 c) Selective nOe experiment with excitation of the peak at δ 7.78, due to H_6, showing through space interaction to H_4 and a strong interaction with H_5. x 64 indicates a vertical expansion of the right hand portion of the spectrum relative to the left hand portion of the spectrum.

The corresponding ^{1}H-^{13}C HMQC spectrum allows for the rapid identification of the carbon chemical shifts that correspond to C_2, C_4, C_5 and C_6 as they have attached protons and therefore exhibit strong short-range couplings. C_3 is located through the use of longer ranged couplings. Using a weaker coupling for the ^{1}H-^{13}C HMQC measurement reveals a coupling between ^{1}H δ 7.94 and C_3 but not between δ 7.79 and C_3. This confirms that the peak at δ 7.94 corresponds to H_2 and δ 7.79 corresponds to H_6.

The protons that make up the amine group could not be identified in methanol due to rapid exchange with the solvent. These protons were identified in the aprotic solvent, *d₂*-DCM, although they still exchange with residual water in the sample resulting in a broad peak at δ 3.76. A strong coupling to these ^{1}H resonances allowed identification of the amine nitrogen at δ 49.1.

This assignment is in good agreement with that given in the literature for alternative solvents. [53, 54]

The methodology used here was followed during the characterisation of all of the species used in this thesis. Clearly, even a simple molecule requires extensive investigation if unambiguous assignments are to be made.

2.2 [Ir(IMes)(cod)(3-aminopyridine)]$^{+}$ - precatalyst

The reaction of [Ir(IMes)(cod)Cl], (**1-cod-Cl**), to form [Ir(IMes)(cod)(**L**)]Cl, (**1-cod-L**), occurs rapidly in solution. The substrate **L** acts to displace the halide from **1-cod-Cl**.[12] The resulting complex **1-cod-L** is formed, as shown in Figure 17.

Figure 18 shows the associated ^{1}H NMR spectrum for **1-cod-3AmPy**. However, even at 243 K, rapid exchange occurs, implying that **3AmPy** is labile in this complex.

At room temperature it is difficult to distinguish the peaks corresponding to the complex from those corresponding to the free substrate due to rapid exchange between the two and significant overlap of the peaks. Cooling the sample slows the exchange of the substrate and tumbling of the molecules in solution, this reduces line broadening allowing for greater resolution. Changing the temperature also causes a change in chemical shifts. At 243 K the bound substrate can be distinguished from the free substrate and its identity as part of the complex **1-cod-3AmPy** (shown in Figure 19) confirmed by NMR.

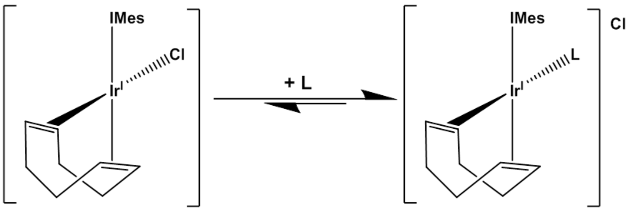

Figure 17: Displacement of chlorine from **1-cod-Cl** by a substrate molecule, **L**, in solution to give **1-cod-L**.

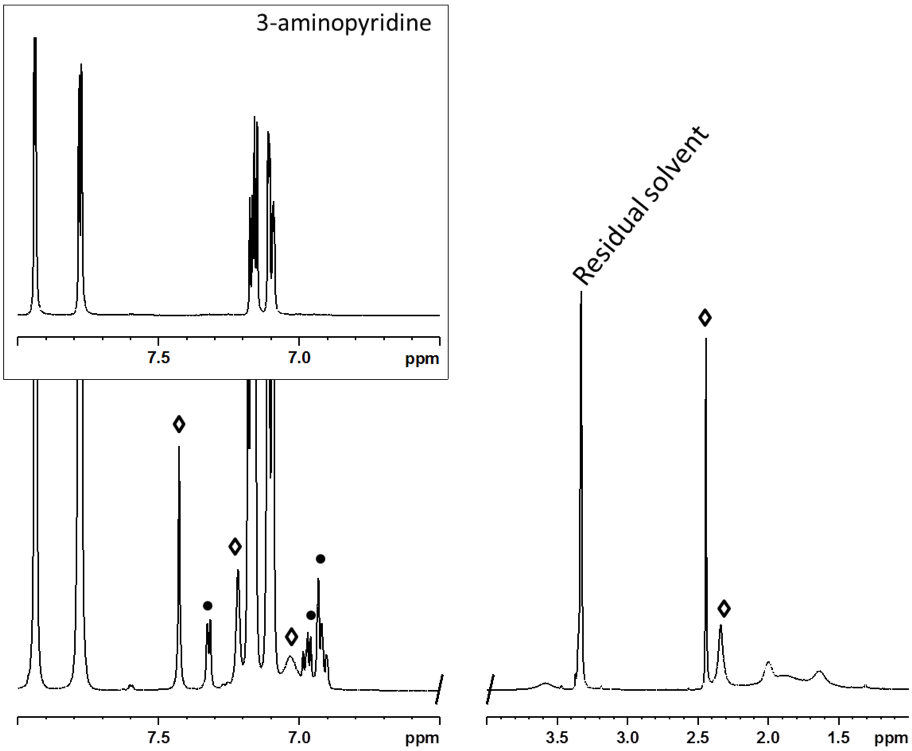

Figure 18: ^1H NMR spectrum of **1-cod-3AmPy** in d_4-methanol at 243 K. ^1H spectrum of **3AmPy** at this temperature is inset. ● indicates a resonance corresponding to the bound **3AmPy**; ◊ indicates a resonance corresponding to the IMes ligand.

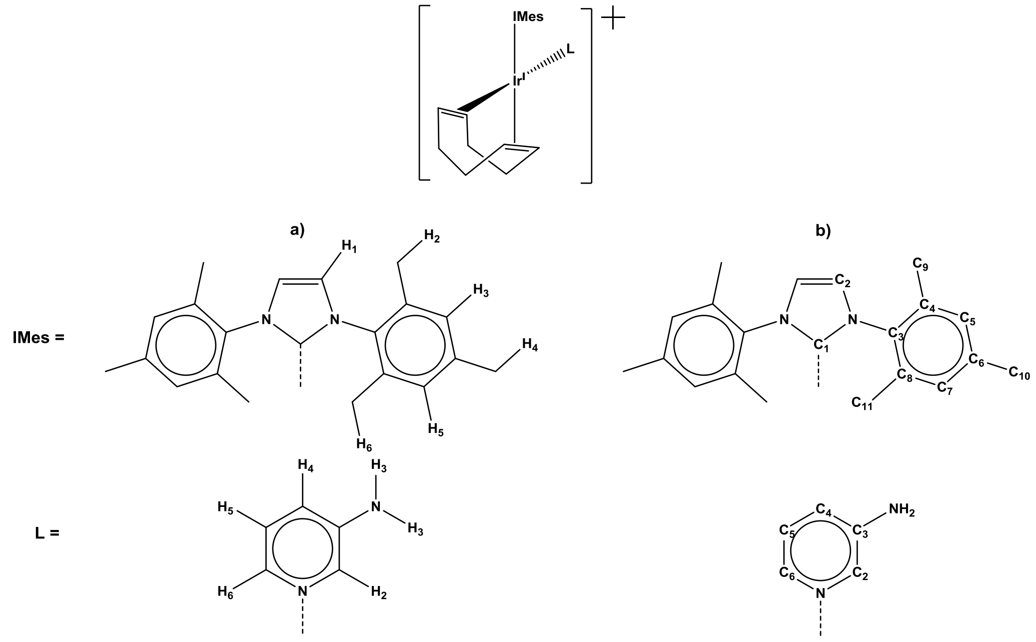

Figure 19: Schematic of **1-cod-3AmPy** showing a) ^1H and b) ^{13}C notation.

A 2D ^1H-^{15}N HMQC spectrum was recorded to locate the ^{15}N nuclei of **1-cod-3AmPy**. Coupling can be seen between ^1H environments and two new ^{15}N peaks at δ 241.2 and 195.5. A third new nitrogen resonance may be expected which would correspond to the amine nitrogen of the bound substrate. However, as in the case of the free substrate, this resonance was not seen in methanol. The ^{15}N peak at δ 241.2 corresponds to the bound substrate aromatic nitrogen whereas the peak at δ 195.5 is due to the N-heterocyclic carbene ligand. This nitrogen is part of the imidazole ring and couples to a ^1H environment at δ 7.42 – the olefinic protons of the imidazole ring, $H_{IMes,1}$.

$H_{IMes,1}$ is close in space to the protons of the *ortho* methyl groups within the mesityl group ($H_{IMes,2}$ and $H_{IMes,6}$). These two ^1H environments can be identified, using a 2D NOESY experiment to see the through-space interaction with $H_{IMes,1}$, with chemical shifts of δ 2.00 and 2.34. The remaining methyl group, $H_{IMes,4}$, has a single resonance at δ 2.44.

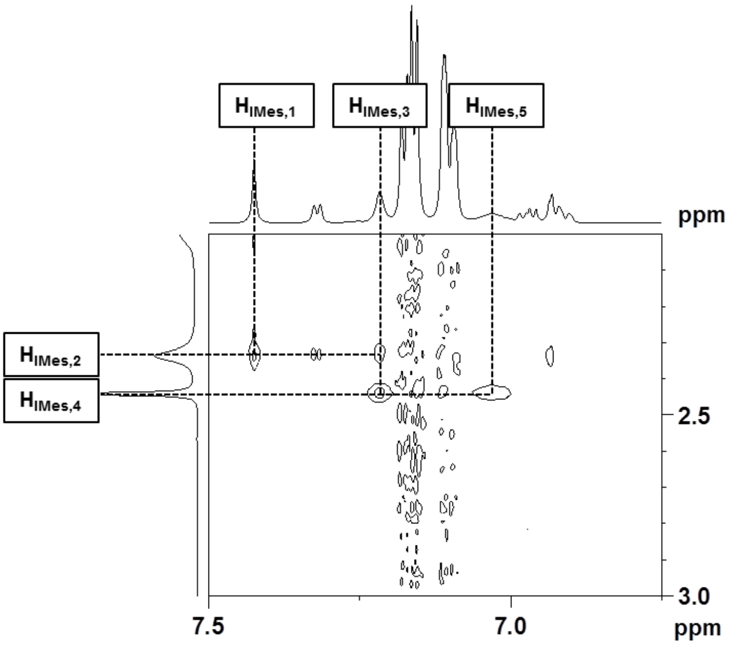

Figure 20: Annotated 2D ^1H-^1H NOESY experiment on a sample of **1-cod-3AmPy** in *d4*-methanol at 243 K, showing cross peaks between the methyl groups of the IMes ligand ($H_{IMes,2}$ and $H_{IMes,4}$) and the aromatic ($H_{IMes,3}$ and $H_{IMes,5}$)and carbene ($H_{IMes,1}$) environments of this ligand. Also visible are through space interactions between $H_{IMes,2}$ and the bound substrate environments $H_{L,2}$ and $H_{L,6}$.

This 2D NOESY spectrum also reveals that the two phenyl protons, $H_{IMes,3}$ and $H_{IMes,5}$, are inequivalent ,with shifts of δ 7.03 and 7.22, through their interactions with $H_{IMes,4}$. The ^1H environment with a shift of δ 7.22 is also close to the methyl group at δ 2.34 as shown in Figure 20. This allows assignment of $H_{IMes,2}$, $H_{IMes,3}$, $H_{IMes,5}$ and $H_{IMes,6}$.

The two *ortho* methyl groups are broad, whereas the *para* methyl and imidazole olefinic protons are sharp; the exchange between the two *ortho* sites is rapid at 243 K. This shows that there is a plane of symmetry is perpendicular to a plane through the *para* methyl group and the imidazole ring.

The bound **3AmPy** peaks are significantly shifted from those of the free substrate in solution. The aromatic nitrogen has shifted from δ 295.7 in the free substrate to 241.2 once coordinated to iridium. This indicates an increase in shielding upon coordination, this is expected due to the σ-donation of the cyclooctadiene ligand *trans* to the substrate. This nitrogen couples to a ^1H at δ 7.32 and more weakly to a ^1H at δ

6.92. These are the protons $H_{L,2}$ and $H_{L,6}$ but it is not immediately clear which resonance corresponds to which environment.

Both COSY and 2D NOESY suggest that the remaining ^{1}H environments are a doublet of doublets at δ 6.97 and part of the multiplet at δ 6.92.

Applying ^{1}H-^{13}C HMQC identifies a coupling between the ^{1}H peaks δ 6.97 and 6.92 and $C_{L,3}$ – this identifies $H_{L,2}$ as being part of the multiplet at δ 6.92 as it couples to both the aromatic nitrogen and $C_{L,3}$. $H_{L,6}$ is therefore the doublet at δ 7.32. The 5.3 Hz splitting of $H_{L,6}$ can be seen in the doublet of doublets along with a coupling of 8.2 Hz. This suggests that the signal at δ 6.98 is due to $H_{L,5}$ as these closely match the couplings seen in the free substrate. The expected coupling between $H_{L,6}$ and $H_{L,4}$ would be closer to 1 Hz.

The protons corresponding to the cyclooctadiene ligand are much harder to characterise due to their significant broadness. Peaks can be identified at δ 3.59, 3.34, 1.89 and 1.64 – the first two corresponding to the alkene protons and the latter to the alkane protons. The alkene environment at δ 3.56 is close in space to the proton $H_{IMes,2}$. The alkene environment at δ 3.34 is close in space to the substrate protons $H_{L,2}$ and $H_{L,6}$. The carbon resonances corresponding to the cyclooctadiene ligand could not be identified through ^{1}H-^{13}C HMQC due to the rapid exchange.

It can therefore be said that:

- **1-cod-3AmPy** readily forms through the displacement of chloride from **1-cod-Cl**
- Bound **3AmPy** can be identified using nOe. Observed nOe between the IMes ligand and the bound substrate protons adjacent to the aromatic nitrogen suggests that **3AmPy** coordinates to the iridium center through the aromatic nitrogen. This is supported by the significant shift in the aromatic nitrogen resonance upon coordination.
- **1-cod-3AmPy** undergoes rapid exchange causing significant signal broadening

I now go on to consider the effect of addition of H_2 to the mixture.

2.3 $[Ir(IMes)(H)_2(3\text{-aminopyridine})_3]^+$ - active catalyst

Addition of hydrogen to the sample causes a reaction to occur. The solution changes during this process from yellow to colourless as the iridium is oxidised from oxidation state Ir^I in **1-cod-L** to Ir^{III} in the product $[Ir(IMes)(H)_2($**L**$)_3]^+$ (**1-L**). The 1,5-cyclooctadiene ligand is hydrogenated to form cyclooctane during this process which accounts for a new peak in the ^1H spectrum at δ 1.57. A further 2 substrate molecules bind to the iridium to give complex **1-L** shown inFigure 21.[12] The ^1H NMR spectrum of the complex $[Ir(IMes)(H)_2($**3AmPy**$)_3]^+$ (**1-3AmPy)** is shown in Figure 22.

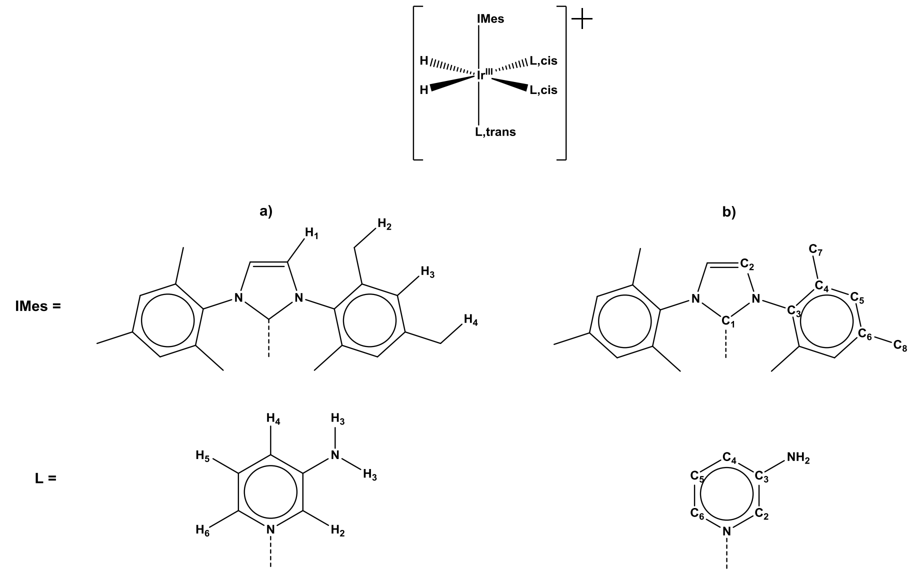

Figure 21: Schematic of **1-3AmPy** showing a) ^1H notation and b) ^{13}C notation. The two bound substrate environments are distinguished as *cis* and *trans* to the IMes ligand as shown.

The two hydride protons appear as a singlet with a chemical shift of δ -23.00 confirming that in this complex they are chemically equivalent. A peak corresponding to the partially deuterated complex $[Ir(IMes)(H)(D)($**3AmPy**$)_3]^+$ can be seen at δ -22.94 which grows in intensity over time. Partially deuterated hydrogen (HD) can also be seen as a 1:1:1 triplet at δ 4.56 with $^1J_{HD} = 42.7$ Hz.[55] The inclusion of deuterium from the d_4-methanol solvent into the catalyst species is described by Lloyd *et al.*[36]

Selectively exciting the hydride resonance at δ -22.94 shows an nOe to a peak at δ 2.08 – this through space interaction locates a methyl environment of the mesityl group in **1-3AmPy**.

^1H-^{15}N HMQC reveals a coupling between a proton at δ 7.06 and a nitrogen nucleus at δ 194.4. This is part of the imidazolium N-heterocyclic carbene ligand. In a 2D NOESY experiment, a cross peak between the ^1H environment at δ 2.08 and δ 7.06 can be seen – this confirms that they are both on the IMes ligand and the relative integral suggests that the environment at δ 2.08 corresponds to the $H_{IMes,2}$ as it integrates to 12 when the peak at δ 7.06 which corresponds to $H_{IMes,1}$ is calibrated to integrate to 2. The through space interaction supports this as the protons in the $H_{IMes,2}$ environment are much closer to $H_{IMes,1}$ than $H_{IMes,4}$ is.

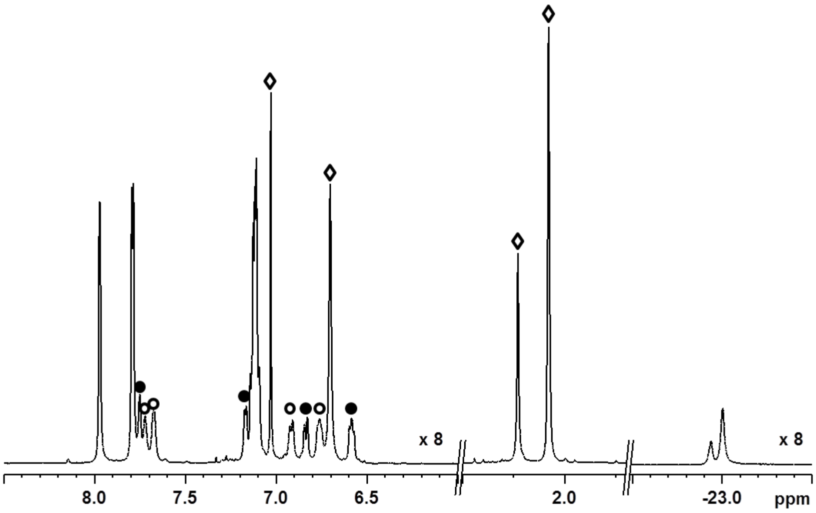

Figure 22: ^1H NMR spectrum of **1-3AmPy** in d_4-methanol. ◊ indicates resonances corresponding to the IMes ligand. ● indicates resonances corresponding to the ligand **3AmPy** *trans* to the IMes ligand. ○ indicates resonances corresponding to the ligand **3AmPy** *cis* to the IMes ligand. x 8 indicates the vertical expansion of the left and right hand sections of the spectrum relative to the central section.

A COSY spectrum shows coupling from $H_{IMes,2}$ to peaks at δ 6.70 and 2.23. A through space interaction between $H_{IMes,2}$ and δ 6.70 can be seen as well as an interaction between δ 6.70 and δ 2.23. This is the mesityl ring – the aromatic proton $H_{IMes,3}$ having a chemical shift of δ 6.70 and the remaining methyl group, $H_{IMes,4}$ having a chemical shift of δ 2.23. The relative intensities of these peaks agree with their identities. A summary of these interactions is given in Figure 23.

The chemical shifts of the carbon environments with protons attached can be readily identified through a ^{1}H-^{13}C HMQC measurement set up to detect only large couplings. To assign the carbon environments that are not directly attached to a proton –$C_{IMes,1}$, $C_{IMes,3}$, $C_{IMes,4}$ and $C_{IMes,6}$ – longer range experiments are necessary. Through coupling with $H_{IMes,1}$, the carbene carbon, $C_{IMes,1}$, resonance can be assigned as δ 153.8. Within the phenyl ring the two methyl groups and the aromatic proton can be used to identify the remaining carbons. $H_{IMes,1}$, $H_{IMes,3}$ and $H_{IMes,2}$ all show long range coupling $C_{IMes,3}$ and each methyl group shows mid-range coupling to the corresponding aromatic carbon.

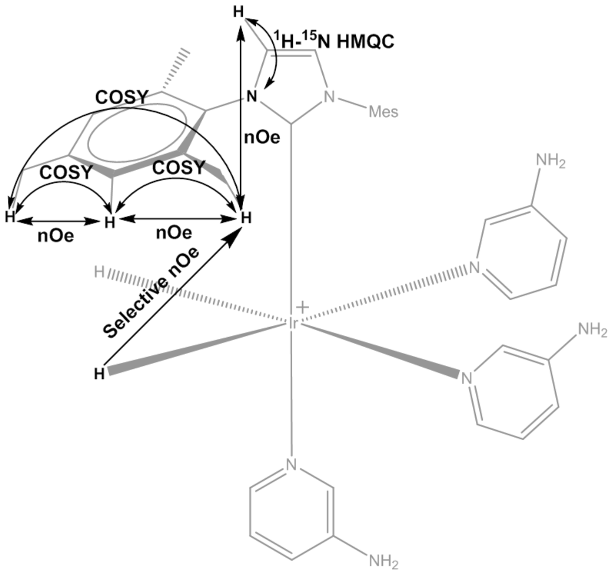

Figure 23: Illustration of through space and through bond interactions seen for the IMes ligand of **1-3AmPy**

After discounting the free **3AmPy** signals, it is possible to identify two remaining **3AmPy** species through a COSY spectrum. These correspond to the two different bound environments – *cis* to the IMes ligand and *trans* to the IMes ligand. The chemical shifts of the protons in these two different environments are given below in Table 1.

Table 1 : ^1H chemical shifts of bound **3AmPy** in d_4-methanol at 298 K

	cis environment	*trans* environment
$H_{L,2}$	7.72	7.76
$H_{L,4}$	6.93	6.84
$H_{L,5}$	6.77	6.59
$H_{L,6}$	7.68	7.17

Assignments within each environment were made using COSY data. The peak at δ 7.76 only couples to the peak δ 6.84, whereas the peak at δ 7.17 couples to both δ 6.84 and 6.59. This points towards δ 7.17 corresponding to $H_{L,trans,6}$, δ 6.84 to $H_{L,trans,4}$ and δ 6.59 to $H_{L,trans,5}$. This gives δ 7.76 being the isolated proton, $H_{L,trans,2}$ as is evident from its lack of coupling to $H_{L,trans,5}$.

The coupling seen between the peaks at δ 7.68, 6.93 and 6.77 also indicates that they arise from a chain of protons in positions $H_{L,cis,6}$, $H_{L,cis,4}$ and $H_{L,cis,5}$ respectively. The proton in position $H_{L,cis,2}$ is difficult to locate through coupling as it relies on the weaker, longer range coupling with $H_{L,cis,4}$; however, it can be identified as it exchanges with the proton in position $H_{L,2}$ of the free **3AmPy**.

A nOe spectrum collected by selectively exciting the hydrides confirms that both the *cis* and *trans* environments are part of the same complex. The two environments could not be distinguished through integration of their resonances due to significant overlap between the two environments, the free species and the IMes ligand. The two environments were distinguished as the environment *cis* to the NHC ligand is closer in space to $H_{IMes,2}$ than the substrate environment *trans* to the NHC. Through space nOe interactions between the $H_{IMes,2}$ environment and the *cis* substrate environment were observed which confirmed the identity of the *cis* substrate (Figure 24).

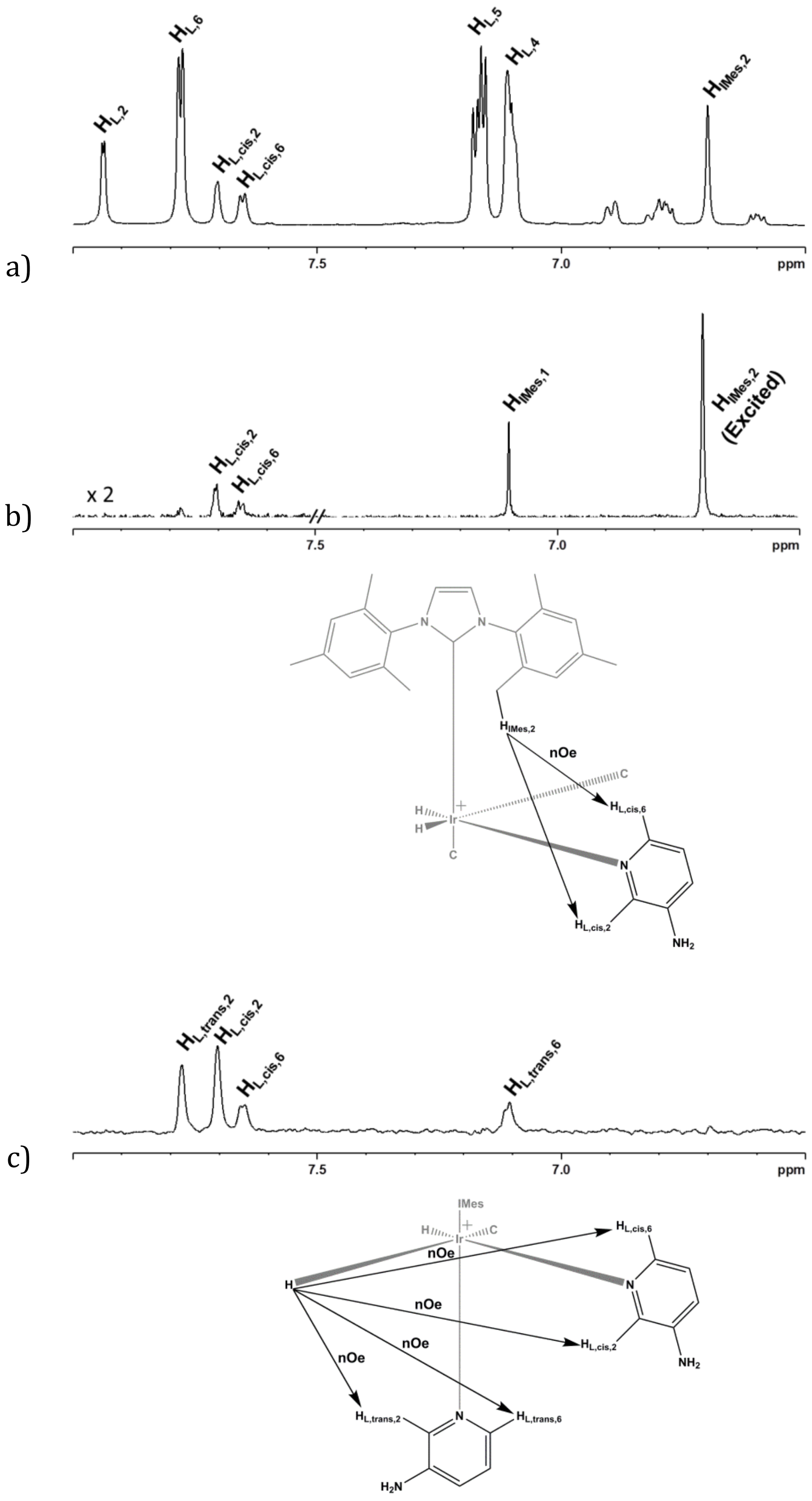

Figure 24: a) ^{1}H NMR spectrum of **1-3AmPy** at 243 K b) nOe spectrum collected after selective excitation of $H_{IMes,2}$, showing nOe to the environments of **3AmPy** bound *cis* to the IMes ligand c) nOe spectrum collected after selective excitation of $H_{Hydride}$ showing nOe to **3AmPy** bound *cis* and *trans* to the IMes ligand.

The nitrogen environments of the bound substrates could not be seen through HMQC at room temperature. After cooling to 243 K the aromatic nitrogen environments of the bound substrates could be identified through coupling to the protons $H_{L,2}$ and $H_{L,6}$. The nitrogen of **3AmPy** bound *cis* to the IMes ligand coupled to the hydrides whereas the substrate bound *trans* to the IMes ligand did not show any coupling to the hydrides. The amine environments could not be identified, even at this reduced temperature, likely due to deuteration of the amine protons. At this reduced temperature many of the peaks which were difficult to identify or broad at room temperature were much clearer, allowing confirmation of their identity.

Exchange with the free **3AmPy** can only be seen for the protons in the environments *cis* to the NHC ligand; this matches previous findings for this type of complex that the substrate *cis* to the IMes ligand readily exchanges with the substrate that is unbound in solution, whereas the substrate *trans* to the carbene ligand exchanges much more slowly.[12]

Based on this data, the identity of **1-3AmPy** is confirmed as $[Ir(IMes)(H)_2(\textbf{3AmPy})_3]^+$. Full data is presented in chapter 7. The bonding of **3AmPy** through the pyridyl nitrogen and not the amino nitrogen is supported through the presence of nOe to the hydride species, the IMes ligand, and between the bound **3AmPy** species $H_{L,2}$ and $H_{L,6}$ environments – and also through the absence of these interactions for the $H_{L,4}$ and $H_{L,5}$ environments.

2.4 SABRE polarisation of 3-aminopyridine

The purpose of this study was to test the SABRE effect of **1-L** when **L** was 3-aminopyridine. **3AmPy** has been shown to react with **1-cod-Cl**, a typical SABRE precatalyst, and hydrogen to form **1-3AmPy**. After activation, bound **3AmPy** exchanges with free **3AmPy** and its hydride species exchange with dihydrogen in solution.[12] An NMR sample of **3AmPy** and **1-cod-Cl** in a ratio of 5:1 was activated and then put under an atmosphere of 3 bar pH_2.

In Figure 25 a thermal spectrum, collected as a single scan after the sample had been allowed to reach equilibrium in the high magnetic field of the spectrometer, is compared to a hyperpolarised spectrum. The hyperpolarised spectrum was collected after a 10 second polarisation period at low field (65 G) and rapid insertion of the sample into the spectrometer. The hyperpolarised signal is much larger than the thermal signal – this demonstrates the SABRE effect on the substrate **3AmPy**. Comparison of the relative integrals gives a measure of the polarisation seen as given in Table 2.

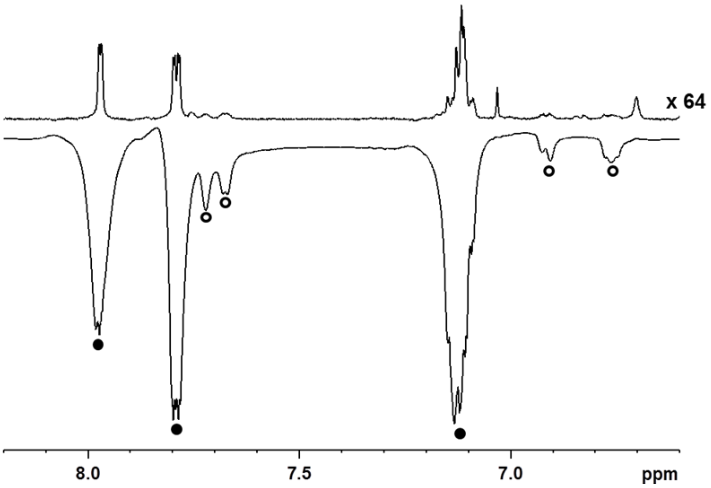

Figure 25 : Comparison of a) thermal and b) hyperpolarised spectra of 25 mM **3AmPy** with 20 % catalyst loading of **1-cod-Cl** and 3 bar *p*H_2 in *d_4*-methanol. ● indicates the resonances of free **3AmPy** and ○ indicates the resonances of **3AmPy** bound *cis* to the IMes ligand. x 64 indicates a vertical expansion of 64 fold for the thermal spectrum relative to the hyperpolarised spectrum.

Table 2 : Comparison of the signal received for thermal and hyperpolarised spectra of **3AmPy**

^{1}H environment	Thermal Integral	Hyperpolarised Integral	Enhancement	Polarisation / %
H_2	1.0	-694.9	964.9	3.0
H_6	1.1	-692.2	629.3	2.0
H_4 + H_5	2.6	-1236.2	475.5	1.5

The protons in environments $H_{L,2}$ and $H_{L,6}$ show a greater polarisation than those in $H_{L,4}$ and $H_{L,5}$ as these environments are closer to the site that binds to the iridium center. $H_{L,2}$ and $H_{L,6}$ therefore have a greater coupling to the hydrides of **1-3AmPy** when **3AmPy** is bound and this leads to a more efficient polarisation transfer to these environments and therefore a greater polarisation. Polarisation of $H_{L,4}$ and $H_{L,5}$ relies on a smaller, longer ranged coupling or on secondary polarisation transfer from the other substrate protons and as a result polarisation transfer to these protons is less efficient.

An alternative method for measuring the enhancement from SABRE is to compare the signal-to-noise (SNR) ratio of the thermal spectrum to that of the enhanced spectrum. For **3AmPy**, a single SABRE enhanced scan has a SNR that has been improved by over 200 fold compared to a single thermal scan. To achieve this improvement through signal averaging methods 40,000 scans would need to be collected. With a delay of 10 seconds between each scan to ensure complete relaxation this corresponds to an experiment time of 4.6 days. In comparison, the hyperpolarised spectrum was collected in under a second.

Some of the bound **3AmPy** peaks of **1-3AmPy** can also be seen in the hyperpolarised signal despite their lower population and shorter lifetime. These bound peaks are all polarised to approximately 1 %. Only the peaks corresponding to the **3AmPy** ligands that are *cis* to the IMes ligand are polarised – this is due to symmetry requirements of the polarisation transfer mechanism[56] and has been reported previously for SABRE.[12, 32, 39] Polarisation does not get transferred into the *trans* environment through exchange with the free substrate due to the poor exchange rates described previously.

In this example, the sample was polarised at 65 G – polarisation at this field gives in-phase emission peaks in the NMR spectrum for **3AmPy**. Using the flow system previously described, the effect of the polarisation transfer field on the observed polarisation of **3AmPy** was investigated. The maximum enhancement was seen at 60 G (Figure 26), although this polarisation was almost an order of magnitude lower than that seen when the sample was manually polarised. This reduction in polarisation is typical when the flow system is used.

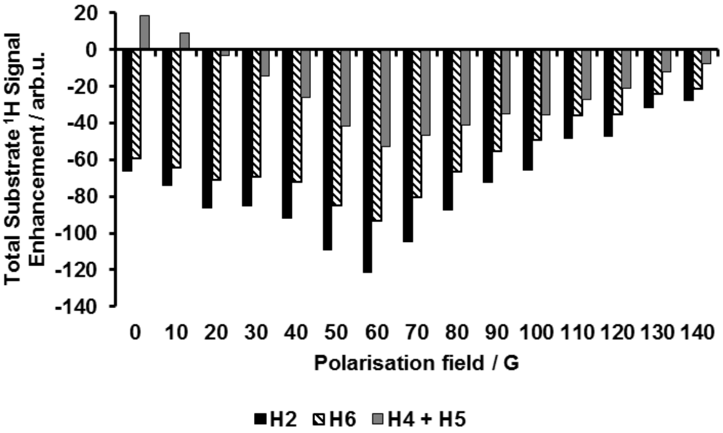

Figure 26: Field plot showing the effect of polarisation transfer field on the SABRE polarisation of 25 mM **3AmPy** by 5 mM **1-cod-Cl** in *d₄*-methanol using the flow method. $H_{L,4}$ and $H_{L,5}$ could not be individually resolved and so their combined enhancement is shown.

2.5 Conclusions

A new substrate, 3-aminopyridine, was successfully polarised using SABRE. Under non-optimised conditions, a 3 % polarisation was achieved on the proton in the H_2 environment of this substrate. Further optimisation, as carried out on **Py** by Lloyd *et al.*,[36] could lead to an increased level of polarisation.

The nOe data collected during this study supports the conclusion that **3AmPy** coordinates to iridium in **1-3AmPy** through its aromatic nitrogen and not through the terminal amine nitrogen. Further investigation in aprotic solvents, such as DCM, could be undertaken to confirm this as they would allow further information about the terminal amine to be obtained. However, care would be needed to ensure that changing the solvent did not change the coordination system. An alternative route would be to examine the complex in the solid state using x-ray crystallography.

3. Applying SABRE to organometallics and metal complexes

3.1 Introduction

3.1.1 Hyperpolarisation of metal catalysts

One of the key successes of hydrogenative PHIP techniques has been the study of reaction mechanisms involving a metal catalyst. Giernoth *et al*. used PASADENA enhancement to identify an intermediate in the hydrogenation of dehydroamino acids by a rhodium complex.[15] Through transfer of the polarisation to labelled carbon atoms they were able to determine the structure of an intermediate containing an agostic C-H interaction as shown in Figure 27. PHIP enhancement of the carbon signal relating to the reactant dehydroamino acid was also observed. This suggests that the process is reversible. An intermediate in the hydrogenation of diphenylacetylene on a platinum catalyst was also identified using *p*H_2.[16] This species did not show an agostic C-H interaction, but instead the hydrogenated alkene species bound to the platinum metal center was identified as shown in Figure 27.

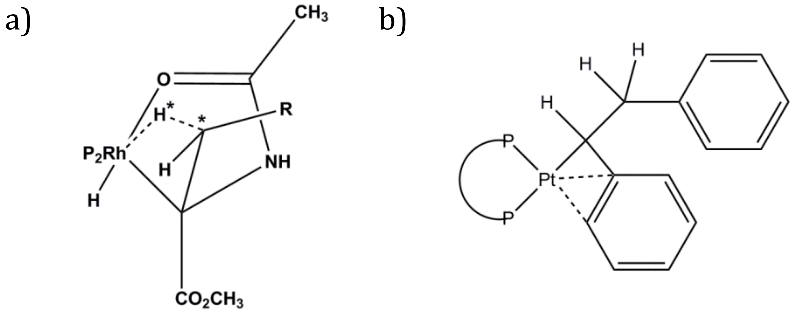

Figure 27: a) Schematic of agostic C-H interaction described by Giernoth *et al*.[15] Key nuclei identified by PHIP are indicated with a *. b) Coordinated hydrogenated alkene intermediate identified by Noutain *et al*.[16]

3.1.2 SABRE as a mechanistic probe

As a non-hydrogenative polarisation technique, SABRE has the potential to be used to study a greater variety of reactions than PHIP. One approach that might be used to study a reaction mechanism by SABRE would be to polarise a simple organic reactant and use this species as a hyperpolarised probe. Another approach would be to directly polarise the catalytic species itself. Whilst SABRE has been shown to be effective at polarising small organic molecules,[8-10, 12, 14, 39, 40, 42] it has not yet been applied to larger molecules or indeed molecules with a metal center (excluding the polarisation transfer catalyst itself). Polarisation of these more complex molecules would be beneficial as it would allow for a more in depth study of the changes that take place in a reaction mechanism around the metal center; potentially including the detection of low population intermediates. More complex molecules can have other interesting, non-catalytic, properties, such as photo-activity,[57, 58] that could also be investigated using SABRE hyperpolarisation. Transfer of SABRE hyperpolarisation to more complex systems will almost certainly feature as a future development of this technique.

In this chapter, I seek to demonstrate the SABRE polarisation of more complex targets. I focus on stable organometallic systems and metal complexes. Limiting the reactivity of the substrate will be a key requirement of this study as it will ensure that any polarisation seen comes from SABRE and not from the hydrogenation of the target substrate and subsequent polarisation through a PASADENA[26] type mechanism. To achieve this goal, the selected substrates possess ligands that are either bidentate or η^5 coordination – this provides them with kinetic stability. To allow SABRE activity, each substrate will then contain a second site that has been shown to undergo SABRE polarisation in a related system that was not coordinated to a metal. To assess the impact of the secondary metal center on SABRE polarisation, the target substrates will be compared to a simple organic analogue of them.

3.2 SABRE polarisation of ferrocenyl systems

3.2.1. Ferrocenyl systems

One class of organometallic complex that has found wide interest is that of ferrocene. Ferrocenes are of interest as the η^5 binding mode is stable[59] and ferrocenes are often used as catalysts themselves[60] or incorporated into catalysts as non-labile ligands.[61-63] The incorporation of a functionalised ferrocene species into catalysts could provide a route to utilise SABRE polarisation to investigate a wide variety of catalytic mechanisms through the direct polarisation of the catalyst species. The increased signal intensity resulting from SABRE polarisation would reveal reaction intermediates that are present only at low concentrations. Other metallocenes have also found significant use, particularly in polymerisation.[64, 65] Ferrocenes have also been shown to possess antitumour activity.[66]

It has been shown that both cyanide[39, 40] and pyridyl[8] functionalities can be employed for SABRE. These would need adding to a cyclopentadienyl ring in order to apply SABRE to ferrocene. It has been shown that benzylcyanide (**PhMeCN**) is polarised much more efficiently than cyanobenzene, therefore a CH_2 spacer group will be incorporated into the cyanide species used in this study.

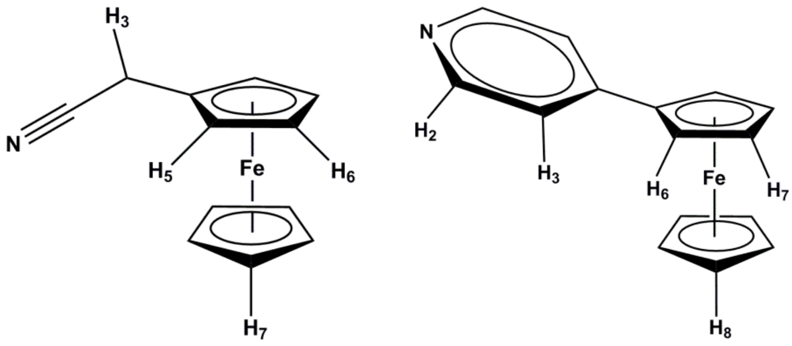

FcMeCN **FcPy**

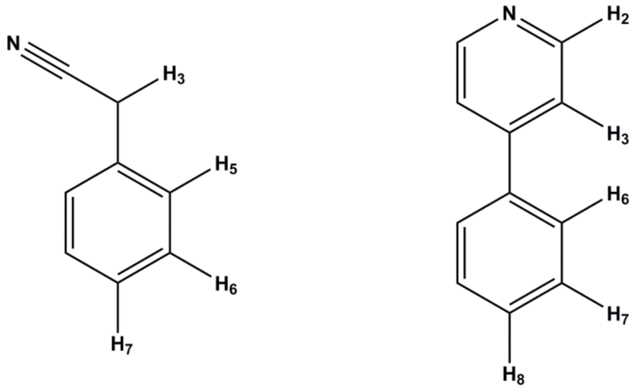

PhMeCN **PhPy**

Figure 28: Annotated schematic of substrates **FcMeCN**, **FcPy**, **PhMeCN** and **PhPy** with their ^1H environments labelled

I show in Figure 28 the two target substrates used in this study. Ferroceneacetonitrile (**FcMeCN**) was commercially available, (4-pyridyl)ferrocene (**FcPy**) was synthesised as part of this study. The details of the synthesis of **FcPy** can be found in Section 7.3.4. I also show the organic analogues of these systems that are used for comparative purposes in this study – benzylcyanide (**PhMeCN**) and 4-phenylpyridine (**PhPy**). **PhMeCN** has been studied previously,[40] **PhPy** will be tested as a control substrate in this study.

3.2.2 Ferroceneacetonitrile

FcMeCN was the first organometallic substrate selected to be investigated for SABRE polarisation. This commercially available ferrocene derivative should polarise in a similar manner to **PhMeCN**. The iron centre is in the iron(II) oxidation state and therefore diamagnetic.[67] This is important as paramagnetic ions will cause significant line broadening in the NMR spectrum making the results difficult to reliably interpret.

A methanol solution of **FcMeCN** was prepared and examined by ^{1}H NMR. The resulting NMR spectrum contained a singlet at δ 4.24 for the 5 equivalent protons of the η^5-C_5H_5 ring (H_7). The two inequivalent pairs of protons on the substituted ring appeared at δ 4.28 and 4.20 (H_5 and H_6 respectively). These three signals appear as a collection of overlapping, broad singlet peaks. In addition, a broad singlet peak of area 2 appears at δ 3.57 due to the equivalent CH_2 protons of the CH_2CN functionality (H_3).

FcMeCN was tested for stability in the presence of hydrogen; when using pH$_2$ no polarised signals were seen indicating that PHIP polarisation had not occurred.

A sample containing **FcMeCN** and **1-cod-Cl** was prepared and placed under hydrogen. A broad hydride signal was observed at δ -21.5 indicating a reaction had occurred, although the broad substrate peaks precluded full characterisation. When the resulting SABRE spectrum was obtained, weak hyperpolarisation was evident as shown in Figure 29. The most notable feature was a 1.5 fold enhancement in the CH_2 signal at δ 3.57. At δ 4.24, the overlapping signals of H_5, H_6 and H_7 also show SABRE polarisation, however the observed effect is complicated. The unfunctionalised C_5H_5 ring is not enhanced and appears as a positive signal, it is flanked by two emission peaks due to the inequivalent protons H_5 and H_6 of the C_5H_4R ring. These broad peaks overlap. As a result, the observed signal amplitude for these peaks is reduced.

The SABRE enhancement seen is poor for this substrate. The effect of substrate:catalyst ratio was tested with a view to increasing the level of polarisation but this was unsuccessful. Nonetheless, the premise that SABRE can be used to polarise a metal complex has been demonstrated.

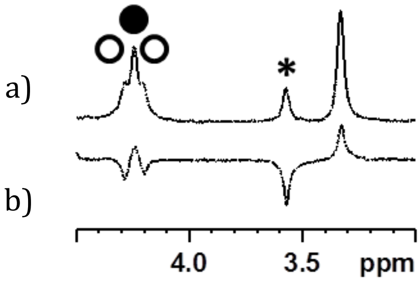

Figure 29: ^{1}H NMR spectra of 25 mM **FcMeCN** and 5 mM **1-cod-Cl** in d_4-methanol. a) thermal spectrum b) hyperpolarised spectrum collected after polarisation for 10 s at 65 G under 3 bar pH$_2$. A 1.5 fold enhancement of the CH$_2$ protons is seen. * indicates signal corresponding to the CH$_2$ protons, ● corresponds to the unfunctionalised C$_5$H$_5$ ring and ○ corresponds to the functionalised C$_5$H$_4$R ring.

The control substrate **PhMeCN** is reported as showing an 18 fold enhancement of the CH$_2$ protons and a 2 fold enhancement of the aromatic protons.[40] Therefore, while polarisation of organometallic complexes by adapting proven substrates is possible, obtaining levels of polarisation that equal those seen for simple organic substrates is not a simple process.

3.2.3 (4-pyridyl)ferrocene

Organic substrates based on pyridine have been found to polarise more strongly than those based on acetonitrile.[12, 39] To improve upon the level of polarisation seen for **FcMeCN**, a pyridine functionalised ferrocene derivative, (4-pyridyl)ferrocene (**FcPy**), was synthesised in low yield via a Suzuki coupling reaction.[68, 69] In d_4-methanol, the unfunctionalised C$_5$H$_5$ ring gives a singlet at δ 4.06, whilst the functionalised ring gives two singlets at δ 4.95 and 4.55. The pyridyl group gives two peaks at δ 8.42 and 7.55 as shown in Figure 30.

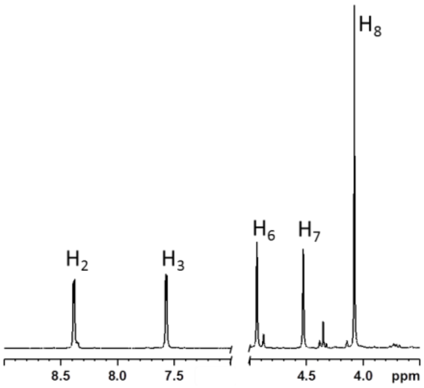

Figure 30: ^1H NMR spectrum of **FcPy** collected in *d4*-methanol at 298 K

Activation of **1-cod-Cl** by **FcPy** and hydrogen yielded a hydride at δ -22.52. However, in this sample, the peak corresponding to H_6 was obscured by the residual solvent peak at δ 4.60. SABRE polarisation of **FcPy** was successful – H_2 showed a 4 fold polarisation and H_3 showed a 6 fold polarisation as shown in Figure 31. As expected, this polarisation is stronger than that seen for **FcMeCN**. H_7 was obscured by the large hydrogen signal in the hyperpolarised spectrum, and H_8 showed no polarisation. As such, no assessment of polarisation transfer into the cyclopentadienyl rings could be made. A number of additional polarised peaks in the aromatic region can also be seen – these are likely bound **FcPy** environments.

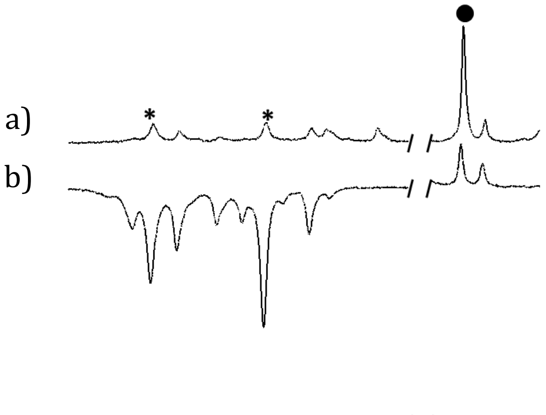

Figure 31: ^1H NMR spectra of 25 mM **FcPy** and 5 mM **1-cod-Cl** in *d4*-methanol. a) thermal spectrum b) hyperpolarised spectrum collected after polarisation for 10 s under 3 bar *p*H_2 at 65 G. * indicates signals corresponding to H_2 and H_3. A 4 fold

polarisation of H_2 and a 6 fold polarisation of H_3 can be seen. The unfunctionalised cyclopentadienyl (●) signal does not appear to be polarised.

Under the same conditions, the H_2 protons of **PhPy** polarise over 1000 fold as shown in Figure 32. It can be seen that the polarisation of the organometallic compound **FcPy** is significantly lower than its simpler organic analogue. This reduction in polarisation efficiency is likely due to the increased steric bulk of **FcPy** compared to **PhPy**. Extension of the linker region between the iridium binding site and the rest of the molecule may improve the polarisation transferred to the substrate;[69, 70] however it would also reduce the efficiency of polarisation transfer to the region around the metal center due to a reduced scalar coupling between the source of polarisation and the target protons.

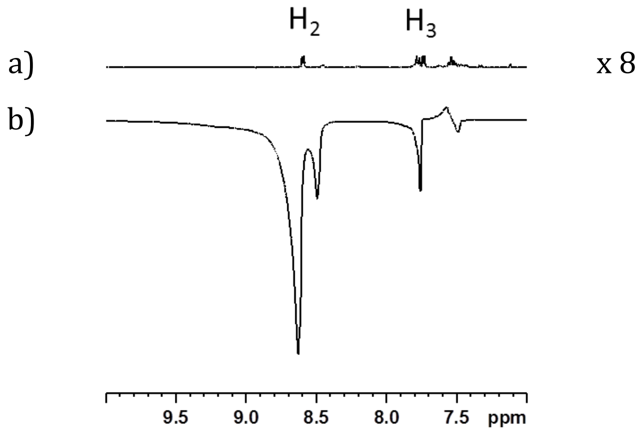

Figure 32: ^1H NMR spectra of 25 mM **PhPy** and 5 mM **1-cod-Cl** in d_4-methanol. a) thermal spectrum b) hyperpolarised spectrum collected after polarisation for 10 s under 3 bar pH_2 at 65 G. x 8 indicates an 8 fold vertical expansion of the thermal spectrum relative to the hyperpolarised spectrum

3.3 SABRE polarisation of tris(bipyridyl)ruthenium(II)

3.3.1 Tris(bipyridyl)ruthenium(II) systems

Another system that has been studied extensively is tris(bipyridyl)ruthenium(II). Of particular interest for its photochemical properties,[57] this complex has also found use as a catalyst.[71] The related complex $[Ru(phen)_2(dppz)]^{2+}$ (phen = phenanthroline, dppz = dipyrido phenazine) has been shown to bind to DNA,[72] hyperpolarisation of this type of species could be used as a probe into the binding mode or into the local structure of the binding site. The related complex [tris(bipyrazyl)ruthenium(II)]$^{2+}$ (**Ru(bpz)$_3$**), shown in Figure 33, incorporates a number of pyrazine motifs that could be used for the transfer of SABRE polarisation and has itself been used as a photocatalyst.[73-75]

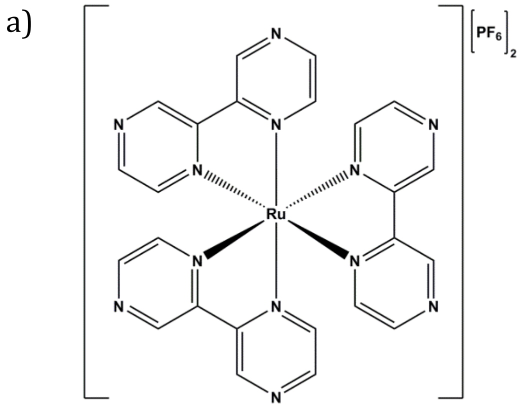

Ru(bpz)$_3$

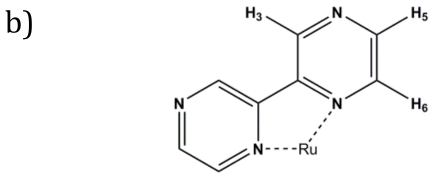

Figure 33: a) Schematic of **Ru(bpz)$_3$**.[PF$_6$]$_2$ b) annotated ^{1}H environments of **Ru(bpz)$_3$**

3.3.2 Tris(bipyrazyl)ruthenium(II).di(hexafluorophosphate)

The substrate **Ru(bpz)$_3$** has several barriers that must be overcome prior to SABRE polarisation. **Ru(bpz)$_3$**.[PF$_6$]$_2$ is poorly soluble in methanol, this prevents it from fully activating **1-cod-Cl** to form [Ir(IMes)(H)$_2$(**Ru(bpz)$_3$**)$_3$]$^+$ (**1-Ru(bpz)$_3$**) in the presence of hydrogen. Acetonitrile is often used as a solvent for reactions using **Ru(bpz)$_3$**.[PF$_6$]$_2$ but this would be unsuitable for SABRE polarisation as the acetonitrile will bind to the iridium and interfere with the exchange processes needed for polarisation, particularly if used at solvent concentrations. Whilst a lower concentration of **1-cod-Cl** could be used, this has been shown to limit SABRE polarisation at concentrations below 5 mM.[36] This can be solved by activating the catalyst with a substrate such as pyridine to form **1-Py** prior to the addition of the target substrate,[38] or by using a weakly binding "co-substrate".[13]

Secondly, activation of **1-cod-Cl** in the presence of **Ru(bpz)$_3$** leads to significant degredation of the sample and significant broadening of the NMR peaks observed. This indicates that a paramagnetic species is being formed. The degredation of the sample does not occur in the absence of hydrogen, and is not seen when the activated **1-Py** is in solution with **Ru(bpz)$_3$** and hydrogen. This suggests that the degredation is due to decomposition of an intermediate in the activation process – possibly being trapped as Ir^{II}. The high oxidation and reduction potentials[76, 77] of photo-excited **Ru(bpz)$_3$**.$[PF_6]_2$ are likely the reason that the paramagnetic species is seen in the presence of this substrate but not in the presence of organic substrates.

To solve these problems, the iridium catalyst was activated with pyridine (**Py**) prior to addition of ruthenium. After activation, the catalyst was dried under vacuum to remove as much **Py** as possible. **Ru(bpz)$_3$**.$[PF_6]_2$ was dissolved in *d$_4$*-methanol and added to the activated catalyst. While this solved the degredation problem, no polarisation of the ruthenium species was seen – only polarisation of **Py** was observed.

Acetonitrile (**MeCN**) was added to displace some of the **Py** species bound to the catalyst.[39] The solvent was again removed under vacuum – along with any free **Py** and **MeCN**. The remaining solid, made up of **Ru(bpz)$_3$**.$[PF_6]_2$ and $[Ir(IMes)(H)_2(\mathbf{Py})_{3-x}(\mathbf{MeCN})_x]Cl$, was dissolved in *d$_4$*-methanol and polarised under typical conditions. The resulting NMR spectrum is shown in Figure 34.

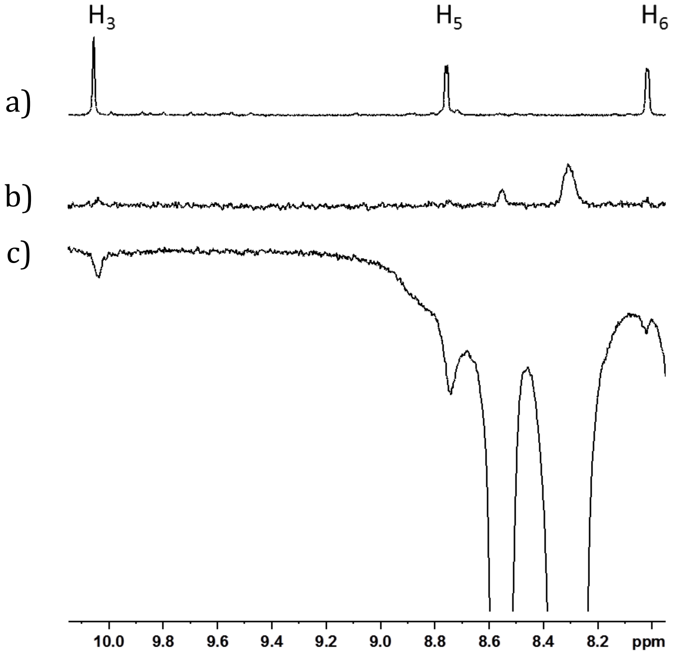

Figure 34: a) 256 scan ^1H spectrum of **Ru(bpz)$_3$**.[PF$_6$]$_2$ in *d$_4$*-methanol b) thermal ^1H spectrum of **Ru(bpz)$_3$**.[PF$_6$]$_2$ and 5 mM [Ir(IMes)(H)$_2$(**Py**)$_{3-x}$(**MeCN**)$_x$]Cl in *d$_4$*-methanol c) hyperpolarised ^1H spectrum of **Ru(bpz)$_3$**.[PF$_6$]$_2$and 5 mM [Ir(IMes)(H)$_2$(**Py**)$_{3-x}$(**MeCN**)$_x$]Cl in *d$_4$*-methanol after 10 s polarisation at 65 G under 3 bar *p*H$_2$

Polarisation of **Ru(bpz)$_3$** can be seen in the above case. Unfortunately only the H$_3$ environment can be seen distinctly due to the large polarised **Py** signals; however this environment is enhanced 10 fold. The remaining environments can be seen overlapping the **Py** signal, and seem to also be polarised. Use of an alternative co-substrate[13] in place of **Py** may resolve this problem and could potentially allow for a less complex system, with fewer competing exchange pathways, to be developed. Attempts to use **MeCN** as the activating ligand failed as degradation of the sample still occurred in the presence of **Ru(bpz)$_3$**.[PF$_6$]$_2$ and hydrogen. These experiments were repeated whilst shielding the sample from light, however no difference was observed. Optimisation of the catalyst, co-substrate and polarisation conditions could improve the level of polarisation; however, this was not investigated due to the time constraints of this project.

3.4 Conclusions

SABRE polarisation of ferrocene and tris(bipyridyl)ruthenium(II) type substrates has been achieved. This demonstrates the potential to apply SABRE hyperpolarisation to a broader range of substrates including both organometallic and metal complex type substrates.

The polarisation levels of these substrates were not optimised, and remained significantly lower than those observed for the free organic analogues described under the same conditions.

In the case of ferroceneacetonitrile, this is likely to be due to the increased steric bulk of the complexed ligand in comparison to the free ligand analogue which prevents efficient binding to the iridium center. The polarisation of ferroceneacetonitrile was approximately 10 % of that previously reported for benzyl cyanide.[40]

A 6 fold polarisation of (4-pyridyl)ferrocene was achieved – this is a promising result that is worth optimising further. However, this is significantly lower than the organic analogue, 4-phenylpyridine, selected for comparison in this study. The organic analogue was shown to undergo a 1000 fold enhancement by SABRE under the same polarisation conditions. This highlights the difficulty of applying SABRE to larger, more complex substrates. Whilst the polarisation of (4-pyridyl)ferrocene is promising, the system was not well resolved – a number of resonances that likely corresponded to bound substrate species were observed suggesting that this system is more complex than a typical system involving a simple organic substrate.

The SABRE polarisation of [tris(bipyrazyl)ruthenium(II)]$^{2+}$ highlights a number of important issues to be considered when attempting to polarise more complex substrates. Polarisation of a sample containing only **Ru(bpz)$_3$**[PF$_6$]$_2$ could not be achieved by **1-cod-Cl** due to degredation of the sample in the presence of hydrogen. The addition of **Py** and **MeCN** to activate the sample before addition of **Ru(bpz)$_3$** overcame this but obscured the subsequent polarisation of **Ru(bpz)$_3$**. To truly assess the level of polarisation attained for this substrate,*d$_5$*-**Py** could be used to remove the large polarised resonances that overlap with those of **Ru(bpz)$_3$**.

Poor solubility of the substrates used in this study was a significant problem which limited the scope of this research. Future development of SABRE in different solvents may make polarisation of substrates that have poor solubility in methanol viable.

4 The effect of pH on SABRE polarisation

4.1 Introduction

4.1.1 The effect of pH in chemical reactions

The pH of a solution has great importance in both chemistry and biology. It can affect reaction mechanisms,[78, 79] products[79, 80] and kinetics[79-81] in a chemical system and must be tightly controlled in biological systems due to the toxic effect of variations in pH.[82]

One of the most obvious effects of the addition of a strong base to a chemical reaction is the removal of a proton from the reactants. This is well documented and often forms the first step of a reaction[83, 84] as the deprotonated species is more reactive than the neutral compound. The addition of an acid or base can also be used to drive a reaction through a catalytic mechanism such as acid catalysed hydrolysis.[85] However, the effect of pH on a reaction can be less direct.

The mechanism of pyrogallol (1,2,3-benzenetriol) autoxidation (Figure 35) has been reported to be pH dependent[78] – the mechanism that dominates at high pH cannot be significantly inhibited by superoxide dismutase whereas the mechanism that dominates at lower pH is almost completely inhibited by these enzymes.

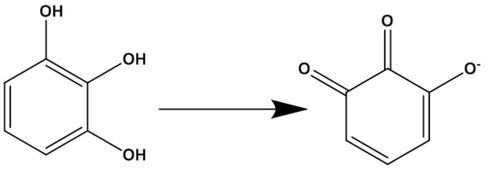

Figure 35: Autoxidation of pyrogallol

Transfer hydrogenation of aromatic ketones by Ru-(R,R)-Ts-dpen (Ts-dpen = N-(p-toluenesolfonyl)-1,2-diphenylethlenediamine) is significantly faster under basic conditions than under acidic conditions.[79] Two mechanisms were proposed – one that proceeded under acidic conditions and involved the protonation of the (R,R)-Ts-dpen ligand and one under basic conditions that did not. The mechanism under acidic conditions was less efficient and resulted in slower hydrogenation of the aromatic ketones. Introduction of (S,S)-Ts-dpen under acidic conditions led to a loss of enantiomeric selectivity, but under basic conditions did not (Figure 36), confirming the acidic mechanism could lead to loss of the (R,R)-Ts-dpen ligand.

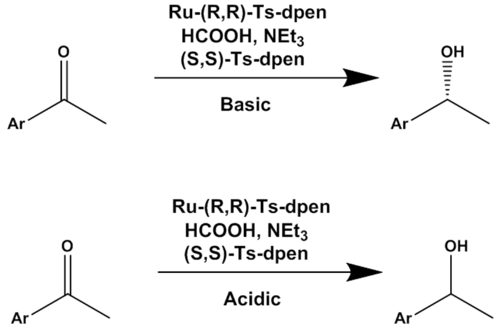

Figure 36: Transfer hydrogenation of aromatic ketones by Ru-(R,R)-Ts-dpen proceeds through a different mechanism at high and low pH which may result in a loss of stereochemistry.[79]

Oxidation of nitrates and nitrites by monometallic palladium and bimetallic catalysts has been reported to be negatively impacted by an increase in pH due to the adsorption of hydroxide species on the metal surface preventing binding of the nitrogen species.[80] The number of unwanted, partially oxidised by products also increased with the pH. This dependency on pH was specific to the catalyst used and to the choice of reducing agent (hydrogen or formic acid). The oxidative coupling of aniline by manganese oxide to form azobenzene was shown to have an increased rate under more acidic conditions.[81]

Any of these effects could affect the SABRE polarisation mechanism, which is known to be highly dependent on the kinetics of exchange of both the target substrate and hydrogen.[10, 12] As such, the effect of pH on the SABRE process must be considered for a greater understanding of the polarisation transfer process and its potential application to *in vivo* imaging studies. This chapter will focus on the effect of pH on the SABRE polarisation transfer process; chapter 5 will explore the potential applications of SABRE to imaging and the effect of pH on these applications.

4.1.2 The effects of pH on NMR

The effect of pH on the NMR chemical shift has also been well documented.[86, 87] The greatest effect is seen around the pKa of the molecule being investigated – if the protonated and deprotonated forms are in rapid equilibrium then the chemical shift observed will be an average of their respective chemical shifts, weighted by their relative populations. Under more acidic conditions the protonated form will become more favoured and the chemical shift observed will be closer to the protonated chemical shift, and under basic conditions the same will be true of the deprotonated structure. An example of this is the protonation of histidine.[86] Plotting the chemical shift against the pH for a system such as this gives a sigmoidal trend with the steepest slope at the molecule's pKa as shown in Figure 37. SABRE polarisation transfer depends on both scalar coupling and difference in chemical shift;[88] changing the pH of the system may change the chemical shift of the substrate sufficiently that this propagation mechanism is affected.

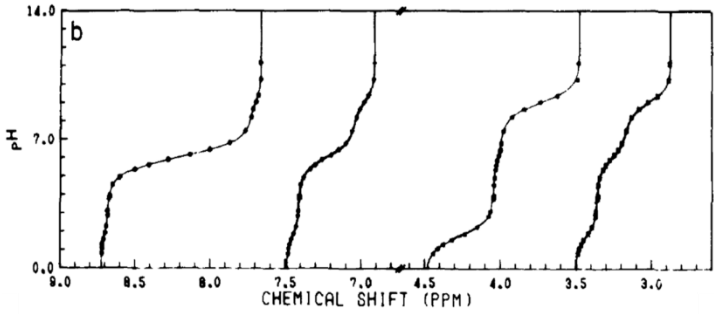

Figure 37: pH titration of L-histidine taken from Tanokura *et al.*[86]

4.1.3 The effect of pH on SABRE

Recent work within the Duckett group has shown that the polarisation of nicotinic acid is greatly affected by pH.[89] The pH titration of the SABRE enhancement was carried out; at higher pH the polarisation seen is much greater than in the native system (Figure 38). This dependence of SABRE enhancement on the sample pH could be harnessed to improve SABRE polarisation of a substrate or to apply SABRE polarised substrates as a pH probe for molecular imaging.

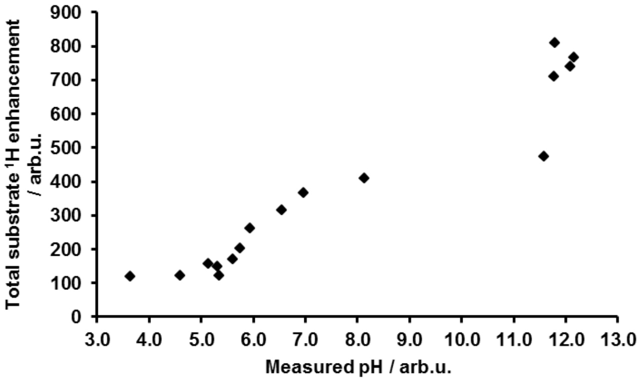

Figure 38: Effect of pH on SABRE polarisation of nicotinic acid in methanol by 1-cod-Cl and pH_2. pH varied by addition of Cs_2CO_3.Data taken from Olaru *et al.*[89]

In this study, I will investigate the effect of pH on the SABRE polarisation of a number of different substrates derived from pyridine. The substrates selected were 3-hydroxypyridine, 3-methoxypyridine, 4-hydroxypyridine and 4-methoxypyridine. By varying the functionalization I will determine whether any effect seen is primarily due to the change in chemical shift, or a more subtle function of the addition of base. The two hydroxypyridine substrates have acidic protons whereas the methoxypyridines do not, this will allow for a distinction between general electronic effects and deprotonation effects to be made. I will study the effect of addition of a base, caesium carbonate, to the sample with respect to chemical shift and SABRE enhancement. Cesium carbonate was selected for its solubility in methanol. I will also investigate the addition of an acid to the sample. The addition of acid is expected to reduce polarisation due to protonation of the basic nitrogen site preventing efficient association of the substrate to the iridium catalyst.

4.2 The effect of pH on SABRE polarisation of 3-hydroxypyridine

4.2.1 3-hydroxypyridine

4.2.1.1 Comparison of pyridine, nicotinic acid and 3-hydroxypyridine substrates

3-hydroxypyridine (**3OHPy**) was selected for study as it is a pyridine ring with a substituent in the same position as in nicotinic acid. This will allow a direct comparison of the effect of the functionalization of pyridine on the hyperpolarisation observed and its pH dependence to the results previously obtained. The carboxylic acid group in nicotinic acid is electron withdrawing whereas the alcohol group in **3OHPy** is electron donating. This contrast may be an important factor in the SABRE polarisation of these substrates. The change in functional group from a carboxylic acid group to an alcohol also results in the proton of the functional group becoming much less acidic (Figure 39). This may have a significant impact on the effect of base with nicotinic acid likely being more affected than **3OHPy**.

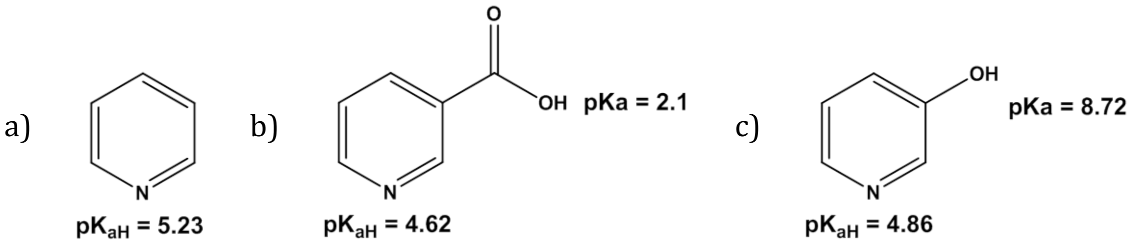

Figure 39: Schematic showing the pK$_a$ and pK$_{aH}$ values for the basic pyridine sites and the acidic functional groups of a) **Py**[46] b) nicotinic acid[90] and c) **3OHPy**.[46] pK$_{aH}$ is the pK$_a$ of the conjugate acid in which the aromatic nitrogen is protonated

4.2.1.2 Characterisation of [Ir(IMes)(H)$_2$(3-hydroxypyridine)$_3$]$^+$

Upon coordination to [Ir(IMes)(H)$_2$(**3OHPy**)$_3$]$^+$ (**1-3OHPy**), the nitrogen of **3OHPy** becomes more shielded, as revealed by the change in chemical shift. As seen previously for **3AmPy**, the ligand *trans* to the NHC is more shielded than the ligand cis to the NHC due to the significant electron donating ability of IMes (Table 3). A single hydride ^{1}H resonance is seen for the activated species **1-3OHPy** at δ -22.96. Full characterisation data is available in Chapter 6.

Table 3: Key chemical shifts for **3OHPy**, **1-3OHPy**, **Py**, and **1-Py** in *d$_4$*-methanol.

Species	**3OHPy**	**Py**
	^{15}N δ / ppm	
Free substrate, **L**	298.8	317 [91]
cis to NHC in **1-L**	257.2	255.6 [36]
trans to NHC in **1-L**	241.3	239.1 [36]
	^{1}H δ / ppm	
Hydride in **1-L**	-22.96	-22.56 [36]

4.2.1.3 Exchange processes in [Ir(IMes)(H)$_2$(3-hydroxypyridine)$_3$]$^+$

The system was further characterised by measuring the rate of dissociation for both hydride and substrate species as described in Appendix 1. Comparison of these values to those previously obtained for **Py** should offer an insight into the SABRE mechanism and the effect that the choice of substrate has on this. Comparison of these values to those obtained from a more basic sample will offer an insight into the effects of pH on the SABRE process.

It can be seen that **1-3OHPy** has a much slower substrate dissociation rate than **1-Py** (Table 4). The positive values for $\Delta H^{\ddagger}$ and $\Delta S^{\ddagger}$ indicate that this exchange occurs via the same dissociative mechanism as reported for **1-Py**. [12]

Whilst the ^{15}N shift of the free substrate indicates that the nitrogen of **3OHPy** is more shielded than **Py**, when the nitrogen environments of **1-3OHPy** and **1-Py** are considered both systems have similar chemical shifts (Table 3). This suggests that the bound substrates in **1-Py** receive more electron density from the iridium centre than those in **1-3OHPy**, and this suggests a stronger bond between the iridium center and the substrate ligands in **1-Py** than in **1-3OHPy**. This is supported by the higher activation enthalpy for substrate dissociation from **1-Py** than from **1-3OHPy**. This is further supported by the shorter Ir-N bond lengths (Table 5) in the crystal structure of **1-Py**[12]than **1-3OHPy** (Appendix 2). This difference in bond length may also be the cause of the difference in entropy of activation – the longer bonds in **1-3OHPy** reduce the entropy gained upon dissociation. The significantly lower entropy of activation may be the explanation for the slower exchange rate – the smaller increase in entropy does not sufficiently compensate the increase in enthalpy required to reach the transition state.

The hydride exchange rate is also much slower for **1-3OHPy** than **1-Py**. As the activation entropies are similar, it is the difference in activation enthalpy that is the likely cause of this change in exchange rates. The dissociation of hydrides from **1-3OHPy** has a greater enthalpy of activation than hydride dissociation from **1-Py** and therefore requires a higher amount of energy to reach the transition state. This explains the slower rate of exchange. The hydride chemical shifts (Table 3) indicate an increased shielding of the hydrides in **1-3OHPy** than **1-Py**, supporting the conclusion that the iridium-hydride bond is stronger in **1-3OHPy** than in **1-Py**.

Table 4: Exchange and activation parameters for **1-3OHPy** and **1-Py**

	1-3OHPy		**1-Py**[12]	
Substrate				
k_{Dissoc}(298 K) / s^{-1}	6.37	± 0.02	23	
$\Delta H^{‡}$ / kJ mol^{-1}	73.8	± 0.7	95	± 1
$\Delta S^{‡}$ / J K^{-1} mol^{-1}	19	± 2	96	± 2
$\Delta G^{‡}_{298}$ / kJ mol^{-1}	68.39	±0.01	64	± 2
Hydride				
$k_{Hydride}$(298 K) / s^{-1}	4.1	± 0.5	9	
$\Delta H^{‡}$ / kJ mol^{-1}	85.5	± 0.6	79	± 0.2
$\Delta S^{‡}$ / J K^{-1} mol^{-1}	59	± 2	54	± 1
$\Delta G^{‡}_{298}$ / kJ mol^{-1}	69.5	± 0.3	66.4	± 0.3

Table 5: Selected bond lengths for **1-3OHPy** and **1-Py** obtained by single crystal x-ray diffraction

Bond	**1-3OHPy**	**1-Py**[12]
Ir-N (*cis* to NHC)	2.239(2)	2.220(3), 2.192(3),
Ir-N (*trans* to NHC)	2.104(3)	2.129(3)

4.2.1.4 Longitudinal relaxation, T_1, of 3-hydroxypyridine

The longitudinal relaxation constant, T_1, gives a measure of the lifetime of the polarisation. A short T_1 will result in rapid decay of the hyperpolarised signal, whereas a longer T_1 will make measurement of a hyperpolarised signal more feasible. This is particular important when considering MRI applications of SABRE.

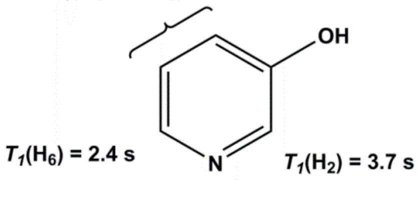

Figure 40: T_1 values recorded for **3OHPy** in the presence of **1-3OHPy** in d_4-methanol

4.2.2 SABRE polarisation of 3-hydroxypyridine

Initial testing of **3OHPy** (Figure 41) for SABRE activity revealed that it polarises very well (Figure 42); optimisation of the SABRE polarisation of **3OHPy** was carried out before studying the effect of pH on the polarisation.

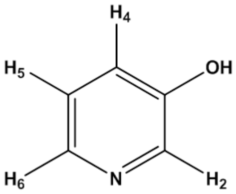

Figure 41: Schematic of **3OHPy** with proton environments annotated

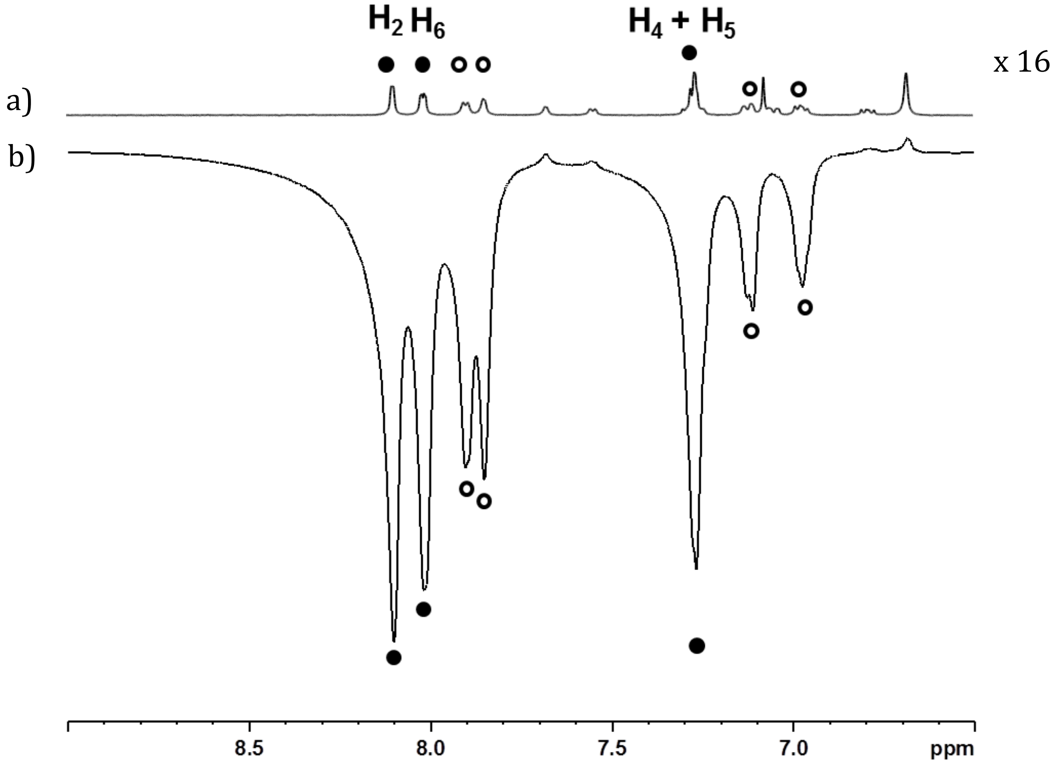

Figure 42: Comparison of a) thermal and b) hyperpolarised spectra of 25 mM **3OHPy** with 20% catalyst loading of **1-cod-Cl** and 3 bar pH_2 in d_4-methanol. ● indicates the resonances of free **3OHPy** and ○ indicates the resonances of the substrate molecules bound *cis* to the IMes ligand. x 16 indicates a vertical expansion of 16 fold for the thermal spectrum relative to the hyperpolarised spectrum.

4.2.3 Optimising the ^{1}H SABRE polarisation of 3-hydroxypyridine

4.2.3.1 Factors that affect SABRE polarisation efficiency

Lloyd *et al.*[36] showed that SABRE polarisation of pyridine by **1-cod-Cl** exhibits a high dependence on a number of factors, including:

- The ratio of substrate:catalyst
- The concentration of the catalyst
- The field at which polarisation transfer occurs
- The pressure of pH$_2$ in the system

A balance must be achieved between polarisation build up and relaxation of the polarisation within the system. Polarisation can only be transferred from pH$_2$ to the substrate through the scalar coupled species [Ir(IMes)(H)$_2$(**L**)$_3$]$^+$ (**1-L**), and so the lifetime of this species must be sufficiently long as to allow this transfer to occur. As the polarisation comes from the hydrogen species, exchange of this species must also be maximised. The hydrogen exchange follows the dissociation of the substrate, and is hindered by the association of substrate. These interconnected rates create a system that must be carefully balanced if optimisation of the polarisation transfer is to be achieved. In this investigation the system was optimised for proton polarisation of **3OHPy** by varying the substrate:catalyst ratio,the concentration of the catalyst and the polarisation transfer field.

4.2.3.2 Optimisation of substrate:catalyst ratio

The effect of the substrate:catalyst ratio was investigated by varying the amount of substrate added to a sample, without changing the catalyst concentration. The ratio of substrate:catalyst was determined by NMR integration. This ratio is important as it controls the association rate of the substrate onto the iridium species. This has an effect on the polarisation as it limits the hydrogen binding rate and therefore limits the source of polarisation. The dissociation rate should be independent of the substrate concentration.

The optimal ratio for **3OHPy** and **1-cod-Cl** was found to be 5.5:1 (Figure 43). For **Py** the optimal ratio has been reported as being 4:1[36] with a similar decrease in observed polarisation at higher ratios. The trend below this optimum ratio was not explored for **Py**.

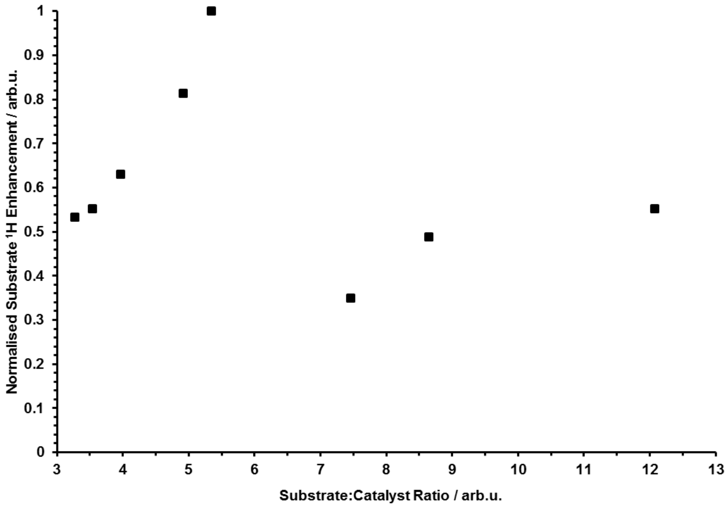

Figure 43: A comparison of the normalised signal enhancement for **3OHPy** upon changing the ratio of substrate:catalyst at a constant 5mM concentration of **1-cod-Cl** in d_4-methanol. The enhancement values have been normalised.

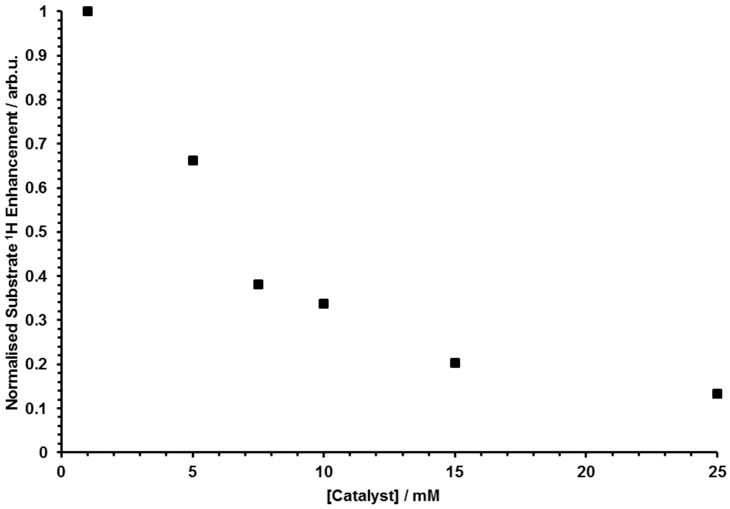

Figure 44: A comparison of normalised signal enhancement for **3OHPy** upon changing the catalyst concentration at a constant substrate:catalyst ratio of 5:1 in d_4-methanol. Observed enhancements have been normalised.

4.2.3.3 *Optimisation of catalyst concentration*

The effect of the catalyst concentration on enhancement was investigated for a substrate:catalyst ratio of 5:1. The concentration was varied by diluting a stock solution of **1-cod-Cl** and **3OHPy** in d_4-methanol. As previously seen with **Py**,[36] the polarisation of the substrate increases with decreasing catalyst concentration for a given substrate:catalyst ratio (Figure 44).

4.2.3.4 *Optimisation of polarisation transfer field*

As has been previously reported,[10] SABRE polarisation is highly dependent on the magnetic field at which the polarisation occurs. A field plot of the SABRE polarisation of **3OHPy** was produced (Figure 45) using the flow system previously described.[12] By increasing the polarisation transfer field stepwise it is apparent that the ideal field for **3OHPy** polarisation is at 70 G for each proton environment.

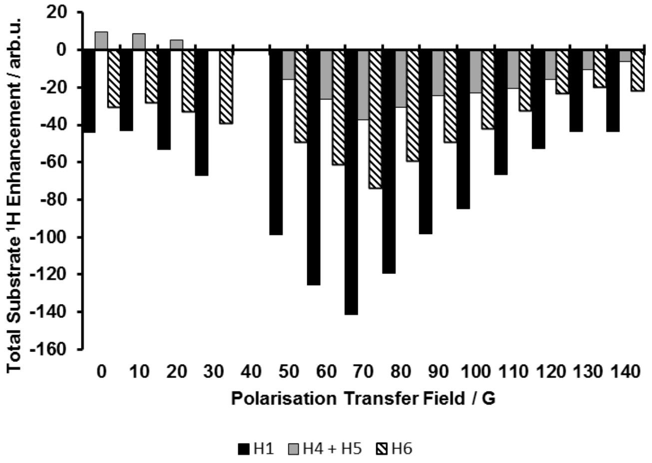

Figure 45: Field plot obtained for **3OHPy** showing the effect of the polarisation transfer field on the observed polarisation. Polarisation of a sample of **3OHPy** in a ratio of 20:1 with 5 mM **1-cod-Cl** in d_4-methanol was achieved by bubbling pH$_2$ through the sample for 6 seconds using a flow probe system set up. The measurement at 40 G is not included due to an error during data collection

The following studies of **3OHPy** were carried out with a 5:1 ratio of substrate to catalyst and a catalyst concentration of 5 mM. Although not the ideal concentration for maximum polarisation, a catalyst concentration of 5 mM was chosen for practical purposes including increased signal and to reduce the errors introduced when weighing out very small amounts of base. Polarisation was carried out at 65 G for the remainder of this study as this is the maximum field that it is practical to polarise at using polarisation method 1 (Chapter 6) and the stray field of the NMR spectrometer used.

4.2.4 The effect of pH on 3-hydroxypyridine SABRE polarisation: Addition of Cs_2CO_3

4.2.4.1 Preliminary study

A comparison of the polarisation of **3OHPy** with no added base and with excess Cs_2CO_3 added reveals that there is a stark change, both in polarisation and in chemical shift of the substrate, upon addition of base (Figure 46). The polarisation of the substrate decreases in the presence of Cs_2CO_3 – this is in contrast to the results obtained for nicotinic acid. This invites further investigation into the effect of pH on SABRE polarisation as it is clearly not a straightforward relationship.

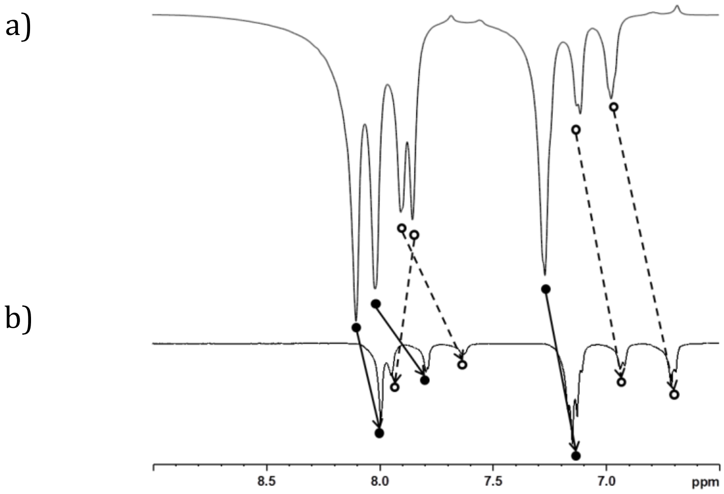

Figure 46: Comparison of hyperpolarised spectra for 25 mM **3OHPy** with a 20% catalyst loading in d_4-methanol after 10 s polarisation at 65 G under 3 bar pH_2 at a) pH = 7.24 b) pH = 10.07 showing the effect of addition of excess Cs_2CO_3 on the SABRE polarisation and chemical shifts of the substrate. ● indicates the resonances of free **3OHPy** and ○ indicates the resonances of the substrate molecules bound *cis* to the IMes ligand in **1-3OHPy**

4.2.4.2 *The effect of solution basicity on SABRE polarisation of 3-hydroxypyridine: chemical shift*

By carrying out a pH titration on this system we can see the effect of addition of base. The pH of a solution having an effect on the chemical shift observed has been reported previously[86, 87] and the sigmoidal trend described can also be seen for the protons of **3OHPy** and **1-3OHPy**. However, the different ^{1}H environments are affected to different degrees by addition of base – those corresponding to the IMes ligand are barely affected whereas those corresponding to the hydrides and **3OHPy** species are significantly affected (Figure 47). It is worth noting that whilst the majority of signals move to a lower chemical shift indicating an increase in shielding, the peaks corresponding to the hydrides and the protons in the $H_{L,2}$ position of the bound substrates of **1-3OHPy** move to higher chemical shifts. This causes overlap of signals and a reordering of peaks so care is needed in the analysis of these results.

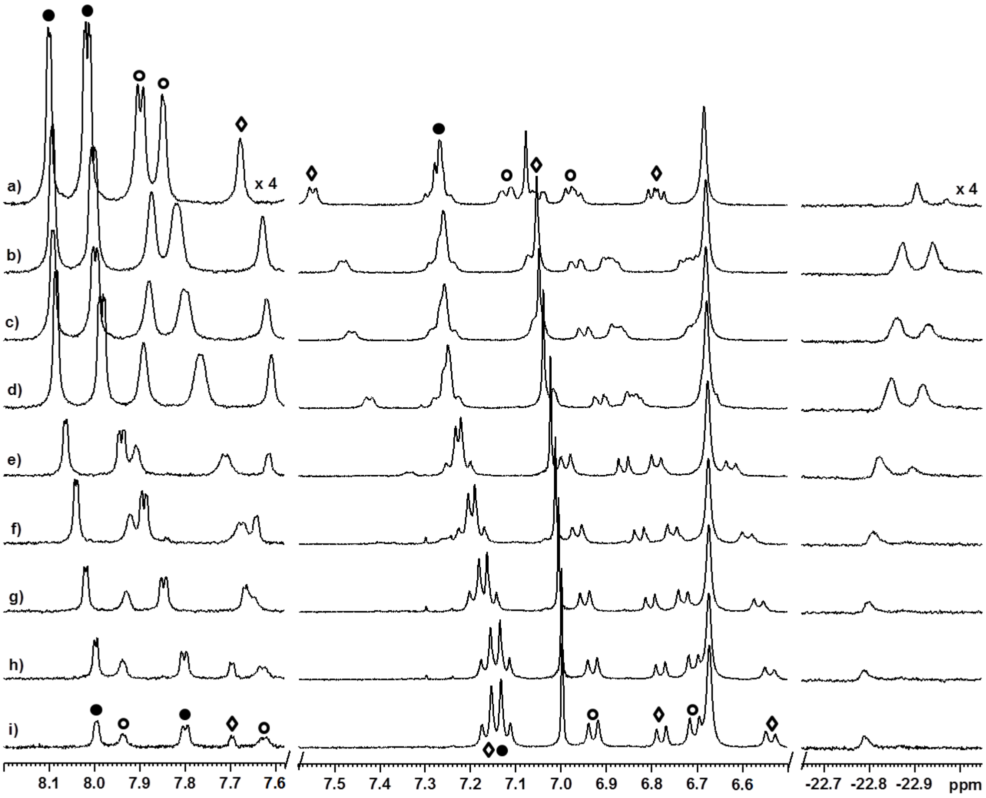

Figure 47: ^{1}H NMR spectra of samples containing 25 mM **3OHPy** with a 20% **1-cod-Cl** catalyst loading. pH of sample varied by addition of Cs_2CO_3 a) pH = 7.24 b) pH = 8.25 c) pH = 8.54 d) pH = 8.78 e) pH = 9.23 f) pH = 9.64 g) pH = 9.88 h) pH = 10.07 i) pH = 10.48. ● indicates free **3OHPy**. ○ indicates bound **3OHPy** *cis* to the IMes ligand. ◊

indicates bound **3OHPy** *trans* to the IMes ligand. x 4 indicates the vertical expansion of the left and right hand sections of the spectrum relative to the central section of the spectrum.

As the sample is made more basic, all aromatic protons of the free substrate (Figure 47 - ●) move to lower chemical shifts with a sigmoidal trend (Figure 48). This shift to a lower frequency indicates increased shielding – this is likely due to the increased electron density being donated into the ring by the oxyanion formed on deprotonation of the alcohol group. The protons are not all equally affected – this is particularly obvious when comparing H_5 and H_4 as the multiplet made up from their signals separates sufficiently that the two environments can be individually resolved at pH = 10.48. The reason for this is due to the difference in the extent of electron donation from the hydroxyl group to these sites. The ^{15}N chemical shift moves from δ 298.8 to 294.9 when excess Cs_2CO_3 is added indicating an increase in shielding corresponding to increased donation from the oxygen anion in comparison to the alcohol group.

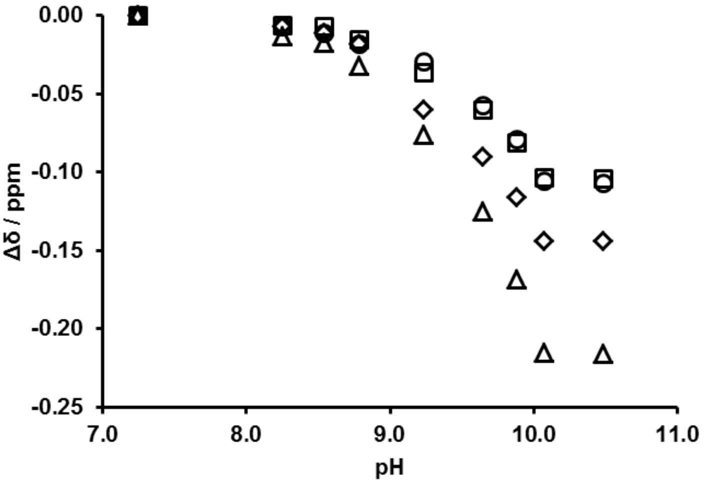

Figure 48: pH titration of free **3OHPy** in d_4-methanol showing the change in chemical shift upon addition of Cs_2CO_3 indicating increased shielding of all aromatic proton environments. □ shows the change in chemical shift of the H_2 environment, Δ shows the change in chemical shift of the H_6 environment. ◊ shows the change in chemical shift of the H_4 environment and ○ Shows the change in chemical shift of the H_5 environment relative to the native chemical shift.

This trend to lower chemical shift is carried through to most of the bound substrate peaks as shown in Figure 49. However, $H_{L,2}$ for both bound substrates moves to a higher chemical shift. It is evident that binding of the substrate to iridium changes the electronic and steric environment of the protons and this is the cause for this change in trend. An increase in hydrogen bonding or a change in interaction with neighbouring aromatic groups are potential causes for this change in shielding but it is not clear what the cause is from this data. The hydride signal also moves downfield indicating a reduction in shielding of this species.

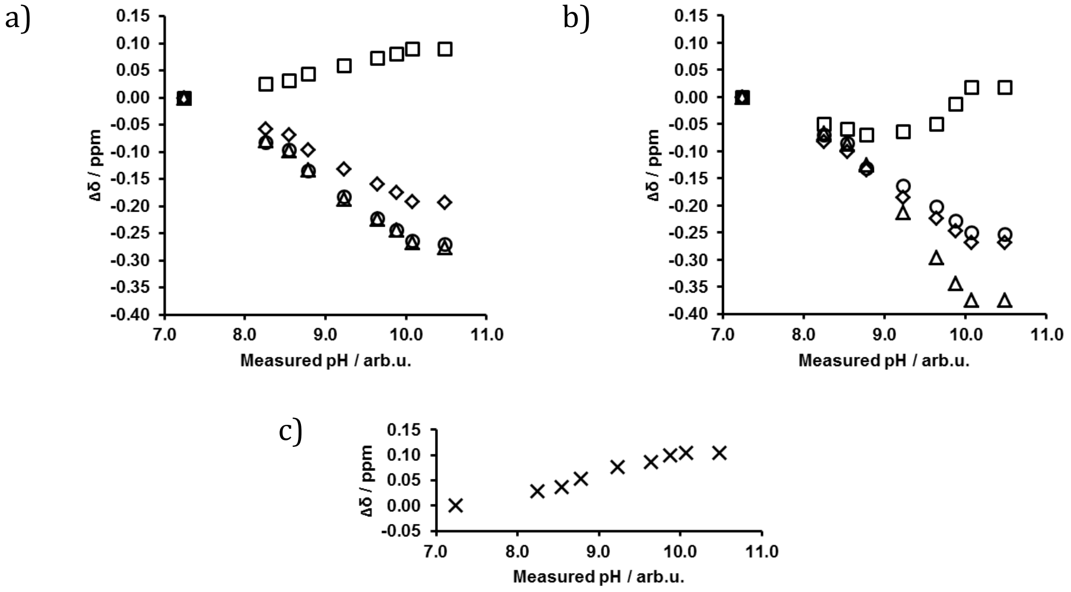

Figure 49: pH titration of the signals corresponding to **3OHPy** bound to **1-3OHPy** in d_4-methanol showing the change in chemical shift upon addition of Cs_2CO_3 relative to the native chemical shift. a) shows the bound substrate environment *cis* to the IMes ligand, b) shows the bound substrate environment *trans* to the IMes ligand, c) shows the hydride environment. ◊ shows the chemical shift of the H_4 environment and ○ shows the chemical shift of the H_5 environment. X shows the chemical shift of the hydride environment.

4.2.4.3 The effect of solution basicity on SABRE polarisation of 3-hydroxypyridine: enhancement

A more quantitative study of the effect of pH on the SABRE polarisation was carried out alongside the pH titration. The total enhancement of the system drastically falls from 4500 fold to a minimum of 1500 fold at pH 9.5. It then rises again at the basic extreme (Figure 50). This trend is seen for both the free and the bound substrates.

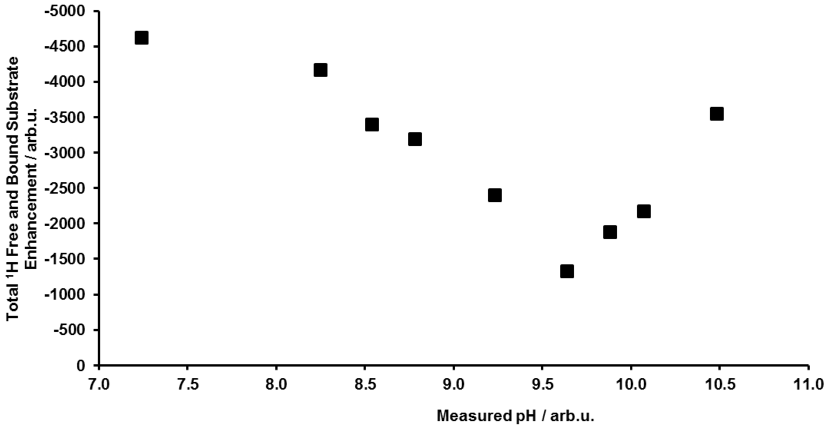

Figure 50: pH titration of the total SABRE enhancement of **3OHPy**. Each sample contained 25 mM **3OHPy** with a 20% **1-cod-Cl** catalyst loading in d_4-methanol and was polarised for 10 s in a 65 G field under an atmosphere of 3 bar pH_2.

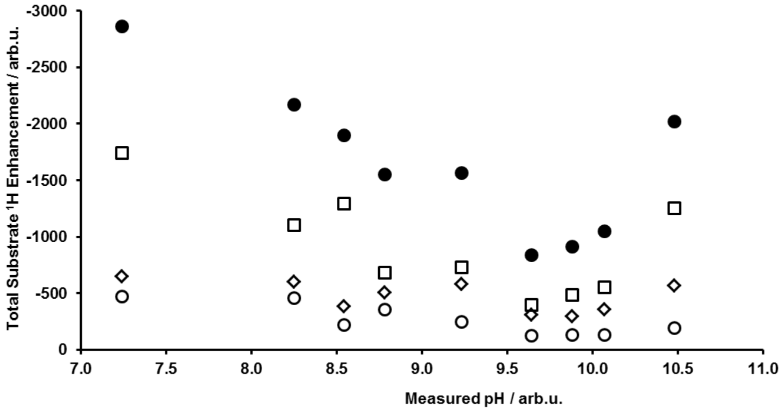

Figure 51: pH titration of the SABRE enhancement of free **3OHPy** in solution. Each sample contained 25 mM **3OHPy** with a 20% **1-cod-Cl** catalyst loading in d_4-methanol and was polarised for 10 s in a 65 G field under an atmosphere of 3 bar pH_2. ● represents the total enhancement of the free **3OHPy** environments, □ represents the enhancement of the H_2 environment, ◊ represents the H_6 environment and ○ represents the enhancement of the combined H_4 and H_5 peaks

Looking at the polarisation of the free substrate in more detail (Figure 51) it is evident that this trend is primarily from the polarisation of the proton in the H_2

position. This proton is located between the pyridine nitrogen and the alcohol group that is deprotonated and so is likely to be most affected by any transfer of electrons from the oxyanion to the basic nitrogen that binds to the iridium. Of note is the slight increase at pH 9.23 due to the overlap of the H_6 of free **3OHPy** and $H_{L,2}$ of the bound **3OHPy** *cis* to the NHC. This is reflected in both the free and bound trends where it was impossible to distinguish between the two peaks, but not in the total polarisation where their contribution was only counted once.

4.2.4.4 The effect of solution basicity on SABRE polarisation of 3-hydroxypyridine: substrate dissociation rate, relaxation constant T_1, polarisation transfer field

The underlying cause for the changes seen in the polarisation of **3OHPy** by **1-3OHPy** and pH_2 upon addition of Cs_2CO_3 is not immediately apparent. To understand this further a number of parameters were measured.

- The dissociation rate constant of the substrate in the presence of excess base was determined to be $k_{Dissoc} = 12.76 \pm 0.09\ s^{-1}$ at 298 K. This is substantially higher than the associated rate constant in the absence of Cs_2CO_3. This could negatively impact polarisation by preventing efficient build up on the substrate or by promoting rapid exchange of hydrogen depleting the reservoir of polarisation. If multiple ligands are deprotonated, and the caesium ions are not closely associated with the negative charge, there will be increased repulsion between the bound ligands which will increase the rate of dissociation. If the caesium ions are closely associated with the oxyanion group then the increased bulk will also increase the dissociation rate.
- The T_1 relaxation constants for each proton environment of **3OHPy** were determined in the presence of excess Cs_2CO_3 and are shown below in Figure 52. These constants are higher than in the absence of base – assuming the initial polarisation is the same, this increase in the T_1 values should be reflected in the polarisation by an increased signal due to less relaxation occurring prior to measurement. This reduction in the relaxation rate is likely due to the faster dissociation rate recorded in the presence of base.
- The field plot acquired for **3OHPy** in the presence of excess base is shown in Figure 53. The maximum polarisation of **3OHPy** occurs at around 70 G – this is not significantly different to the native sample.

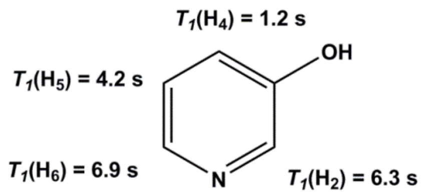

Figure 52: T_1 relaxation constants recorded **3OHPy** in the presence of base and **1-3OHPy** in d_4-methanol

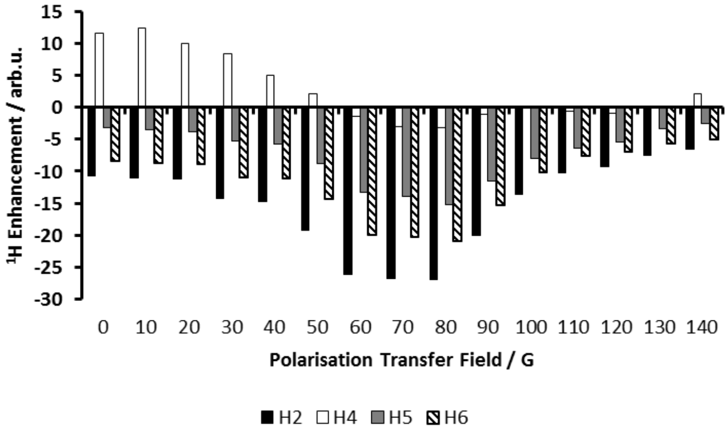

Figure 53: Field plot depicting dependence of **3OHPy** polarisation on the polarisation transfer field. Sample contains 100 mM **3OHPy**, 5 mM **1-cod-Cl** and excess Cs_2CO_3 in d_4-methanol

4.2.5 The effect of pH on SABRE enhancement of 3-hydroxypyridine: addition of acetic acid

To investigate the effect of acidic conditions on SABRE polarisation, a pH titration using acetic acid (Figure 54) was carried out. This will allow for a comparison of acidic, basic and native conditions for the same substrate to give a more complete analysis of the effect of pH on SABRE polarisation.

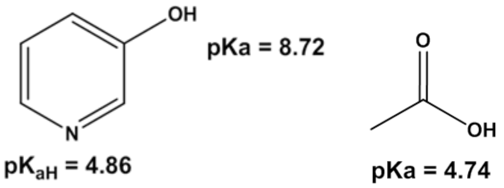

Figure 54: pKa values of **3OHPy**[46] and acetic acid[92]

Upon addition of acetic acid it is expected that the aromatic nitrogen of **3OHPy** will be protonated as acetic acid is sufficiently acidic to protonate this basic site.

The change in chemical shift upon addition of acetic acid was a transition to higher chemical shifts for all protons in the free substrate (Figure 55)– this is due to the protonation of the substrate leading to a decrease in shielding as the protonated nitrogen becomes more electronegative and the species overall has a positive charge. The bound substrates show no measurable change in chemical shift – this is because the aromatic nitrogen cannot be protonated in these substrates as it has already donated its lone pair to the iridium and therefore cannot also donate it to a proton. This confirms that it is the aromatic nitrogen that is protonated first upon addition of an acid.

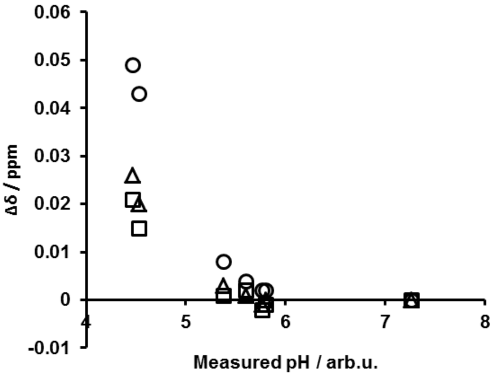

Figure 55: pH titration of free **3OHPy** in *d_4*-methanol showing the change in chemical shift upon addition of acetic acid from the native chemical shift indicating decreased shielding of all aromatic proton environments. □ shows the chemical shift of the H_2 environment, Δ shows the chemical shift of the H_6 environment. ○ Shows the chemical shift of the H_4 and H_5 environment.

The polarisation of **3OHPy** fell upon addition of acetic acid (Figure 56). The protonated substrate species no longer has an available nitrogen lone pair with which to bind to the iridium.

No polarisation of the acetic acid was seen in this system, and no species were seen that suggested binding of the acid to the iridium.

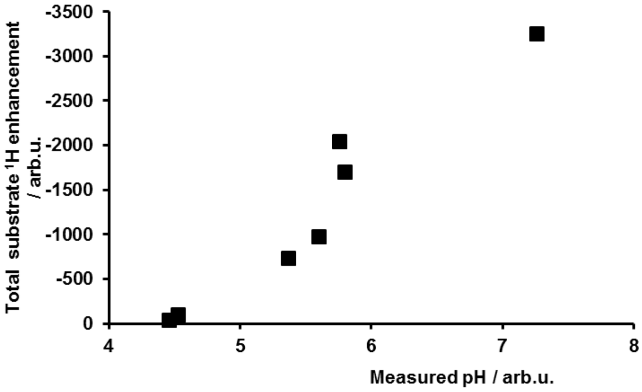

Figure 56: pH titration of the total SABRE enhancement of free **3OHPy** by addition of acetic acid. Each sample contained 25 mM **3OHPy** with a 20% **1-cod-Cl** catalyst loading in d_4-methanol and was polarised for 10 s in a 65 G field under an atmosphere of 3 bar pH$_2$.

4.3 The effect of pH on SABRE polarisation of 4-hydroxypyridine

4.3.1 4-hydroxypyridine

4.3.1.1 Comparison of hydroxypyridine isomers

The second substrate selected for this study was 4-hydroxypyridine (**4OHPy**). Moving the alcohol group to the 4 position on the ring (Figure 57) will change the electronics of the substrate – this will reveal the importance of the electron donation from the functional group on SABRE polarisation and the effect that pH has on this. The pK_a of **4OHPy** (pK_a = 3.27, pK_{aH} = 11.09[46]) is also significantly lower than **3OHPy** (pK_a = 4.86, pK_{aH} = 8.72[46]) and **Py** (pK_a = 5.23[46]), this confirms a change in the electronics of the substrate and may result in a different dependence on pH. It is worth noting that the ^{15}N shift for **4OHPy** (δ 152.5 in methanol) is significantly lower than that seen for **3OHPy** (δ 298.8) – this indicates a much greater shielding of the nitrogen which may result in a stronger binding between the substrate and iridium. This much greater shielding points to a significant difference between **3OHPy** and **4OHPy** – **4OHPy** readily tautomerises.

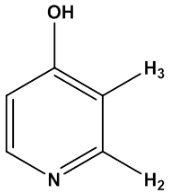

Figure 57: Schematic of **4OHPy** with proton environment labels as annotations

4.3.1.2 Tautomerisation of 4-hydroxypyridine

4OHPy has been reported to undergo significant tautomerisation[93, 94] – this results in 4-pyridone being favoured in polar solvents (Figure 58).[93] This explains the increased shielding of the nitrogen – this is typical of amines. This tautomerisation may have a significant impact on SABRE polarisation.

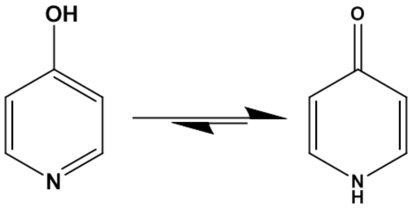

Figure 58: Tautomerisation of **4OHPy** and 4-pyridone

4.3.2 SABRE polarisation of 4-hydroxypyridine

Upon activation of **1-cod-Cl** in the presence of **4OHPy**, the expected complex [Ir(IMes)(H)$_2$(**4OHPy**)$_3$]$^+$ (**1-4OHPy**) is formed. This results in a significant deshielding of the nitrogen nuceli of the bound substrates as seen by their chemical shifts of δ 228.8 (*cis* to the NHC) and δ 212.1 (*trans* to the NHC). These are more similar to the previously reported shifts for **1-Py** (δ 255.6, 239.1)[36] and **1-3OHPy** (δ 257.2, 241.3) than the free ligand is to **Py** and **3OHPy**. This suggests that the 4-hydroxypyridine tautomer binds through its nitrogen lone pair to iridium in **1-4OHPy**.

Unusually, the **1-4OHPy** complex is not the primary species in solution – another species with inequivalent hydrides also forms in approximately a 5:1 ratio with **1-4OHPy**. This species is thought to be [Ir(IMes)(H)$_2$(**4OHPy**)$_2$Cl] and will be discussed in section 4.3.3.

Polarisation of **4OHPy** was much lower than that observed for **3OHPy**. A titration of the polarisation against equivalents of substrate revealed that the polarisation increased at around 10 equivalents of substrate:catalyst before levelling off. The maximum polarisation was seen for 20 equivalents substrate:catalyst (Figure 59).

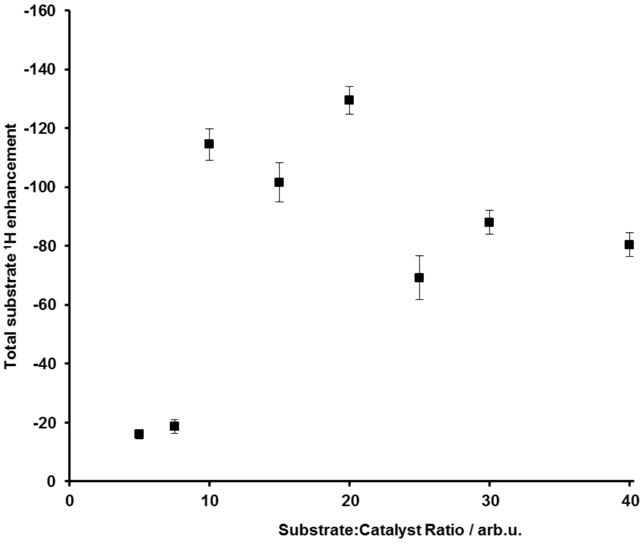

Figure 59: A comparison of the observed signal enhancement for **4OHPy** upon changing the ratio of substrate:catalyst at a constant 5mM concentration of **1-cod-Cl** in d_4-methanol after polarisation for 10 s in a 65 G field under an atmosphere of 3 bar pH_2

The rate of dissociation of the substrate from **1-4OHPy** was measured using selective excitation. The dissociation rate constant of **4OHPy** was measured to be k_{Dissoc} = 1.73 ± 0.01 s^{-1}. This is much lower than the dissociation rate constant seen for **Py** and **3OHPy**. This slow dissociation may explain the low polarisation – the slow rate will likely limit the exchange of hydrogen and therefore the amount of polarisation possible in this system. No exchange into the $[Ir(IMes)(H)_2($**4OHPy**$)_2Cl]$ species was observed.

The SABRE polarisation of the H_3 environment of **4OHPy** shows a significant dependence on the polarisation transfer field (Figure 60) – this peak undergoes a phase inversion at approximately 60 G.

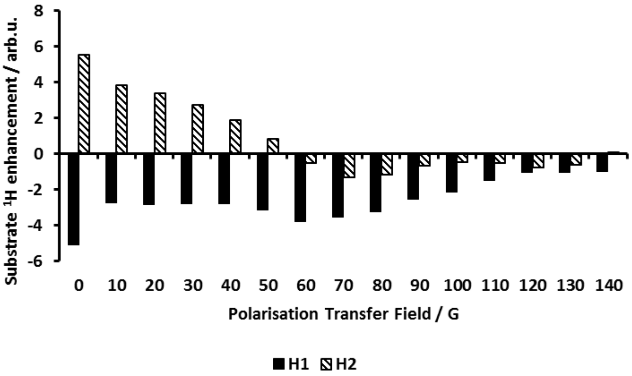

Figure 60: Field plot showing the effect of polarisation transfer field on the SABRE polarisation of **4OHPy**. Sample contained 100 mM **4OHPy**, 5 mM **1-cod-Cl** in d_4-methanol

4OHPy displays longer T_1 values than **3OHPy**, (Figure 61) and therefore the hyperpolarised signal for a sample of **4OHPy** will decay more slowly than for a sample of **3OHPy**. Despite this, the polarisation observed with **4OHPy** was lower than observed with **3OHPy**. This suggests that the initial polarisation of **4OHPy** is lower than that of **3OHPy** and the lower polarisation observed for **4OHPy** is not due to rapid relaxation of the hyperpolarised signal.

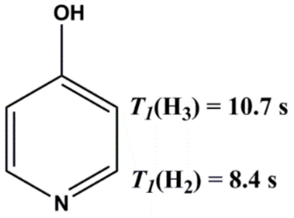

Figure 61: Measured T_1 values for **4OHPy** in the presence of **1-4OHPy** in d_4-methanol

4.3.3 [Ir(IMes)(H)$_2$(4OHPy)$_2$Cl]

The observed species [Ir(IMes)(H)$_2$(**4OHPy**)$_2$Cl] has two chemically distinct hydride environments (δ -22.09, -27.43). These allow for a precise characterisation of the species. Selective excitation of each of the two hydrides reveal that one of the two substrate species is bound *trans* to the NHC as it shows an nOe effect to both hydrides, whereas the other substrate species is *cis* to the NHC as it only shows a through space interaction to the hydride at δ - 22.09.

The species that is *trans* to the NHC is bound through nitrogen – this can be seen through an nOe experiment; both of the hydride environments are close in space to the $H_{L,trans,2}$ environment and not the $H_{L,trans,3}$ environment. The ^{15}N shift for this species is δ 212.2 – this is very close to that of the substrate bound *trans* to the NHC in **1-4OHPy** confirming that they are similar environments.

The remaining **4OHPy** species shows a through space interaction between its $H_{L,cis,3}$ environment and the hydride at δ -22.09. This suggests that it might be bound through the oxygen instead of the nitrogen. The ^{15}N shift of δ 148.9 supports this as this is reasonably close to the free substrate shift. **4OHPy** has been seen to bind to metal centers through oxygen[95, 96] as well as through nitrogen[97, 98] so this is plausible.

The remaining site, *cis* to the hydride at δ –27.43 and *trans* to the hydride at δ - 22.09, could not be identified by NMR. It is possible that the site is vacant, occupied by solvent, by the chlorine counter ion or occupied by a third hydride.

As each hydride signal is a doublet, with $^2J_{HH}$ = 9 Hz, and the two signals have a 1:1 ratio, the option of a third hydride can be discounted. An example of an iridium species with three hydrides gives the chemical shift of hydrides *trans* to each other as being around δ – 12,[99] this further rules this structure out.

If the solvent, methanol, occupied this site then it would be likely that the hydride *trans* to it would have a higher shift, at around δ -25, as reported by Lloyd *et al.*[36] The presence of a nOe to bound methanol would also be expected but is not seen. A number of species in which the hydride is trans to water have been reported by Carmona *et al.* as having a chemical shift close to δ -27.[100]

An iridium species with a hydride *trans* to a vacant site has been reported with a chemical shift of -36.26,[101] whereas hydride species *trans* to chlorine have been reported at δ -25.13[99] and -23.16,[102] and a species with the hydride *trans* to iodine reported as δ -23.4.[103] This suggests that it is most likely the hydride that is seen here is not *trans* to a vacant site, and possibly is *trans* to a chlorine ion, although this has not yet been confirmed. This is represented in Figure 62 as an unoccupied site as the occupying species is unknown.

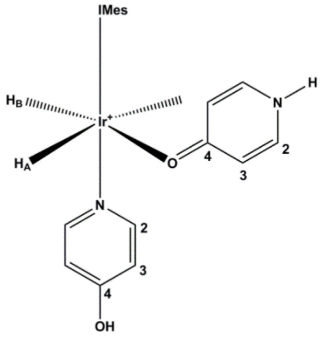

Figure 62 : Schematic of proposed structure for [Ir(IMes)$(H)_2$(κ-N-4-hydroxypyridine)(κ-O-4-hydroxypyridine)$]^+$

4.3.4 The effect of pH on SABRE polarisation of 4-hydroxypyridine: addition of Cs_2CO_3

The SABRE polarisation of **4OHPy** increases significantly (from 100 fold to 500 fold) upon addition of excess base – this is shown in Figure 63. The chemical shift of the proton signals also changes slightly. Upon addition of Cs_2CO_3 the [Ir(IMes)$(H)_2$(**4OHPy**)$_2$Cl] species is no longer formed.

Investigating the chemical shifts of free (Figure 64) and bound (Figure 65) substrates during a pH titration reveals significantly different trends for the free substrate than was seen previously for **3OHPy**.

The deshielding of H_2 and the shielding of H_3 cannot be explained by a simple deprotonation of the alcohol group. The bound substrate follows trends more like those seen previously (Figure 65) – the increased shielding suggesting increased donation from the alcohol group.

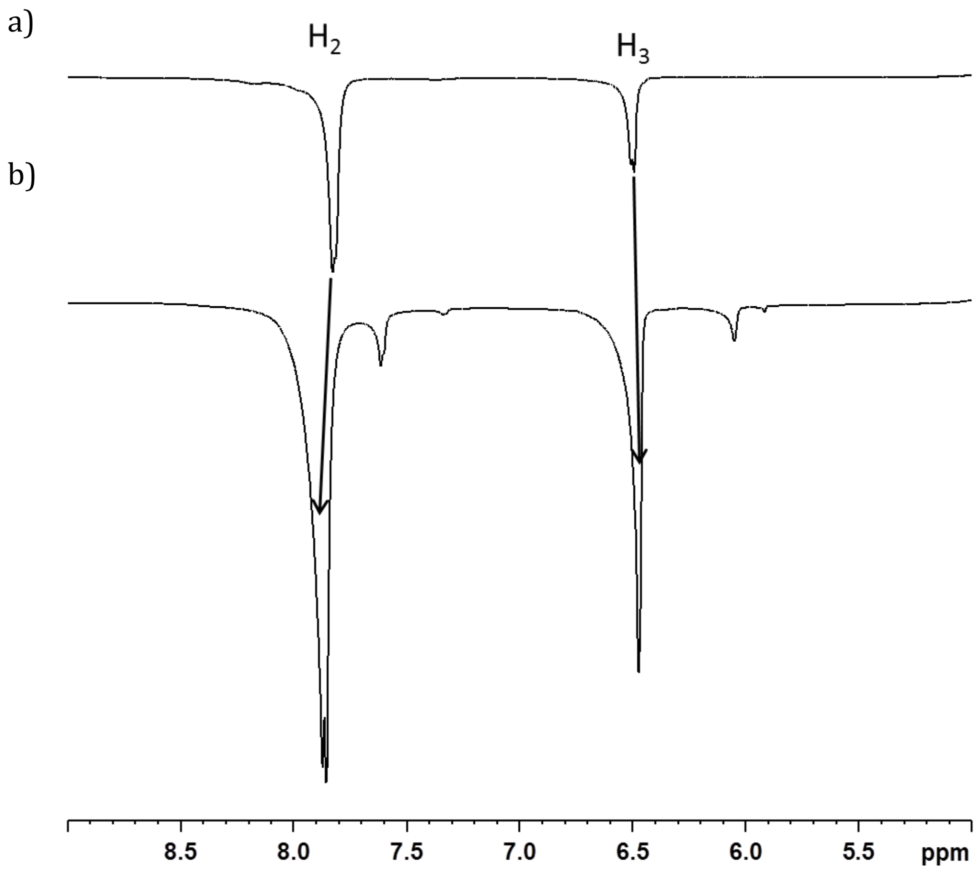

Figure 63: Comparison of hyperpolarised spectra for 100 mM **4OHPy** with a 5% catalyst loading in d_4-methanol after 10 s polarisation at 45 G under 3 bar pH_2 at a) pH = 6.69 b) pH = 11.67 showing the effect of addition of excess Cs_2CO_3 on the SABRE polarisation and chemical shifts of the substrate

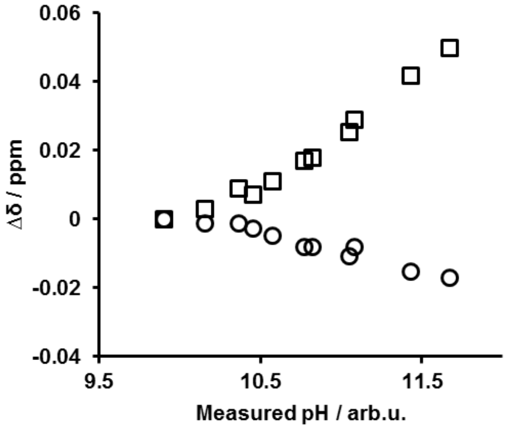

Figure 64: pH titration the chemical shifts of free **4OHPy** in a sample of 100 mM **4OHPy** with a 5% **1-cod-Cl** catalyst loading in d_4-methanol by addition of Cs_2CO_3. □ indicates the H_2 environment, ○ indicates the H_3 environment

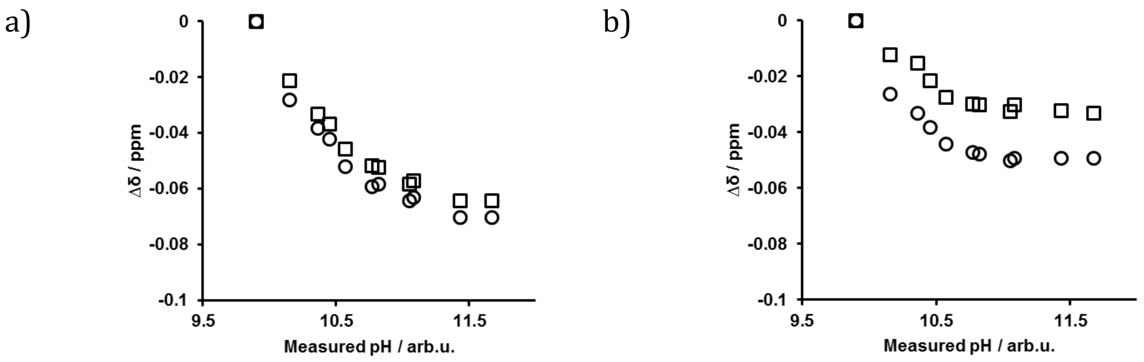

Figure 65: pH titration of the bound environments of **4OHPy** in a sample of 100 mM **4OHPy** with a 5% **1-cod-Cl** catalyst loading by addition of Cs_2CO_3. a) shows the bound substrate *cis* to the IMes ligand, b) shows the bound substrate *trans* to the IMes ligand. □ indicates the $H_{L,2}$ environment, ○ indicates the $H_{L,3}$ environment

The effect of pH on the chemical shift of the free substrate can be explained by considering the tautomerisation. The ^{15}N shift of free substrate in a basic solution moves to a higher shift at δ 246.6 – this indicates that the hydroxypyridine tautomer is more favoured at higher pH than the pyridone tautomer. As the carbon-oxygen double bond loses electron density it reduces the electron withdrawing effect of the electronegative oxygen on the pyridine ring. This results in an increase in shielding – particularly in the adjacent protons. As the ring becomes more aromatic and increases the carbon-nitrogen bond strength the nitrogen pulls electron density away from the adjacent carbon and proton environments deshielding them. Another effect is that in the 4-pyridone tautomer the nitrogen lone pair is able to donate into the π system, whereas in the hydroxypyridine tautomer it is pointing out of the ring and so only a single electron is donated into the π system. This further reduces shielding of the protons of the ring. As the pH increases, the equilibrium moves to favour **4OHPy**. As a result the H_2 proton environment is deshielded and the H_3 environment shielded in comparison to in 4-pyridone.

4OHPy exhibits an increase in SABRE polarisation upon addition of Cs_2CO_3 (Figure 66). This is in contrast to **3OHPy** suggesting that the position of the substituent on the pyridine ring is as important as its identity when considering SABRE polarisation.

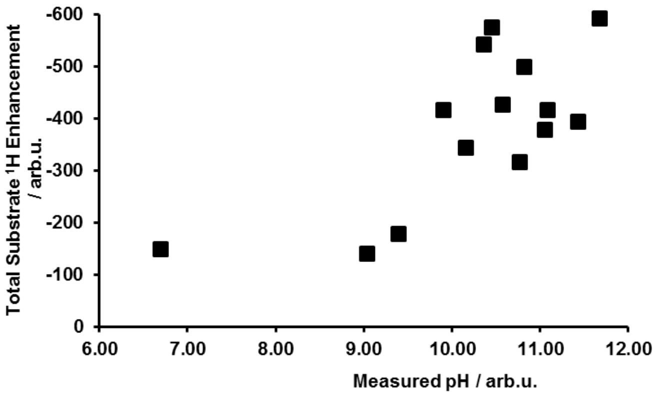

Figure 66: pH titration of the total SABRE enhancement of **4OHPy**. Each sample contained 100 mM **4OHPy** with a 5% **1-cod-Cl** catalyst loading in *d₄*-methanol and was polarised for 10 s in a 65 G field under an atmosphere of 3 bar $p\text{H}_2$.

An increase in the dissociation rate is also seen. In the presence of excess base $k_{\text{Dissoc}} = 4.97 \pm .01\ \text{s}^{-1}$. This may explain the increase in polarisation as more rapid hydrogen exchange is allowed.

The dependence on the polarisation transfer field is different for **4OHPy** in the presence of base (Figure 67) – at no point are both H_2 and H_3 in emission. This will affect the application of **4OHPy** to MRI as the emission and absorption components of the signal will cancel each other out resulting in a reduced signal. This contrasts with the results observed using polarisation method 1 in which the two resonances were in phase across the pH range measured at a polarisation field of 65 G.

The longitudinal relaxation constants for **4OHPy** are slightly reduced on addition of base (Figure 68). This contrasts with the results for **3OHPy** in which the T_1 relaxation constants increased upon addition of base. As both species display a higher dissociation rate constant under basic conditions this must be due to another factor – possibly the suppression of tautomerisation of **4OHPy** under basic conditions.

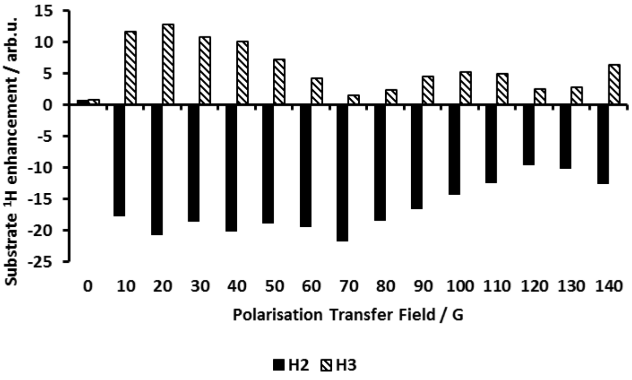

Figure 67: Field plot showing the effect of the polarisation transfer field on SABRE polarisation of **4OHPy** in the presence of excess base. Sample contained 100 mM **4OHPy**, 5 mM **1-cod-Cl** and excess Cs_2CO_3 in d_4-methanol

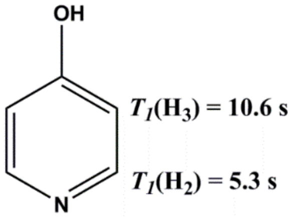

Figure 68: T_1 relaxation constants for **4OHPy** in the presence of excess base, collected in the presence of **1-4OHPy** and excess Cs_2CO_3 in d_4-methanol

4.4 The effect of pH on SABRE polarisation of 3-methoxypyridine and 4-methoxypyridine

4.4.1 Eliminating the effect of acidic alcohol protons

To determine the role of the acidic alcohol proton on SABRE polarisation in a basic environment, the methyl ether derivatives of both 3- and 4-hydroxypyridine (**3OMePy** and **4OMePy** respectively) (Figure 69) were studied. The ether groups should have similar electronic effects to the alcohol groups and this will allow distinction between any pH dependence due to the deprotonation of the alcohol proton and that which is due to electronic factors (Figure 70).

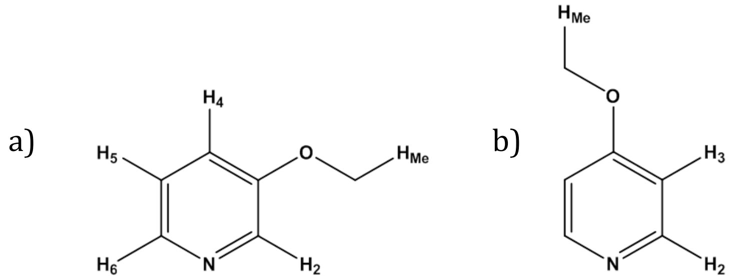

Figure 69: Annotated schematic of a) **3OMePy** and b) **4OMePy** with ^{1}H environments labelled

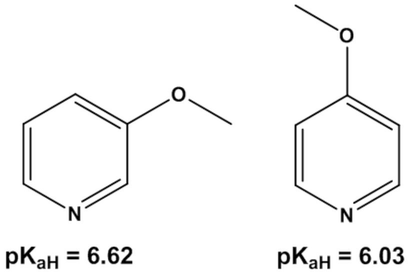

Figure 70: pK_{aH} values of **3OMePy** and **4OMePy**.[104]

4.4.2 SABRE polarisation of 3-methoxypyridine

Like its alcohol analogue, 3-methoxypyridine (**3OMePy**) showed good polarisation at a 5:1 substrate:catalyst ratio – this is shown in Figure 71. In addition to polarisation of the aromatic protons, polarisation of the methyl ether was also seen. Transfer of polarisation across an oxygen bond has not been previously reported for SABRE so this modest polarisation is very promising as it suggests that it may be possible in the future to polarise a substrate that binds through oxygen instead of nitrogen – this would make SABRE polarisation a much more general technique.

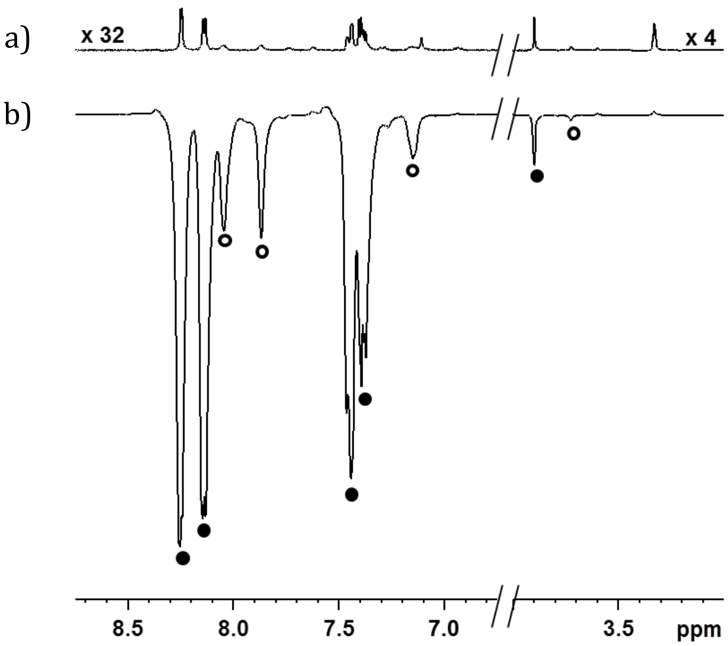

Figure 71: Comparison of a) thermal and b) hyperpolarised spectra of 25 mM **3OMePy** with 20% catalyst loading of **1-cod-Cl** and 3 bar *p*H_2 in *d*$_4$-methanol. ● indicates the resonances of free **3OMePy** and ○ indicates the resonances of the substrate molecules bound *cis* to the IMes ligand. x 32 indicates a vertical expansion of 32 fold for the thermal spectrum relative to the hyperpolarised spectrum.

4.4.3 The effect of pH on SABRE polarisation of 3-methoxypyridine: addition of Cs_2CO_3

No noticeable change in chemical shift could be seen for any species in this system upon addition of base. This is likely due to the lack of electronic changes, in contrast to **3OHPy**, as no deprotonation of **3OMePy** occurs. However, rapid deuteration of H_2 and H_6 was seen in the samples that contained Cs_2CO_3 – these protons were over 90 % deuterated before activation of **1-cod-Cl** was completed in extreme cases (Figure 72). A potential solution to this would be to use *d*$_3$-methanol (CD_3OH), although care would have to be taken due to the large residual peak for this solvent.

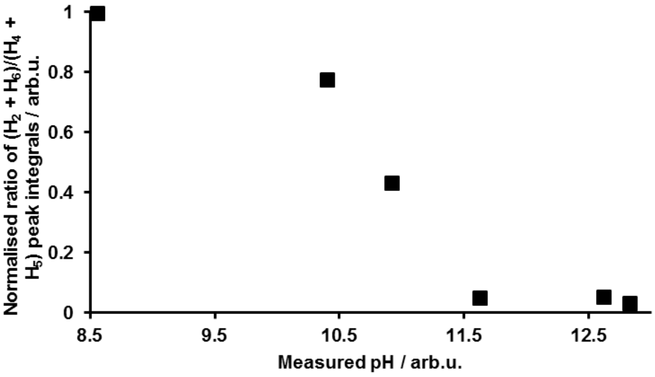

Figure 72: pH titration of the deuteration of H_2 and H_6 of **3OMePy**. Each sample contained 25 mM **3OMePy** with a 20% **1-cod-Cl** catalyst loading in *d_4*-methanol and was under an atmosphere of 3 bar hydrogen. Deuteration was measured using NMR integration relative to H_4 and H_5 after activation

Although the catalysts typically used for polarisation transfer are known to deuterate the substrates used, this rapid deuteration was not expected as it was not seen to such an extent for the previous substrates.

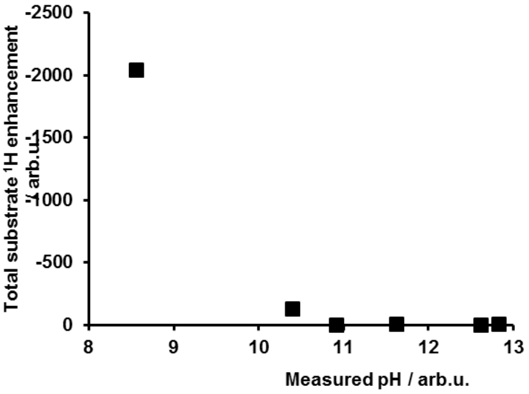

Figure 73: pH titration of the total SABRE enhancement of **3OMePy**. Each sample contained 25 mM **3OMePy** with a 20% **1-cod-Cl** catalyst loading in *d_4*-methanol and was polarised for 10 s in a 65 G field under an atmosphere of 3 bar pH_2.

The polarisation of **3OMePy** sharply dropped upon addition of base. This is likely due to the rapid deuteration of the protons in the 2- and 6-positions observed in the presence of a base (Figure 72). Polarisation of these protons is thought to be key to the polarisation transfer to the rest of the molecule as indicated by selective deuteration experiments on **Py**.[36]

4.4.4 SABRE polarisation of 4-methoxypyridine

Unlike **4OHPy**, 4-methoxypyridine (**4OMePy**) polarises well at a 5:1 ratio with **1-cod-Cl**. **4OMePy** will not tautomerise as readily as **4OHPy** because the tautomerisation would result in a zwitterionic species with an oxygen cation with 3 covalent bonds instead of a neutral ketone, and an amine anion instead of an amine (Figure 74). Unlike **4OHPy**, **4OMePy** is primarily in the pyridine-ether tautomer and the aromatic nitrogen is free to bind to iridium. The ^{15}N shift for **4OMePy** (δ 275.8) supports the pyridine-ether tautomer being dominant. The strong polarisation of **4OMePy** supports the conclusion that the reason **4OHPy** polarises poorly is due to its tautomerisation and relatively low abundance of available nitrogen sites to act as 2 electron donors. As with **3OMePy**, polarisation of the methyl ether protons can be seen for **4OMePy** (Figure 75).

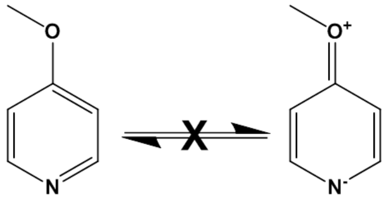

Figure 74: Schematic showing the potential tautomerisation of **4OMePy**.

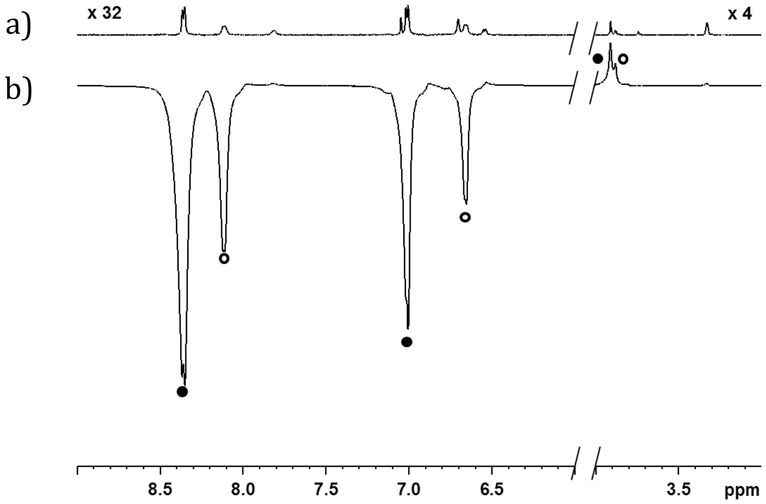

Figure 75: Comparison of a) thermal and b) hyperpolarised spectra of 25 mM **4OMePy** with 20% catalyst loading of **1-cod-Cl** and 3 bar pH_2 in d_4-methanol. ● indicates the resonances of free **4OMePy** and ○ indicates the resonances of the substrate molecules bound *cis* to the IMes ligand. x 32 indicates a vertical expansion of 32 fold for the thermal spectrum relative to the hyperpolarised spectrum.

4.4.5 The effect of pH on SABRE polarisation of 4-methoxypyridine: addition of Cs_2CO_3

As with **3OMePy**, the two protons adjacent to the nitrogen atom of **4OMePy** deuterate rapidly in the presence of Cs_2CO_3 and **1-4OMePy** (Figure 76) and the polarisation falls as the pH increases (Figure 77). Again, no noticeable change in the chemical shift was seen for any protons in this system upon addition of base, this further supports the conclusion that **4OMePy** does not undergo the tautomerisation seen for **4OHPy**.

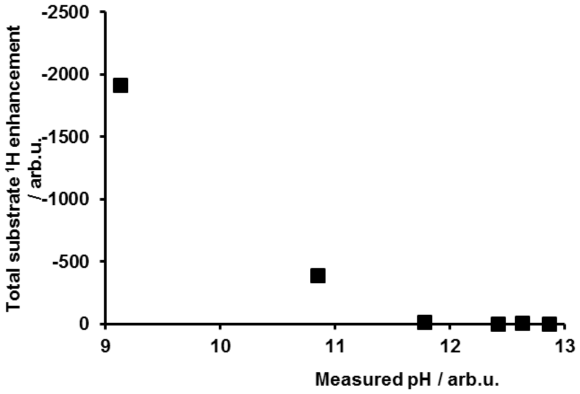

Figure 76: pH titration of the total SABRE enhancement of **4OMePy**. Each sample contained 25 mM **4OMePy** with a 20% **1-cod-Cl** catalyst loading in *d*$_4$-methanol and was polarised for 10 s in a 65 G field under an atmosphere of 3 bar *p*H_2.

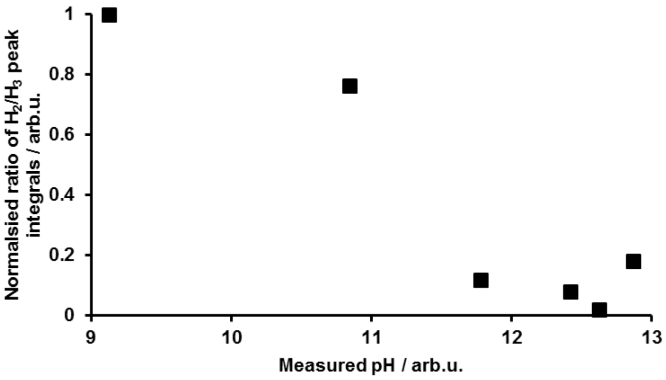

Figure 77: pH titration of the deuteration of H_2 of **4OMePy**. Each sample contained 25 mM **4OMePy** with a 20% **1-cod-Cl** catalyst loading in *d*$_4$-methanol and was under an atmosphere of 3 bar hydrogen. Deuteration was measured using NMR integration relative to H_3 after activation

4.5 Conclusions

The pH of a sample has been shown to have a significant effect on its SABRE polarisation.

Basic conditions do not have a straightforward effect on SABRE– in some cases the polarisation observed is improved, whereas in others it is drastically diminished. The structure of the substrate being investigated must be considered and its vulnerability to basic conditions taken into account.

3-hydroxypyridine was shown to polarise efficiently under standard SABRE conditions. The SABRE polarisation of 3-hydroxypyridine was suppressed in the presence of caesium carbonate – falling to approximately a third of the native polarisation at pH 9.5. The dissociation rate constant of 3-hydroxypyridine from the complex **1-3OHPy** was over 12 s^{-1}, this is double the constant measured under native conditions. This is the most likely cause of the reduced polarisation. A previous study on the SABRE polarisation of pyridine at different temperatures and with different catalysts revealed that there is an ideal rate of exchange for efficient SABRE polarisation.[36]

In the case of 3- and 4-methoxypyridine the addition of base to the sample was seen to impede polarisation transfer as the *J*-coupling network of protons was broken due to rapid deuteration under basic conditions. The polarisation of these two substrates fell from approximately 2000 fold under native pH to less than 5 fold at pH values over 12. Under native conditions no deuteration of the protons adjacent to the aromatic nitrogen of these two substrates was seen during the experimental time frame. In contrast, the deuteration of the protons adjacent to the aromatic nitrogen was almost 100 % at the higher pH values studied.

In the case of 4-hydroxypyridine the removal of the acidic proton encouraged association of the substrate to the polarisation transfer catalyst by changing the tautomeric equilibrium. Under native conditions 4-hydroxypyridine favours the 4-pyridone tautomer – removal of the acidic proton under basic conditions leads to the 4-hydroxypyridine tautomer being favoured. This resulted in an increase in the efficiency of SABRE polarisation of 4-hydroxypyridine -a fivefold increase in the

SABRE polarisation of 4-hydroxypyridine was observed in the presence of excess base.

Acidic conditions can lead to protonation of the substrate nitrogen and prevent efficient binding to the iridium centre. This will reduce the level of polarisation observed under SABRE conditions. For 3-hydroxypyridine the polarisation was seen to drop from 4500 fold under native conditions to 5 fold at pH 4.5.

Future work in this area of research should investigate how general the reported observations are. Whilst the SABRE polarisation of pyridine has been thoroughly investigated, the effect of pH on this polarisation has not yet been studied. It could be expected that the addition of base to a sample would result in rapid deuteration of the protons adjacent to the aromatic nitrogen similar to that seen for 3- and 4-methoxypyridine. Identification of substrates that behave in a manner similar to 4-hydroxypyridine and nicotinic acid in the presence of base could be used to develop the SABRE technique by increasing the level of polarisation achieved and allowing substrates that are normally poorly polarised to be more efficiently polarised.

An alternative research area would be to compare the effect of different bases on SABRE polarisation of a substrate. The use of an organic base such as methylamine or dimethylaminopyridine (DMAP) would allow for the effect of pH to be distinguished from the effect of metal ion concentration.

An alternative aspect of this study to consider is that it may be possible to polarise new substrates through control of the solution pH. Some examples of substrates that may benefit from basic conditions such as those described above are imidazole and pyrrole – both key features in biological and pharmaceutical systems. These maintain a pyridine like motif except their basic nitrogen site is occupied by a proton – removal of this proton may result in their binding to iridium and subsequent polarisation as seen for 4-hydroxypyridine. These are both more basic than caesium carbonate; a stronger base would be needed for such a study.

5. Applications of SABRE polarised substrates as a MRI contrast agents

5.1 Contrast agents and molecular imaging

5.1.1 Molecular imaging

Contrast agents are used to improve image quality. For MRI the most common contrast agents are gadolinium based. These work by increasing the relaxation rate of the surrounding water which allows for greater contrast of the tissues being observed.[105, 106] As described previously, there are a number of examples of contrast agents prepared through the use other hyperpolarisation techniques.[19-21]

Molecular imaging is a technique used in diagnosis and for following treatment progress in a non-invasive manner. For example, Positron Emission Tomography (PET) techniques use ^{18}F labelled glucose (2-fluoro-2-deoxy-D-glucose) and thymidine (3'-deoxy-3'-fluorothymine) analogues to identify diseases such as cancer and Huntington's disease before symptoms are displayed and often before other diagnostic techniques can identify the diseases.[107] This allows earlier treatment which is simpler and less expensive. 2-fluoro-2-deoxy-D-glucose (FDG) forms a phosphate but is not further metabolised. As a result it accumulates in areas that metabolise more glucose – the resulting signal received during the PET process allows identification of these areas and gives metabolic information such as the location of tumours.

5.1.2 SABRE as a MRI contrast agent

Initial studies into the use of SABRE for the production of hyperpolarised images have been promising. SABRE enhanced proton images have been captured after polarisation at low[8] and high[108] field, and SABRE polarised phosphorus images have shown that it is possible to significantly improve the quality of image obtained for heteronuclei by hyperpolarisation (Figure 78).[11]

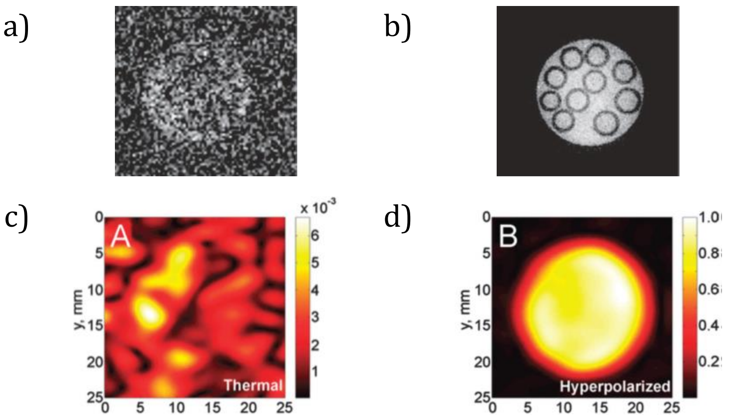

Figure 78: a) ^{1}H MRI image of an 8 mm sample tube containing 1 mm glass cylinders and A and [Ir(PCy$_3$)(cod)(**Py**)]Cl in *d$_4$*-methanol, thermal image, 20 mm slice-thickness b) hyperpolarised image, 0.5 mm slice-thickness. Image taken from Adams *et al.*[8] c) 20 mm sample tube containing 6 mM (PPh$_3$)$_3$Ir(H)$_2$Cl in toluene with thermal polarisation and 128 acquisitions d) after hyperpolarisation by bubbling with *p*H$_2$ at 80 ^{o}C collected without signal averaging. Image taken from Zhivonitko *et al.*[11]

The successes shown above could be translated to medical applications through the polarisation of biological or drug substrates. The high intensity, combined with the high resolution offered by MRI, would allow for a greater understanding of how a substrate behaves in the body by making it easier to track. SABRE is particularly useful in this regard as it does not require a chemically altered substrate; PET requires a radionucleus such as ^{18}F to be incorporated into the probe whereas the nuclei commonly used for MRI – ^{1}H, ^{13}C, ^{15}N, ^{31}P – are all present in natural products. This would allow for study of the exact substrate of interest and not a fluorinated form of it.

The reported polarisation of isoniazid,[43] pyrazinamide[43] and nicotinamide[8] are examples where SABRE has been applied to a medically relevant substrate. This is encouraging as it demonstrates the applicability of SABRE hyperpolarisation directly to substrates of interest without need for modification of the substrate. Studies of nicotinamide derivatives using PET[109, 110] have shown that they can have significant uptake in melanoma cancer cells –

this demonstrates the importance of this substrate as a potential tool for diagnosis of disease, either through PET or through hyperpolarised MRI.

The lifetime of polarisation is a general problem for the development of SABRE – in order to effectively use a contrast agent for molecular imaging it must have time to circulate the body and be sequestered. A short lifetime of polarisation is problematic when attempting this. This problem has been overcome in DNP for the ^{13}C polarisation of pyruvate[19] and carbonate[111]. The majority of SABRE studies are on ^{1}H nuclei, it is possible that transitioning to polarisation of heteronuclei will provide a longer lifetime of polarisation. An alternative application of SABRE which would be of medical use, but would not require as significant an increase in polarisation lifetime, would be as a pH mapping agent. The applications of this would be more local and, whilst they would require sufficient time for equilibration, would not have as significant a lead time as metabolic molecular imaging applications.

5.1.3 pH mapping

A deviation from physiological pH can be symptomatic of a number of diseases, including cancer[112] and renal failure.[113] Therefore, non-invasive measurement of pH can be an important diagnostic tool. A number of approaches to developing such a technique have been made.

Huang *et al.*[114] used pH "switches" to control the formation of micelles. These switches were polymers containing hydrophobic sections, pH sensitive sections and ^{19}F reporter sections. At pH values greater than the pK_a of the unimers the micelle structure was formed due to the hydrophobic sections self-assembling nature. Under acidic conditions the micelles disassembled as the pH sensitive sections, containing amine groups, became protonated (Figure 79) and repulsion increased.

The restrictions imposed on chain motion by the micelle structure led to rapid spin-spin relaxation of the ^{19}F NMR signal which resulted in significant line broadening effectively suppressing the signal. However, when the micelles disassembled into unimers the signal observed from the ^{19}F reporter section was strong. The presence or absence signal was used to indicate if the pH was above or below the pKa of the switch used.

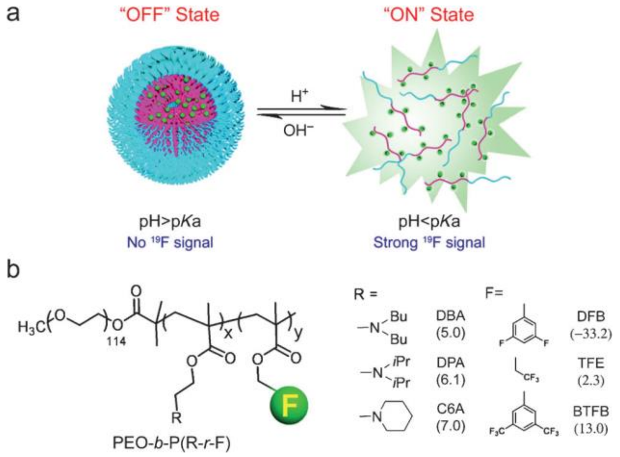

Figure 79: a) Schematic of assembled micelle at pH>pKa and of unimers at pH<pKa. B) Structural formula of diblock copolymer containing a pH sensitive segment (R) and a ^{19}F reporter segment (F). Image taken from Huang et al.[114]

By adapting the copolymers used to form the unimers, a number of different switches were developed with different ^{19}F signals and that switch "on" at different pH values. Using a combination of these probes, Huang *et al*. were able to determine a sample's pH to a specific range with a unique combination of observed signals, as shown below in Figure 80. This may be possible to apply to a hyperpolarised sample if the hyperpolarised signal was suppressed in a similar manner to that shown by Huang *et al*. or the hyperpolarisation step was prevented at a specific pH.

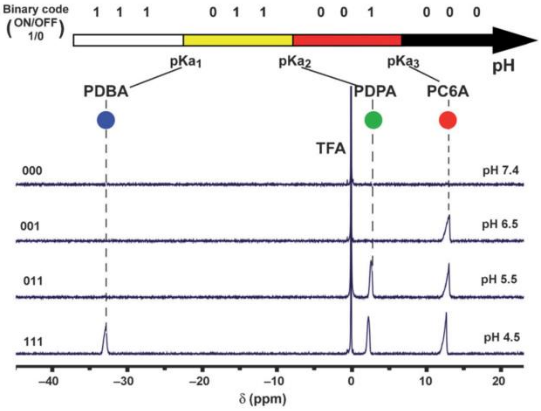

Figure 80: ^{19}F spectra of a mixture of three pH sensitive probes in acetate buffers of different pH values. Trifluoroacetic acid was used as an external reference. Binary code system shown above shows how detection of different signals indicates the pH range of a sample. Taken from Huang *et al.*[114]

Martinez *et al.*[115] used a pH sensitive T_1-relaxation contrast agent ($[Gd(1,4,7,10\text{-tetraazacyclododecane-}1,4,7,10\text{-tetraaminophosphonate})]^{5-}$) to measure the pH. As the relaxation caused by this contrast agent would be dependent on the concentration of the agent as well as the pH, the local concentration needed to be determined *in vivo*. To overcome this, an orthogonal pH insensitive contrast agent ($[Dy(1,4,7,10\text{-tetraazacyclododecane-}N,N',N'',N'''\text{-tetrakis(methylenephosphonic acid)})]^{5-}$), which is assumed to have a similar pharmacological profile, allowed measurement of this parameter. This gave the concentration of $[Gd(1,4,7,10\text{-tetraazacyclododecane-}1,4,7,10\text{-tetraaminophosphonate})]^{5-}$ which allowed a measurement of the pH to be made. Whilst a relaxation mechanism is unsuitable for SABRE hyperpolarised contrast agents, use of a pH insensitive probe in parallel with a pH sensitive probe could improve the reliability of pH measurements.

Garlick *et al.*[116] used a correlation between the intracellular phosphorus (P_i) chemical shift and pH to measure the pH of a rat's heart during a perfusion experiment. The P_i chemical shift depends on pH as it is determined by the equilibrium of HPO_4^{2-} and $H_2PO_4^-$. Comparison of the measured shift to a calibration curve of P_i chemical shift against pH allowed for determination of the pH. From the previous findings on the effect of pH on SABRE substrates

(Chapter 4), this is likely to be a viable method for the use of SABRE hyperpolarised substrates as a pH probe.

An injection of DNP hyperpolarised ^{13}C labelled carbonate allows for pH mapping in a slightly different manner. The carbonate is rapidly converted to carbon dioxide by carbonic anhydrase. The equilibrium position of these two species in solution is dependent on pH – by measuring the ratio of the two using NMR it is possible to get an idea of the pH of the system. Instead of measuring the averaged chemical shift, Gallagher et al.[111] compared the relative signal from each species. This example shows the viability of a hyperpolarised pH probe and its ability to rapidly determine the *in vivo* pH in a non-invasive manner (Figure 81).

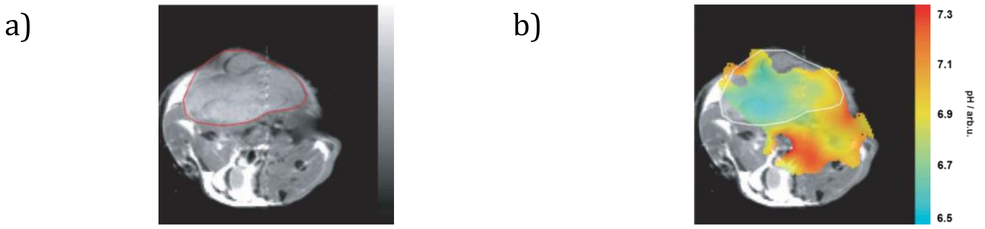

Figure 81: a) ^{1}H magnetic resonance image of a mouse with a subcutaneously implanted tumour (outlined) b) pH map of the same animal calculated from the ratio of the $H^{13}CO_3^-$ and $^{13}CO_2$ voxel intensities in ^{13}C images collected 10 s after intraveneous injection of 600 mM hyperpolarised $H^{13}CO_3^-$.Taken from Gallagher *et al*.[111]

5.1.4 SABRE as a pH mapping technique

SABRE has the potential to be applied as a molecular imaging technique, and development of it as a pH probe would create a specialisation that could see significant use in a clinical setting. This could be realised in the form of Huang's fluorine probe[114] by switching a hyperpolarised signal on and off at a given pH, by following conversion of a substrate in the style of Gallagher,[111] or by following a change in chemical shift as demonstrated by Garlick.[116] Whilst the change in enhancement previously seen is a less practical method of determining the pH, it is worth considering as a substrate that is not dependent on pH could be used to "normalise" the signal as seen for pH dependent relaxation agents.[115] If this is the technique of choice, a distinction must be made between the effects of the polarisation pH and the measurement pH.

This chapter will consider the use of the substrates discussed in chapter 4 as contrast agents and their further application to pH mapping and will look at combining SABRE-MRI with other imaging techniques.

5.2 The effect of pH on SABRE polarised ^{1}H imaging of 3-hydroxypyridine

Whilst the SABRE polarisation of 3-hydroxypyridine (**3OHPy**) has shown significant pH dependence when collecting NMR spectra, this may not translate directly to the imaging properties of the system. Using a flow system with an integrated imaging cell, hyperpolarised images of **3OHPy** in d_4-methanol were collected across a pH range (Figure 82). The pH was varied by addition of base to the sample directly and measured using a pH probe after the images were collected.

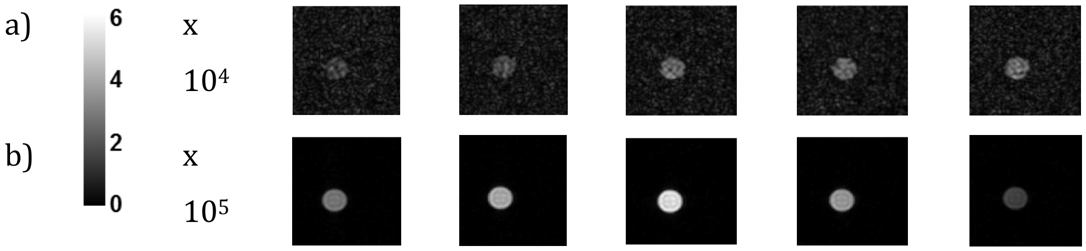

c) Measured pH / arb.u. 6.7 7.6 9.5 10.0 12.3

Figure 82: Single ^{1}H image of a 5.35 mm diameter imaging cell containing 5 mM **1-cod-Cl** and 100 mM **3OHPy** in d_4-methanol. pH was increased by addition of Cs_2CO_3 a) Image collected from a 2 mm slice after thermal equilibrium at 9.4 T was achieved b) Hyperpolarised image collected from a 2 mm slice after 6 s polarisation at 65 G by bubbling pH$_2$ through the sample c) pH measured for sample using pH meter

A comparison of the signal to noise ratio (SNR) for these images shows the effect of pH on the SABRE hyperpolarised imaging of **3OHPy**. The SNR has a roughly bell shaped trend with respect to pH (Figure 83), with lower SNR under native and extremely basic conditions and higher SNR at intermediate pH values.

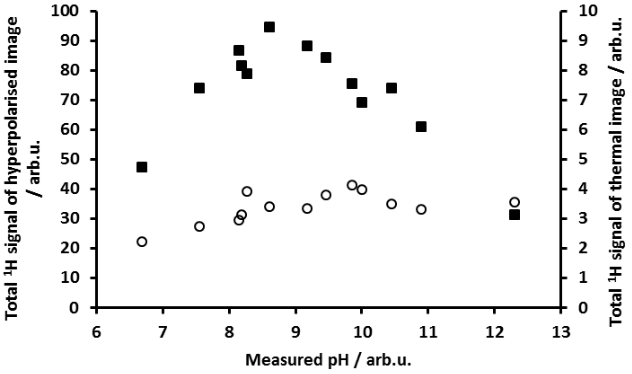

Figure 83: Signal measured for ^1H image collected from a 2 mm transverse slice of a 5.35 mm diameter imaging cell containing 5 mM **1-cod-Cl** and 100 mM **3OHPy** in d_4-methanol across a range of pH values. pH was increased by addition of Cs_2CO_3. ○ indicates thermal signal obtained after equilibration in the high field of the NMR magnet ▪ indicates hyperpolarised signal obtained after bubbling with pH$_2$ for 6 s at 65 G prior to rapid shuttling into the magnet followed by interrogation.

This trend is quite different to that seen for the enhancement collected by NMR. The thermal signal intensity should follow Equation 4.

$$S = \rho \, e^{\frac{-t}{T_2}} \qquad \text{(Equation 4)}$$

Equation 4 : S is the MRI signal intensity, ρ is the proton density, t is the experiment time and T_2 is the transverse relaxation constant

For the thermal images, ρ and t are constant values. As the thermal signal intensity increases with increasing pH we can conclude that T_2 increases with increasing pH for this sample. As the hyperpolarised images do not follow the same trend as the thermal images, another factor must also be dependent on pH. The proton density, ρ, incorporates both the number of protons and the hyperpolarisation. Whilst the number of protons does not change it has been shown that the hyperpolarisation changes as a function of pH. In the hyperpolarised images ρ should display a similar dependency on pH as was seen for the NMR enhancement in chapter 4.

The initial increase in signal intensity of the hyperpolarised images can be attributed to the increase in T_2, from pH = 8.5 onwards the decrease in signal intensity is due to the decrease in ρ dominating.

These results are encouraging – they show that pH has a definite effect on the SABRE polarisation seen in an image as the signal received for the hyperpolarised images follows a different trend to that received for the thermal images. They also confirm that SABRE can be used to produce images in less than one second. However, these results have some flaws when considering their application to a SABRE enhanced pH probe *in vivo*:

- These results were collected with no background signal – in the body there is significant signal from the protons of water which may require a greater received signal to overcome.
- Whilst there is a detectable difference in the SNR as the pH changes, this will be complicated *in vivo* as concentration changes also affect the SNR and will make it difficult to distinguish between the two effects. This could be solved using a second probe as Martinez *et al*.[115] did, although this probe would have to be pH independent.
- The bell-shaped curve results in a given signal intensity corresponding to multiple pH values.

5.3 The effect of pH on ^{13}C SABRE polarisation

5.3.1 Application of heteronuclei as pH probes

An alternative method to using the hyperpolarised signal intensity to follow pH would be to use the hyperpolarised signals to follow the change in chemical shift on addition of base. As shown by Garlick *et al*. this can be used to reliably determine the pH of a sample,[116] and Gallagher *et al*. have shown how such a hyperpolarised signal can be used to create a chemical shift map *in vivo* using DNP.[111]

Both Gallagher and Garlick used heteronuclei in their studies. Using these nuclei for a hyperpolarised study has some advantages over the use of ^{1}H nuclei:

- *Reduced background signal* – the majority of the human body is made up of water which only appears in the proton image, not in heteronuclear imaging. This will increase the contrast between hyperpolarised signal and residual thermal signal improving image quality.
- *Wider chemical shift range*– the typical range considered for ^{13}C nuclei is an order of magnitude greater than that typically considered for ^{1}H nuclei. This wider range of chemical shifts may also be reflected in the change in chemical shift upon pH titration. In Garlick's pH titration of P_i a 2 ppm difference in the ^{31}P chemical shift was observed over a pH range of 9 units.[116] In contrast, in this study a maximum of 0.2 ppm chemical shift difference for the ^{1}H resonances was seen during a pH titration covering 4 pH units. Increasing the chemical shift difference will improve pH resolution.
- *Longer T_1 values* – The T_1 of heteronuclei can often be significantly longer than those seen for protons,[117] this is particularly true of quarternary ^{13}C nuclei.

SABRE polarisation of heteronuclei has been published previously (^{13}C,[8, 42] ^{15}N,[8] ^{19}F,[8] ^{31}P[11]), although pH effects have not previously been explored.

5.3.2 The effect of pH on the ^{13}C SABRE polarisation of 3-hydroxypyridine

5.3.2.1 ^{13}C SABRE polarisation of 3-hydroxypyridine

In addition to the large polarisation of the protons, under SABRE conditions the carbon nuclei of **3OHPy** are also polarised.

The largest signal is received from the carbon in the C_3 position of **3OHPy** (identified in Figure 84) – likely due to its slower relaxation as it is a tertiary carbon and cannot relax through any attached protons – and as a result it is this signal which will referred to throughout this study.

It was possible to identify all carbon environments of the free substrate in a single decoupled hyperpolarised scan, and the proton-carbon couplings could be calculated from an Insensitive Nuclei Enhanced by Polarisation Transfer (INEPT) spectrum (Figure 85). The carbon signals were confirmed and assigned using ^1H-^{13}C HMQC spectra.

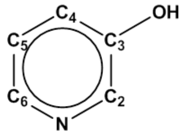

Figure 84: Schematic showing **3OHPy** with carbon environments labelled

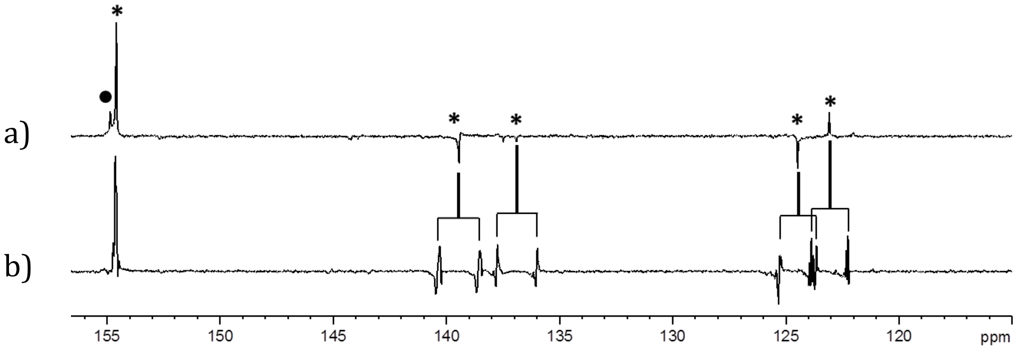

Figure 85: SABRE hyperpolarised ^{13}C spectra of a sample containing 50 mM **3OHPy**, 5 mM **1-cod-Cl** in d_4-methanol under 3 bar pH$_2$. a) INEPT decoupled and refocused spectrum b) INEPT coupled spectrum. * indicates peaks corresponding to free substrate, ● indicates substrate bound cis to NHC. $^1J_{CH}$ splitting trees have been added as annotations.

As with the ^1H enhancement, the signal-to-noise ratio of the ^{13}C signal varies with substrate:catalyst ratio and catalyst concentration, although the trends differ slightly in comparison to the ^1H enhancement (Figure 86). As seen for the ^1H enhancement, the ^{13}C signal to noise ratio has an ideal substrate:catalyst ratio, although this is higher for ^{13}C than for ^1H.

The ^{13}C signal-to-noise ratio has a sigmoidal trend with respect to the catalyst concentration – increasing up to a maximum of 100 at 10 mM before plateauing. This is significantly different to the trend seen for ^1H enhancement which showed a maximum enhancement at lower catalyst concentrations – the main reason for this is that the ^{13}C signal-to-noise ratio does not incorporate a thermal measurement due to the low intensity of the ^{13}C thermal signal preventing its distinction from noise in a single scan.

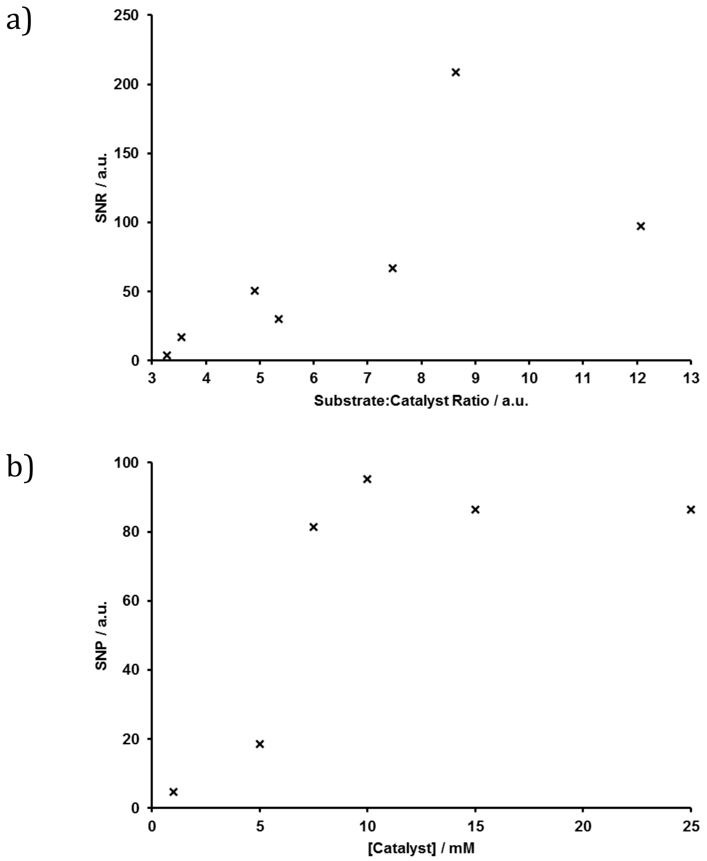

Figure 86: Graphs showing a) the effect of substrate:catalyst ratio at a constant catalyst concentration of 5 mM **1-cod-Cl** b) the effect of catalyst concentration at a constant substrate:catalyst ratio of 5:1 on SABRE enhanced ^{13}C INEPT SNR of **3OHPy**

5.3.2.2 The effect of base addition on ^{13}C SABRE polarisation of 3-hydroxypyridine

It would be reasonable to expect the carbon polarisation to be affected in a similar manner as the proton polarisation. By comparing the two extremes of the pH scale it can be seen that, like the proton signal, the carbon signal shifts with pH and has a reduced intensity at higher pH values (Figure 87).

The addition of base causes a greater deviation of the carbon signal from its native shift than seen for the proton signal. The C_3 carbon signal shifts downfield by almost 4.5 ppm over a pH range of 3.5 units (Figure 88). This larger change in chemical shift means that a greater resolution of the pH can be achieved using ^{13}C than for ^{1}H, in addition to the inherent benefits of using a non-proton nucleus.

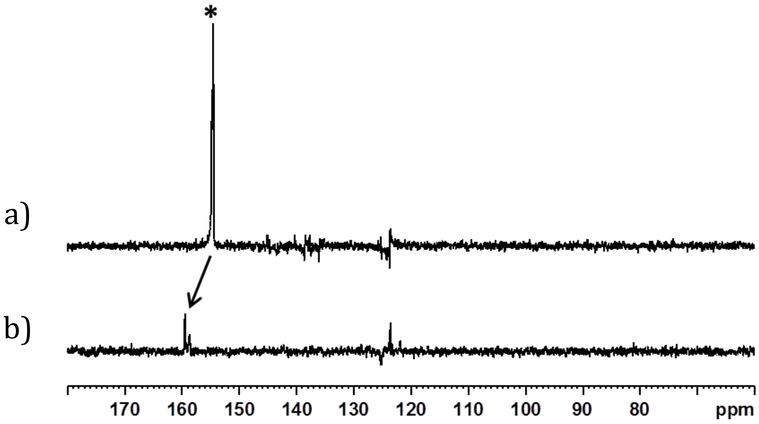

Figure 87: Comparison of ^{13}C INEPT spectra for two samples of 25 mM **3OHPy** and 5 mM **1-cod-Cl** in d_4-methanol under 3 bar pH$_2$ after 10 s polarisation at 65 G. a) contains no additional base, b) contains excess Cs_2CO_3

The shift of the carbon indicates a more deshielded nucleus at higher pH values – this is in contrast to the protons of the substrate which became more shielded. As the hydroxyl group becomes deprotonated, the oxygen will donate more electron density into the carbon-oxygen bond. This will result in the carbon-oxygen bond having more double bonding character in the charged oxyanion species than in the neutral alcohol species – this will increase polarisation of the bond and deshield the carbon nucleus.

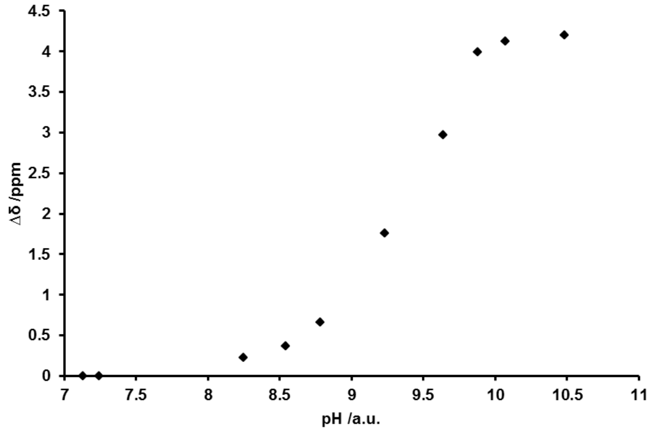

Figure 88: Graph showing the effect of addition of Cs_2CO_3 on the chemical shift of C_3 of **3OHPy**

The overall reduction in enhancement upon addition of Cs_2CO_3 seen for the protons of 3-hydroxypyridine is repeated for the polarised signal of C_3 (Figure 89).

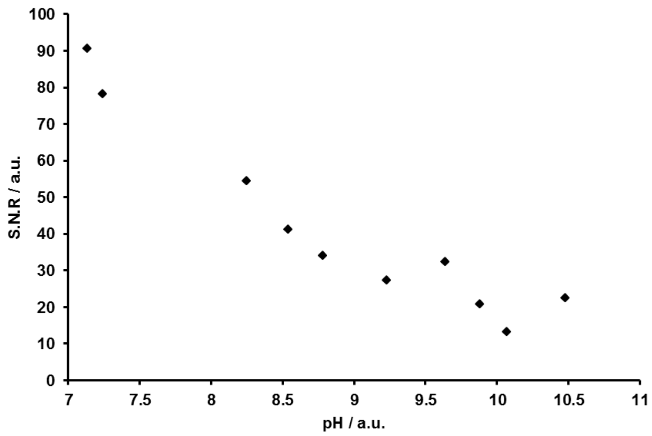

Figure 89: Graph showing the effect of addition of base on the ^{13}C signal to noise ratio of hyperpolarised **3OHPy**

5.3.3 The effect of pH on ^{13}C SABRE polarisation of 4-hydroxypyridine

Whilst the polarisation of 4-hydroxypyridine (**4OHPy**) is much lower than for **3OHPy**, the carbon signal of **4OHPy** can also be used as an indicator of pH. The C_4 carbon signal, indicated in Figure 90, is the only signal that is visible at all pH values tested. As with **3OHPy,** this visible signal is due to a tertiary carbon with no attached protons.

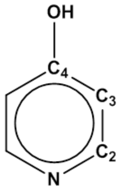

Figure 90: Schematic of **4OHPy** with carbon environments labelled

The C_4 signal of **4OHPy** moves to a lower chemical shift (Figure 91,Figure 92) upon addition of base, this indicates an increase in shielding which corroborates the observations made for the protons of **4OHPy** and is due to the reduction in double bonding character of the carbon-oxygen bond. The signal received was also significantly improved for the high pH sample – again this follows the effect seen for ^1H polarisation.

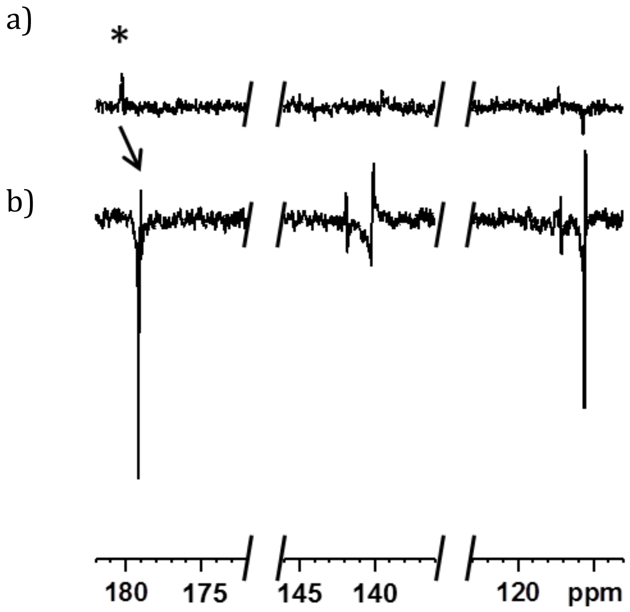

Figure 91: Comparison of ^{13}C INEPT spectra for two samples of 100 mM **4OHPy** and 5 mM **1-cod-Cl** in d_4-methanol under 3 bar $p$$H_2$ after 10 s polarisation at 65 G. a) contains no additional base, b) contains excess Cs_2CO_3. * indicates C_4

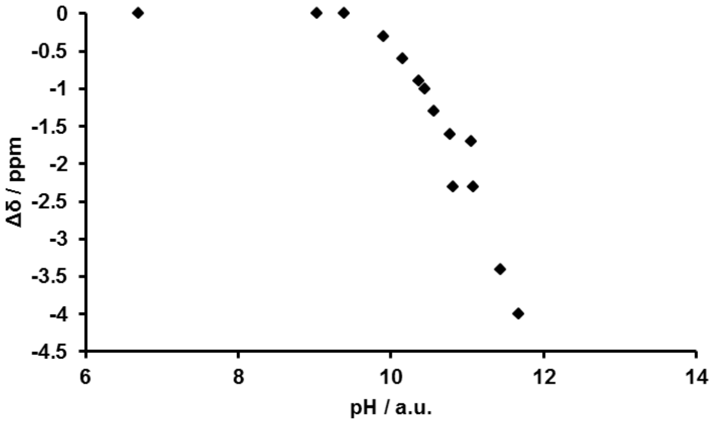

Figure 92: Graph showing the effect of addition of Cs_2CO_3 on the chemical shift of C_4 of **4OHPy**

5.3.4 SABRE polarised ^{13}C NMR of 3-methoxypyridine and 4-methoxypyridine

Both 3-methoxypyridine (**3OMePy**) and 4-methoxypyridine (**4OMePy**) exhibited good carbon polarisation in addition to their significant proton polarisation (Figure 93). This polarisation was also carried across the oxygen bond into the methyl ether carbon (C_7 of **3OMePy** and C_5 of **4OMePy**, indicated in Figure 94).

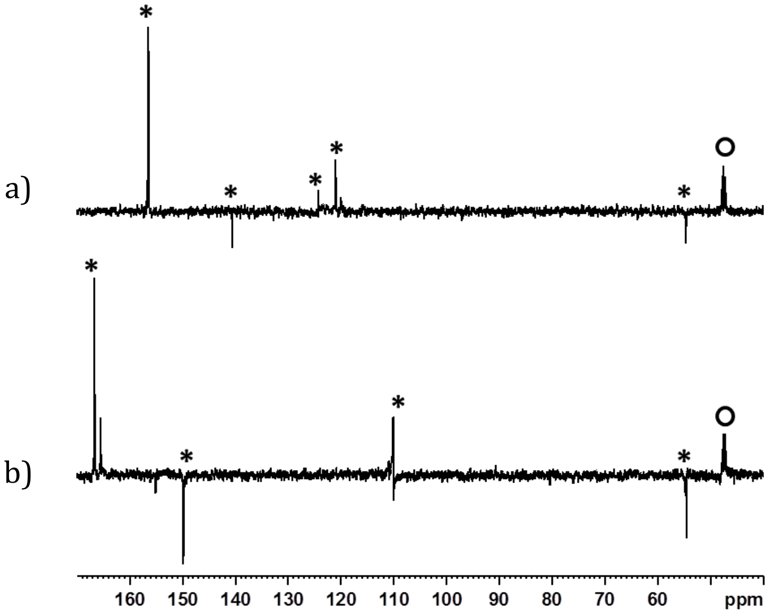

Figure 93: SABRE hyperpolarised ^{13}C INEPT spectra of a) **3OMePy** and b) **4OMePy**. Each sample contained 25 mM of substrate, 5 mM **1-cod-Cl** in *d₄*-methanol under 3 bar pH_2 and was polarised for 10 s at 65 G. * Indicates substrate peaks, ○ indicates residual solvent peak

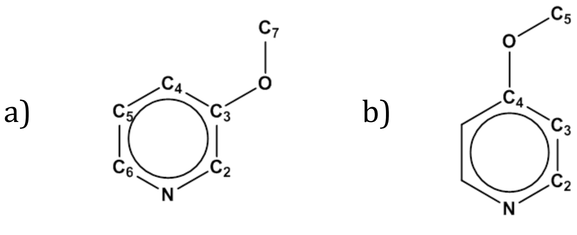

Figure 94: Schematic of a) **3OMePy** b) **4OMePy** with carbon environments labelled

Whilst both **3OMePy** and **4OMePy** showed good carbon polarisation, the sudden drop in their proton polarisation upon addition of Cs_2CO_3 was reflected in the polarised ^{13}C signal as well. This made a pH titration of their carbon signals impractical.

5.4 SABRE polarisation of 2-fluoro-3-hydroxypyridine: a model for the PET agent Nifene

Following the successful polarisation of **3OHPy** and **3OMePy**, 2-fluoro-3-hydroxypyridine (**2F3OHPy**) (Figure 95) was selected as a model for the PET agent Nifene.

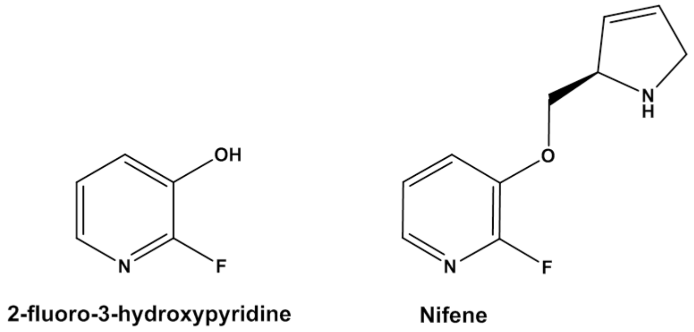

Figure 95 : Schematic of **2F3OHPy** and Nifene

As it has already been used in pre-clinical studies,[118, 119] polarisation of Nifene would advance the development of SABRE as a medical imaging technique significantly. When used for PET Nifene must be isotopically labelled with ^{18}F – this is expensive, increasing the cost of imaging. If used for MRI purposes this labelling would be unnecessary as the signal could come from the protons, carbon nuclei or the naturally abundant ^{19}F nuclei. Alternatively, polarisation of ^{18}F labelled Nifene could create the possibility of a simultaneous SABRE-MRI/PET scan to offer even more diagnostic information from a single appointment.

Initial attempts to polarise **2F3OHPy** were unsuccessful – the substrate did not bind to the precatalyst and activation did not occur, even after 48 hours under hydrogen. Addition of acetonitrile (**MeCN**) as a cosubstrate[42] allowed rapid activation and polarisation as the weakly bound **MeCN** could be displaced by **2F3OHPy**. However the overall polarisation was low on all nuclei. The proton polarisation was approximately 10 fold on two of the sites (Figure 96), and the

^{19}F polarised signal was indistinguishable from the thermal signal. This suggests that the polarisation of Nifene would also be poor and that other substrates would be more suitable for the application of SABRE in a medical context.

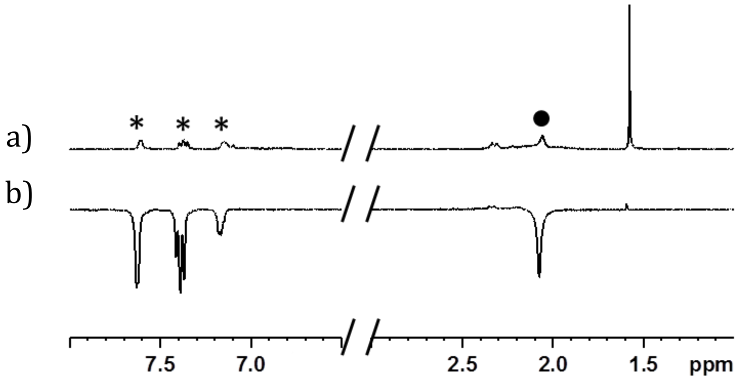

Figure 96: ^{1}H spectra of 25 mM **2F3OHPy**, 25 mM **MeCN**, 5 mM **1-cod-Cl** in d_4-methanol under 3 bar pH_2. a) Thermal spectrum b) SABRE Hyperpolarised spectrum after 10 s polarisation at 65 G. * indicates **2F3OHPy** signals, ● indicates **MeCN** signals

5.5 Conclusions

3-hydroxypyridine was studied to understand the effect of pH on SABRE hyperpolarisation in an imaging context. Initially, increasing the pH of the hyperpolarised sample resulted in an increase in signal intensity to approximately double the native signal intensity. At pH > 8.5 the signal intensity decreased with increasing basicity. This suggests that whilst the pH of a sample has a noticeable effect in the recorded images, the measurement of signal intensity alone is not a viable method for developing a SABRE enhanced pH imaging probe as the signal intensity cannot be specifically assigned to a single pH.

The enhanced signal due to SABRE hyperpolarisation of 3-hydroxypyridine and 4-hydroxypyridine was also used to study the effect of pH on their ^{13}C resonances using NMR spectroscopy. The hyperpolarised ^{13}C signal-to-noise ratio of 3-hydroxypyridine was affected in a similar manner to the ^{1}H signal enhancement. The tertiary carbon environment of each substrate was shown to be pH sensitive by recording its chemical shift. The tertiary carbon environment of 3-hydroxypyridine became deshielded under basic conditions – this was indicated by a chemical shift over 4 ppm higher at pH 10.5 than under native conditions of pH 7.1. The tertiary carbon environment of 4-hydroxypyridine became shielded under basic conditions – this was indicated by a chemical shift 4 ppm lower at pH 11.6 than under native conditions at pH 6.6. Exploiting this large chemical shift range could be a route to application of SABRE for the development of a pH probe.

Further application of this technique is currently limited by the low signal intensity of ^{13}C MRI, even when hyperpolarised. Whilst measurements could be recorded using NMR spectroscopy, MRI measurements of the ^{13}C signal of SABRE hyperpolarised 3-hydroxypyridine were unsuccessful. ^{13}C labelling of the carbon in the C_3 position of 3-hydroxypyridine in conjunction with SABRE hyperpolarisation could overcome this problem and result in a pH sensitive probe for basic conditions. Alternatively, development of a probe utilising a different nucleus, such as phosphorous which has shown some success in SABRE hyperpolarised imaging,[11] could provide a route to further developing this application.

6. Experimental Methods

6.1 Instrumentation and Reagents

6.1.1 NMR spectrometers

Characterisation of complexes and substrates by NMR spectroscopy has been completed using a number of Bruker spectrometers including an Avance III 400 MHz and Avance III 500 MHz where the ^{1}H frequency is measured at 400.1 MHz and 500.1 MHz respectively. These spectrometers have also been used for the calculation of thermodynamic parameters and for hyperpolarisation experiments. Data acquisition and processing was carried out using the Bruker program TopSpin versions 3.2.3 and 3.2.6.

MRI images were collected using a Bruker Avance III 400 MHz spectrometer and the Bruker software ParaVision. The sample was inserted into the spectrometer using hyperpolarisation method 2 described below, allowing for ½ s settling time inside the spectrometer. A RARE imaging sequence[120] was used to collect the images using a 64 x 64 matrix. The field of view was 30 x 30 mm with a slice thickness of 2 mm.

During the course of these experiments three NMR solvents are used: d_4-methanol is referenced to residual CHD_2OD, d_2-dichloromethane (DCM) is referenced to residual $CDHCl_2$, d_6-dimethylsulphoxide (DMSO) is referenced to residual $CD_3S(O)CD_2H$

6.1.2 Preparation of *para*hydrogen

*Para*hydrogen was prepared by cooling hydrogen gas over Fe_2O_3.[24] Two systems were used during this project, the first was made in house and this system used a hydrogen cylinder as a source of hydrogen. The second was provided by Bruker and had a self-contained hydrogen generator that produced the hydrogen used.

Whilst multiple *para*hydrogen sources were used over the course of the project, within each study the source was consistent.

6.1.3 Source of solvents and chemicals

General solvents for synthetic chemistry were distilled from an appropriate drying agent under N_2 as necessary. Deuterated solvents were obtained from Sigma-Aldrich and used as supplied. High purity gases were obtained from BOC and used as received.

Iridium chloride was obtained from Precious metals online. Ferroceneacetonitrile was obtained from Alfa Aesar. 2-fluoro-3-hydroxypyridine was obtained from Fluorochem. Remaining reagents were obtained from Sigma-Aldrich and used as supplied.

6.2 Standard methods

6.2.1 General synthetic techniques

All synthetic procedures were conducted under an inert atmosphere of nitrogen using standard Schlenk line techniques.

6.2.2 Hyperpolarisation method 1 – Shake method

Investigations using hyperpolarisation method 1 were completed using a 5 mm NMR tube fitted with a J Young valve. A solution of catalyst (5 mM, 3.1×10^{-6} mol), substrate (25 mM, 1.6×10^{-5} mol) and solvent (0.6 ml) was used unless otherwise stated. The sample was degassed using standard techniques and activated by hydrogen gas at a pressure of 3 bar.

For each measurement, the headspace of the NMR tube was evacuated and replenished with 3 bar *para*hydrogen. The sample is then shaken using the fringe field of the magnet to provide the polarisation transfer field before being rapidly inserted into the magnet for interrogation by NMR spectroscopy. A single scan ^1H NMR spectrum is collected with a 90^o pulse as standard.

6.2.3 Hyperpolarisation method 2 – Flow method

Samples investigated using hyperpolarisation method 2 were polarised using a flow system as described in the literature.[12]

A polarisation chamber was charged with a solution of substrate (100 mM, 3.2×10^{-4} mol), catalyst (5 mM, 1.6×10^{-5} mol) and deuterated solvent (3 mL), unless otherwise stated. *Para*hydrogen was bubbled through the solution at a pressure of 6 bar for 6 s. This solution was then transferred into the spectrometer equipped with a flow probe head (cell volume = 200 μL) for interrogation by NMR using nitrogen as a flow gas.

Once interrogated, the solution was returned to the polarising chamber with a nitrogen flow gas and the process repeated as required.

It is standard to activate a sample being studied by method 2 in the polariser itself.

The applied magnetic field is controlled by a coil surrounding the reaction chamber which can produce static fields in the range of -150 to 150 G.

6.2.4 Calculation of enhancement factors

For calculation of the enhancement of signals Equation 5 was used.

$$E = \frac{S_{pol}}{S_{unpol}} \qquad \text{(Equation 5)}$$

Equation 5: Calculation of signal enhancement (E). S_{pol} is the signal calculated for the polarised measurement, S_{unpol} is the signal calculated for the thermal measurement.

Where E = enhancement factor, S_{pol} = signal of polarised sample and S_{unpol} = signal of unpolarised (reference) sample. Experimentally, reference spectra were collected after the sample had reached thermal equilibrium within the high magnetic field of the spectrometer. The thermal and polarised spectra were collected using identical acquisition parameters.

For ^{1}H NMR measurements S_{pol} and S_{unpol} were calculated by measuring the integral of the NMR peak. For ^{13}C NMR measurements S_{pol} and S_{unpol} were calculated by measuring the signal to noise. For ^{1}H MRI measurements S_{pol} and S_{unpol} were obtained by comparing the average signal of the region containing the sample to the standard deviation of the noise region as described in Equation 6.

$$S = \frac{\mu_{sample}}{\sigma_{background}} \qquad \text{(Equation 6)}$$

Equation 6: Calculation of signal to noise ratio (S) from an MRI image. μ_{sample} is the mean signal of the sample region and $\sigma_{background}$ is the standard deviation in the background signal

Owing to the nature of *para*hydrogen derived hyperpolarisation, a sample interrogated by NMR in the presence of parahydrogen may result in both enhanced absorption signals and enhanced emission signals. Consequently, the integral for an enhanced emission peak is negative. This sign has been carried through in the equation to the resulting calculated enhancement. This means that where a negative enhancement is quoted the peak was in emission.

6.3 Reactions

6.3.1 Bis(1,5-cyclooctadiene)diiridium(I) dichloride -[Ir(cod)Cl]$_2$

Synthesis adapted from Herde *et al.*[121]

Iridium chloride (2.00 g, 5.67 mmol) was dissolved in water (30 ml) and isopropanol (60 ml). The solution was stirred for 45 minutes before 1,5-cyclooctadiene (7 ml, 57.07 mmol) was added. The reaction was stirred for a further 15 minutes before being heated to reflux for 18 hours. After cooling the solvent was removed under vacuum and the sample cooled to 3 ^{o}C for 18 hours. The precipitate was collected and washed with ice cold methanol (2 x 5 ml) to produce a red solid product (0.93 g, 1.38 mmol, 49 %).

6.3.2 (1,5-cyclooctadiene)(methoxy)iridium(I) dimer - [Ir(μ-OMe)(cod)]$_2$

Synthesis adapted from Uson *et al.*[122]

[Ir(cod)Cl]$_2$ (0.90 g, 1.34 mmol) was dissolved in methanol (50 ml). Potassium hydroxide (0.153 g, 2.73 mmol) was dissolved in methanol (10 ml). The potassium hydroxide solution was added to the iridium solution and stirred for 1 hour. The solution initially turned red before producing a yellow precipitate. The solution was cooled in a freezer for 1 hour and the precipitate collected using a sinter. After washing with water (5 x 10 ml) and ice cold methanol (2 x 2 ml) the solid was dried under vacuum to give the product; a bright yellow solid (0.58 g, 0.87 mmol, 65 %)

6.3.3 (1,5-cyclooctadiene)(1,3-bis(2,4,6-trimethylphenyl)imidazole-2-ylidene)Iridium(I) chloride - [Ir(IMes)(cod)Cl]

Synthesis adapted from Torres *et al.*[123]

$[Ir(\mu\text{-}OMe)(cod)]_2$ (0.58 g, 0.87 mmol) and 1,3-bis(2,4,6-trimethylphenyl)imidazolium chloride (0.61 g, 1.79 mmol) were dissolved in acetone (30 ml) and stirred for 1 hour. The solvent was removed under vacuum to give a yellow solid. The product was purified using a silica column (DCM eluent) and the solvent removed under reduced pressure. The solid was triturated with diethyl ether and the solvent removed under reduced pressure to yield a yellow solid (1.05 g, 1.63 mmol, 94 %)

6.3.4 (4-pyridyl)ferrocene

Synthesis adapted from Braga *et al.*[68]

4-bromopyridinium hydrochloride (0.20 g, 5.14 mmol) was dissolved in dioxane (6.5 ml). 1 M aqueous sodium carbonate (5 ml, 5.03 mmol) was added to the solution and the suspension heated to 50 ^oC. $Pd(dppf)Cl_2$ (0.006 g, 0.007 mmol) was added to the solution.

A solution of ferrocene boronic acid (0.10 g, 0.44 mmol), 3 M sodium hydroxide (0.24 ml) and DME (3 ml) was prepared.

After addition of the DME solution to the dioxane solution the mixture was heated to reflux at 100 ^oC for 3 days. The reaction was hydrolysed with ice water and extracted into DCM (3 x 10 ml), washed with ammonium chloride, water and then dried using sodium sulfate. The resulting product was purified by flash silica column chromatography in 0 -> 2% MeOH in DCM followed by Biotage column chromatography in 0 -> 20% EtOAc in DCM to give an orange solid product (10.2 mg, 8.9 %)

6.4 NMR data for substrates

6.4.1 3-aminopyridine (3AmPy)

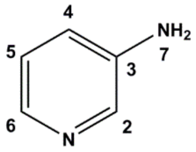

Figure 97: Labelled schematic of **3AmPy**

^{1}H {d_4-methanol, 400.1 MHz, 298 K} δ: 7.97 (dd, 1 H, H$_2$, J = 0.7, 2.7 Hz), 7.79 (dd, 1 H, H$_6$, J = 1.4, 4.7 Hz), 7.15-7.07 (m, 2 H, H$_4$ & H$_5$)

^{1}H {d_4-methanol, 500.1 MHz, 243 K} δ: 7.90 (dd, 1 H, H$_2$, $^4J_{HH}$ = 2.7 Hz, $^5J_{HH}$ = 0.7 Hz), 7.78 (dd, 1 H, H$_6$, $^3J_{HH}$ = 4.7 Hz, $^4J_{HH}$ = 1.4 Hz), 7.17 (ddd, 1 H, H$_5$, $^3J_{HH}$ = 4.7, 8.2 Hz, $^5J_{HH}$ = 0.7 Hz), 7.10 (ddd, 1 H, H$_4$, $^3J_{HH}$ = 8.2 Hz, $^4J_{HH}$ = 1.4, 2.7 Hz,)

^{1}H {d_2-DCM, 500.1 MHz, 298 K} δ: 8.10 (d, 1 H, H$_2$, $^4J_{HH}$ = 2.7 Hz), 7.99 (d, 1 H, H$_6$, $^3J_{HH}$ = 4.7 Hz), 7.09 (dd, 1 H, H$_5$, $^3J_{HH}$ = 4.7, 8.2 Hz), 7.09 (dd, 1 H, H$_4$, $^3J_{HH}$ = 8.2 Hz, $^4J_{HH}$ = 2.7 Hz), 3.76 (br s, 2 H, H$_7$)

^{1}H {d_2-DCM, 500.1 MHz, 243 K} δ: 8.06 (d, 1 H, H$_2$, $^4J_{HH}$ = 2.7 Hz), 7.96 (dd, 1 H, H$_6$, $^3J_{HH}$ = 4.7 Hz, $^4J_{HH}$ = 1.4 Hz), 7.10 (dd, 1 H, H$_5$, $^3J_{HH}$ = 4.7, 8.2 Hz), 7.01 (ddd, 1 H, H$_4$,$^3J_{HH}$ = 8.2 Hz, $^4J_{HH}$ = 1.4, 2.7 Hz), 3.85 (br s, 2 H, H$_7$)

^{13}C {d_4-methanol, 100.6 MHz, 298 K} δ: 145.0 (C$_3$), 136.8 (C$_6$), 135.6 (C$_2$), 123.8 (C$_4$/C$_5$), 121.5 (C$_4$/C$_5$)

^{13}C {d_4-methanol, 125.8 MHz, 243 K} δ: 145.5 (C$_3$), 136.3 (C$_6$), 135.1 (C$_2$), 124.3 (C$_5$), 121.5 (C$_4$)

^{15}N {d_4-methanol, 50.7 MHz, 298 K} δ: 297.7 (N$_{Ar}$)

^{15}N {d_4-methanol, 50.7 MHz, 243 K} δ: 295.8 (N$_{Ar}$)

^{15}N {d_2-DCM, 50.7 MHz, 298 K} δ: 49.1 (N$_{NH}$)

^{15}N {d_2-DCM, 50.7 MHz, 298 K} δ: 50.7 (N$_{NH}$)

6.4.2 ferroceneacetonitrile (FcMeCN)

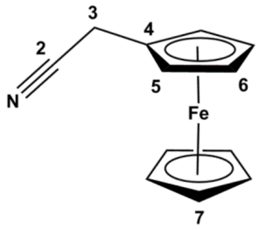

Figure 98: Labelled schematic of **FcMeCN**

^{1}H {*d_4*-methanol, 400.1 MHz, 298 K} δ: 4.28 (br s, 2 H, H_5), 4.24 (br s, 5 H, H_7), 4.20 (br s, 2 H, H_6), 3.57 (br s, 2 H, H_3)

^{13}C {*d_4*-methanol, 100.6 MHz, 298 K} δ: 118.3 (C_2), 77.9 (C_4), 68.6 (C_7), 67.8 (C_6), 67.6 (C_5), 17.2 (C_3)

^{1}H {*d_6*-DMSO, 400.1 MHz, 298 K} δ: 4.27, 4.22, 4.18, 3.65

^{13}C {*d_6*-DMSO, 100.6 MHz, 298 K} δ: 119.4, 78.6, 69, 68.2, 68.1, 17.8

MS (ESI) m/z: 225.0 (M^+), 248.0 (MNa^+)

6.4.3 (4-pyridyl)ferrocene (FcPy)

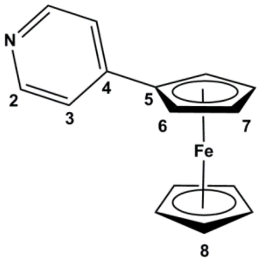

Figure 99: Labelled schematic of **FcPy**

^{1}H {*d_4*-methanol, 500.1 MHz, 298 K} δ: 8.39 (d, 2 H, H_2, $^2J_{HH}$ = 5.8 Hz), 7.57 (d, 2 H, H_3, $^2J_{HH}$ = 5.8 Hz), 4.94 (br s, 2 H, H_6), 4.53 (br s, 2 H, H_7), 4.08 (s, 5 H, H_8)

m/z = 263.9 (MH^+)

6.4.4 (4-phenyl)pyridine (PhPy)

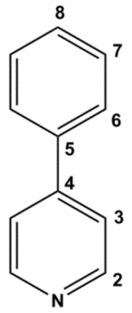

Figure 100: Labelled schematic of **PhPy**

^{1}H {*d$_4$*-methanol, 400.1 MHz, 298 K} δ: 8.59 (dd, 2 H, H_2, $^3J_{HH}$ = 4.7 Hz, $^5J_{HH}$ = 1.5 Hz), 7.77 (br d, 2 H, H_6, J = 7.8 Hz), 7.72 (dd, 2 H, H_3, $^3J_{HH}$ = 4.7 Hz, $^5J_{HH}$ = 1.5 Hz), 7.63-7.46 (m, 3 H, H_7 and H_8)

6.4.5 tris(bipyrazyl)ruthenium(II)hexafluorophosphate (Ru(bpz)$_3$)

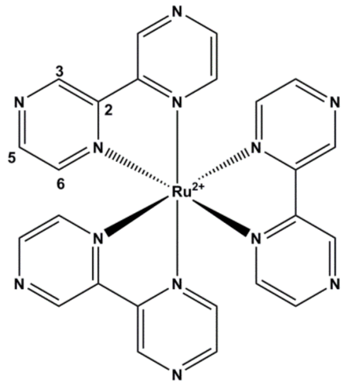

Figure 101: Labelled schematic of **Ru(bpz)$_3$**

^{1}H {*d$_4$*-methanol, 400.1 MHz, 298 K} δ: 10.05 (s, 6 H, H_3), 8.75 (d, 6 H, H_5, $^3J_{HH}$ = 2.5 Hz), 8.02 (d, 6 H, H_6, $^3J_{HH}$ = 2.5 Hz)

^{13}C {*d$_4$*-methanol, 100.6 MHz, 298 K} δ: 147.0 (C_5), 144.7 (C_6), 144.0 (C_3)

In reasonable agreement with literature.[76]

6.4.6 3-hydroxypyridine (3OHPy)

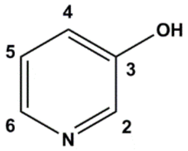

Figure 102: Labelled schematic of **3OHPy**

^1H {d_4-methanol, 500.1 MHz, 298 K} δ: 8.11 (d, 1 H, H_2, J_{HH} = 2 Hz), 8.02 (d, 1 H, H_6, $^3J_{HH}$ = 4 Hz), 7.26 (m, 2 H, H_4 + H_5)

^1H {d_4-methanol, 500.1 MHz, 243 K} δ: 8.09 (d, 1 H, H_2, J_{HH} = 2.2 Hz), 8.03 (br d, 1 H, H_6, $^3J_{HH}$ = 4.6 Hz), 7.34 (dd, 1 H, H_5, $^3J_{HH}$ = 4.6 Hz, 8.2 Hz), 7.29 (br d, 1 H, H_4, $^3J_{HH}$ = 8.2 Hz)

^{13}C {d_4-methanol, 125.8 MHz, 298 K} δ: 154.5 (C_3), 139.4 (C_6), 136.8 (C_2), 124.4 (C_5), 123.1 (C_4)

^{13}C {d_4-methanol, 125.8 MHz, 243 K} δ: 154.8 (C_3), 139.1 (C_6), 136.5 (C_2), 124.7 (C_5), 123.1 (C_4)

^{15}N {d_4-methanol, 50.7 MHz, 243 K} δ: 298.8 (N_{Ar})

6.4.7 4-hydroxypyridine (4OHPy)

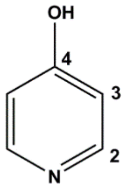

Figure 103: Labelled schematic of **4OHPy**

^1H {d_4-methanol, 500.1 MHz, 243 K} δ: 7.90 (d, H_2, $^3J_{HH}$ = 7.45 Hz), 6.53 (d, H_3, $^3J_{HH}$ = 7.45 Hz)

^{13}C {d_4-methanol, 125.8 MHz, 243 K} δ: 180.0 (C_4), 138.8 (C_2), 116.2 (C_3)

^{15}N {d_4-methanol, 50.7 MHz, 243 K} δ: 152.5 (N_{Ar})

6.4.8 3-methoxypyridine (3OMePy)

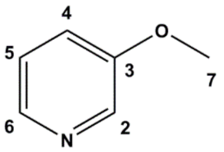

Figure 104: Labelled schematic of **3OMePy**

^{1}H {d_4-methanol, 500.1 MHz, 298 K} δ: 8.25 (d, 1 H, H_2, $^{4}J_{HH}$ = 2.7 Hz), 8.14 (dd, 1 H, H_6, $^{3}J_{HH}$ 4.6 Hz, $^{4}J_{HH}$ = 1.0 Hz), 7.45 (ddd, 1 H, H_4, $^{3}J_{HH}$ = 8.5 Hz, $^{4}J_{HH}$ = 2.7, 1.0 Hz), 7.39 (dd, 1 H, H_5, $^{3}J_{HH}$ = 8.5, 4.6 Hz), 3.90 (s, 3 H, H_7)

^{13}C {d_4-methanol, 125.8 MHz, 298 K} δ: 156.4 (C_3), 140.6 (C_6), 136.5 (C_2), 124.2 (C_5), 121.1 (C_4), 54.7 (C_7)

6.4.9 4-methoxypyridine (4OMePy)

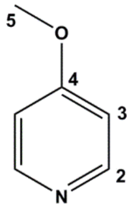

Figure 105: Labelled schematic of **4OMePy**

^{1}H {d_4-methanol, 500.1 MHz, 298 K} δ: 8.36 (d, 2 H, H_2, $^{3}J_{HH}$ = 5 Hz), 7.01 (d, 2 H, H_3, $^{3}J_{HH}$ = 5 Hz), 3.9 (s, 3 H, H_5)

^{13}C {d_4-methanol, 125.8 MHz, 298 K} δ: 166.6 (C_4), 149.8 (C_2), 110.1 (C_3), 54.5 (C_5)

^{15}N {d_4-methanol, 50.7 MHz, 298 K} δ: 275.8 (N_{Ar})

6.4.10 2-fluoro-3-hydroxypyridine (2F3OHPy)

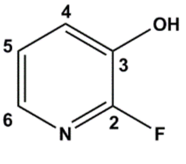

Figure 106: Labelled schematic of **2F3OHPy**

^{1}H {d_4-methanol, 500.1 MHz, 298 K} δ: 7.61 (dd, 1 H, H_6, $^{3}J_{HH}$ = 4.8 Hz, $^{4}J_{HH}$ = 1.5 Hz), 7.38 (ddd, 1 H, H_4, $^{3}J_{HH}$ = 7.8 Hz, $^{4}J_{HH}$ = 1.5 Hz, $^{4}J_{HF}$ = 10.4 Hz), 7.15 (dd, 1 H, H_5, $^{3}J_{HH}$ = 7.8, 4.8 Hz)

^{19}F {d_4-methanol, 470.6 MHz, 298 K} δ: 90.7 (d, F_2, $^{4}J_{HF}$ = 10.4 Hz)

In reasonable agreement with literature.[124]

6.5 Characterisation of catalyst precursors and active polarisation transfer catalysts

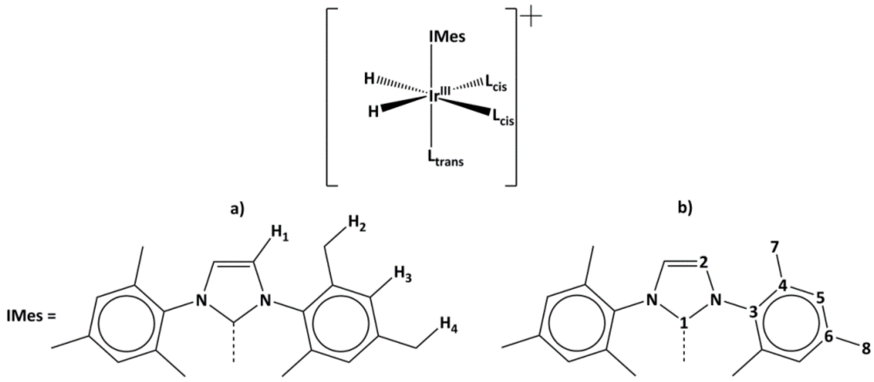

Figure 107: Labelled schematic of $[Ir(IMes)(H)_2(\mathbf{L})_3]^+$ (**1-L**) where **L** is a 2 electron donor

6.5.1 [Ir(IMes)(cod)Cl] (1-cod-Cl)

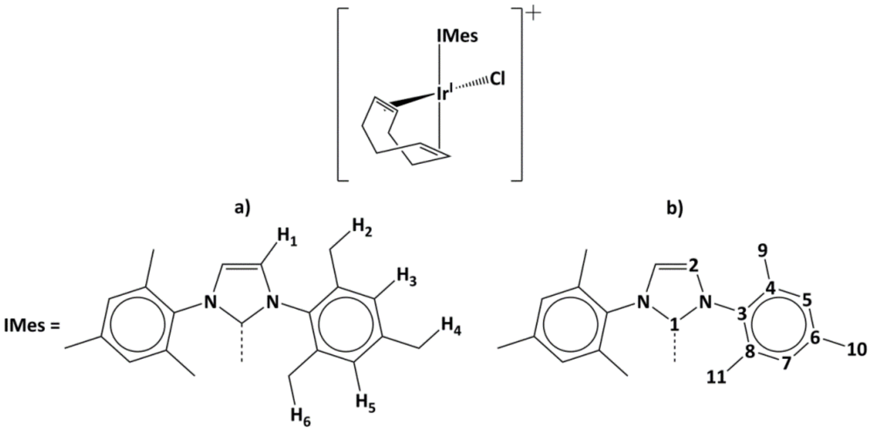

Figure 108: Labelled schematic of **1-cod-Cl**

${}^{1}H$ {d_4-methanol, 400.1 MHz, 298 K} δ: 7.24 (s, 2 H, $H_{IMes,1}$), 7.04 (br s, 4 H, $H_{IMes,3}$), 4.02 (m, 2 H, $H_{cod,CH}$), 3.10 (m, 2 H, $H_{cod,CH}$), 2.38 (s, 6 H, $H_{IMes,4}$), 2.31 (m, 6 H, $H_{IMes,2}$), 2.20 (m, 6 H, $H_{IMes,2}$), 1.60-1.78 (m, 4 H, $H_{cod,CH2}$), 1.23-1.42 (m, 4 H, $H_{cod,CH2}$)

MS (ESI): m/z = 605.2 $[Ir(IMes)(cod)]^+$

6.5.2 [Ir(IMes)(cod)(3-aminopyridine)]Cl (1-cod-3AmPy)

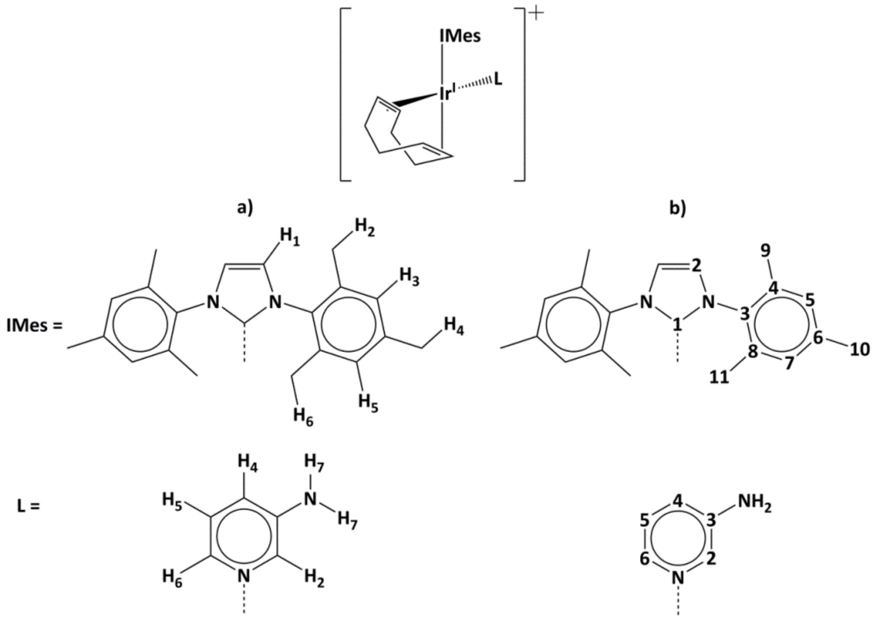

Figure 109: Labelled schematic of **1-cod-3AmPy**

${}^{1}H$ {d_4-methanol, 500.1 MHz, 243 K} δ: 7.42 (s, 2 H, $H_{IMes,1}$), 7.32(d, 1 H, $H_{L,6}$, ${}^{3}J_{HH}$ = 5.6 Hz), 7.22 (br s, 2 H, $H_{IMes,3}$), 7.03 (br s, 2 H, $H_{IMes,5}$), 6.97 (dd, 1 H, $H_{L,5}$, ${}^{3}J_{HH}$ = 5.6, 8.4 Hz), 6.92 (m, 2 H, $H_{L,2}$ & $H_{L,4}$), 3.59 (br s, 2 H, $H_{cod,CH}$), 3.34 ($H_{cod,CH}$), 2.44 (s, 6 H, $H_{IMes,4}$), 2.34 (br s, 6 H, $H_{IMes,2}$), 2.00 (br s, 6 H, $H_{IMes,6}$), 1.89 (br s, 4 H, $H_{cod,CH2}$), 1.64 (br s, 4 H, $H_{cod,CH2}$)

${}^{13}C$ {d_4-methanol, 125.8 MHz, 243 K} δ: 172.8 ($C_{IMes,1}$), 146.4 ($C_{L,3}$), 139.5 ($C_{IMes,6}$), 137.5 ($C_{L,6}$), 136.8 ($C_{L,2}$), 136.0 ($C_{IMes,4}$), 135.5 ($C_{IMes,3}$), 128.8 ($C_{IMes,5}$), 128.7 ($C_{IMes,7}$), 124.9 ($C_{IMes,2}$), 124.9 ($C_{L,5}$), 120.8 ($C_{L,4}$), 19.9 ($C_{IMes,10}$), 17.3 ($C_{IMes,9}$)

${}^{15}N$ {d_4-methanol, 50.7 MHz, 243 K} δ: 241.2 ($N_{L,Ar}$), 195.5 (N_{IMes})

6.5.3 [Ir(IMes)(H)$_2$(3-aminopyridine)$_3$]Cl (1-3AmPy)

Labelled according to Figure 107.

^{1}H {d_4-methanol, 500.1 MHz, 298 K} δ: 7.76 (s, H$_{\mathrm{L,trans,2}}$), 7.72 (s, H$_{\mathrm{L,cis,2}}$), 7.68 (s, H$_{\mathrm{L,cis,6}}$), 7.17 (d, H$_{\mathrm{L,trans,6}}$, J = 5 Hz), 7.06 (s, 2 H, H$_{\mathrm{IMes,1}}$), 6.93 (d, H$_{\mathrm{L,cis,4}}$, J = 8 Hz), 6.84 (br s, H$_{\mathrm{L,trans,4}}$), 6.77 (H$_{\mathrm{L,cis,5}}$), 6.70 (s, 4 H, H$_{\mathrm{IMes,3}}$), 6.59 (dd, H$_{\mathrm{L,trans,5}}$, J = 5, 8 Hz), 2.23 (s, 6 H, H$_{\mathrm{IMes,4}}$), 2.08 (s, 12 H, H$_{\mathrm{IMes,2}}$), -23.00 (s, 2 H, H$_{\mathrm{Hydride}}$)

^{1}H {d_4-methanol, 500.1 MHz, 243 K} δ: 7.78 (d, H$_{\mathrm{L,trans,2}}$, J = 2 Hz), 7.71 (s, 2 H, H$_{\mathrm{L,cis,2}}$), 7.65 (d, 2 H, H$_{\mathrm{L,cis,6}}$, $^{3}J_{\mathrm{HH}}$ = 5 Hz), 7.11 (d, H$_{\mathrm{L,trans,6}}$, $^{3}J_{\mathrm{HH}}$ = 5 Hz), 7.10 (s, H$_{\mathrm{IMes,1}}$), 6.90 (d, 2 H, H$_{\mathrm{L,cis,4}}$, $^{3}J_{\mathrm{HH}}$ = 8 Hz), 6.82 (d, 1 H, H$_{\mathrm{L,trans,4}}$, $^{3}J_{\mathrm{HH}}$ = 8 Hz), 6.79 (dd, 2 H, H$_{\mathrm{L,cis,5}}$, $^{3}J_{\mathrm{HH}}$ = 5, 8 Hz), 6.70 (s, 4 H, H$_{\mathrm{IMes,3}}$), 6.60 (dd, 1 H, H$_{\mathrm{L,trans,5}}$, $^{3}J_{\mathrm{HH}}$ = 5, 8 Hz), 2.23 (s, 6 H, H$_{\mathrm{IMes,4}}$), 2.08 (s, 12 H, H$_{\mathrm{IMes,2}}$), -22.7 (s, 2 H, H$_{\mathrm{Hydride}}$)

^{13}C {d_4-methanol, 125.8 MHz, 298 K} δ: 153.8 (C$_{\mathrm{IMes,1}}$), 143.4 (C$_{\mathrm{L,trans,2}}$), 143.1 (C$_{\mathrm{L,trans,6}}$), 142.3 (C$_{\mathrm{L,cis,2}}$), 142.0 (C$_{\mathrm{L,cis,6}}$), 137.9 (C$_{\mathrm{IMes,6}}$), 137.7 (C$_{\mathrm{IMes,3}}$), 135.1 (C$_{\mathrm{IMes,4}}$), 128.2 (C$_{\mathrm{IMes,5}}$), 124.2 (C$_{\mathrm{L,cis,5}}$), 124.2 (C$_{\mathrm{L,trans,5}}$), 120.4 (C$_{\mathrm{L,trans,4}}$), 122.1 (C$_{\mathrm{IMes,2}}$), 120.0 (C$_{\mathrm{L,cis,4}}$), 19.7 (C$_{\mathrm{IMes,8}}$), 17.6 (C$_{\mathrm{IMes,7}}$)

^{13}C {d_4-methanol, 125.8 MHz, 243 K} δ: 154.2 (C$_{\mathrm{IMes,1}}$), 145.6 (C$_{\mathrm{L,cis,3}}$), 145.5 (C$_{\mathrm{L,trans,3}}$), 143.1 (C$_{\mathrm{L,trans,2}}$), 142.6 (C$_{\mathrm{L,cis,2}}$), 142.4 (C$_{\mathrm{L,trans,6}}$), 141.4 (C$_{\mathrm{L,cis,6}}$), 137.9 (C$_{\mathrm{IMes,6}}$), 137.6 (C$_{\mathrm{IMes,3}}$), 135.0 (C$_{\mathrm{IMes,4}}$), 128.1 (C$_{\mathrm{IMes,5}}$), 127.0 (C$_{\mathrm{IMes,2}}$), 124.5 (C$_{\mathrm{L,cis,5}}$), 124.2 (C$_{\mathrm{L,trans,5}}$), 120.1 (C$_{\mathrm{L,trans,4}}$), 119.6 (C$_{\mathrm{L,cis,4}}$), 19.9 (C$_{\mathrm{IMes,8}}$), 17.8 (C$_{\mathrm{IMes,7}}$)

^{15}N {d_4-methanol, 50.7 MHz, 298 K} δ: 194.4 (N$_{\mathrm{IMes}}$)

^{15}N {d_4-methanol, 50.7 MHz, 243 K} δ: 255.3 (N$_{\mathrm{L,cis,Ar}}$), 239.6 (N$_{\mathrm{L,trans,Ar}}$), 194.0 (N$_{\mathrm{IMes}}$)

6.5.4 [Ir(IMes)(H)$_2$(3-hydroxypyridine)$_3$]Cl (1-3OHPy)

Labelled according to Figure 107.

^{1}H {d_4-methanol, 500.1 MHz, 298 K } δ: 7.88 (d, H$_{\mathrm{cis,6}}$, $^{3}J_{\mathrm{HH}}$ = 4.5 Hz), 7.85 (s, H$_{\mathrm{cis,2}}$), 7.66 (s, H$_{\mathrm{trans,2}}$), 7.53 (d, H$_{\mathrm{trans,6}}$, $^{3}J_{\mathrm{HH}}$ = 5 Hz), 7.10 (d, H$_{\mathrm{cis,4}}$, $^{3}\mathrm{J}_{\mathrm{HH}}$ = 8 Hz), 7.07 (s, H$_{\mathrm{IMes,1}}$), 7.03 (d, H$_{\mathrm{trans,4}}$, $^{3}J_{\mathrm{HH}}$ = 8 Hz), 6.95 (m, H$_{\mathrm{cis,5}}$), 6.77 (m, H$_{\mathrm{trans,5}}$), 6.68 (s, H$_{\mathrm{IMes,3}}$), 2.21 (s, H$_{\mathrm{IMes,4}}$), 2.07 (s, H$_{\mathrm{IMes,2}}$), -22.96 (s, H$_{\mathrm{Hydride}}$)

^{1}H {d_4-methanol, 500.1 MHz, 243 K } δ: 7.89 (br d, 2 H, H$_{\mathrm{L,cis,6}}$, $^{3}J_{\mathrm{HH}}$ = 4.5 Hz), 7.81 (br s, 2 H, H$_{\mathrm{L,cis,2}}$), 7.62 (br s, 1 H, H$_{\mathrm{L,trans,2}}$), 7.58 (br d, 1 H, H$_{\mathrm{L,trans,6}}$, $^{3}J_{\mathrm{HH}}$ = 5 Hz), 7.16 (s, 2 H, H$_{\mathrm{IMes,1}}$), 7.12 (br d, 2 H, H$_{\mathrm{L,cis,4}}$, $^{3}J_{\mathrm{HH}}$ = 8 Hz), 7.06 (br d, 1 H, H$_{\mathrm{L,trans,4}}$, $^{3}J_{\mathrm{HH}}$ = 8 Hz), 7.01

(br dd, 2 H, $H_{L,cis,5}$, $^{3}J_{HH}$ = 4.5, 8 Hz), 6.82 (br dd, 1 H, $H_{L,trans,5}$, $^{3}J_{HH}$ = 5, 8 Hz), 6.69 (s, 4 H, $H_{IMes,3}$), 2.22 (s, 6 H, $H_{IMes,4}$), 2.08 (s, 12 H, $H_{IMes,2}$), -22.69 (s, $H_{Hydride}$)

^{13}C {*d$_4$*-methanol, 125.8 MHz, 298 K} δ: 153.1 ($C_{IMes,1}$), 146.1 ($C_{trans,6}$), 144.1 ($C_{cis,2}$), 144.1 ($C_{trans,2}$), 144.0 ($C_{cis,6}$), 139.6 ($C_{IMes,6}$), 137.5 ($C_{IMes,4}$), 135.0 ($C_{IMes,3}$), 128.3 ($C_{IMes,5}$), 125.0 ($C_{trans,5}$), 124.9 ($C_{cis,5}$), 122.7 ($C_{trans,4}$), 122.2 ($C_{IMes,2}$), 122.0 ($C_{cis,4}$), 19.68 ($C_{IMes,8}$), 17.57 ($C_{IMes,7}$)

^{13}C {*d$_4$*-methanol, 125.8 MHz, 243 K, d$_4$-MeOH} δ: 155.4 ($C_{trans,3}$), 155.1 ($C_{cis,3}$), 153.0 ($C_{IMes,1}$), 146.1 ($C_{trans,6}$), 144.0 ($C_{cis,2}$), 143.8 ($C_{trans,2}$), 143.6 ($C_{cis,6}$), 139.8 ($C_{IMes,6}$), 137.8 ($C_{IMes,4}$), 137.4 ($C_{IMes,3}$), 128.2 ($C_{IMes,5}$), 125.1 ($C_{cis,5}$), 125.0 ($C_{cis,5}$), 122.26 ($C_{IMes,2}$), 122.5 ($C_{cis,4}$), 121.8 ($C_{cis,4}$),19.79 ($C_{IMes,8}$), 17.74 ($C_{IMes,7}$)

^{15}N {*d$_4$*-methanol, 50.7 MHz, 243 K} δ: 257.2 (s, $N_{L,cis,Ar}$), 241.3 (s, $N_{L,trans,Ar}$), 194.2 (s, N_{IMes})

6.5.5 [Ir(IMes)(H)$_2$(4-hydroxypyidine)$_3$]Cl (1-4OHPy)

Labelled according to Figure 107.

^{1}H {*d$_4$*-methanol, 500.1 MHz, 243 K} δ: 7.97 (d, 4 H,$H_{L,cis,2}$, $^{3}J_{HH}$ = 6.7 Hz), 7.70 (d, 2 H, $H_{L,trans,2}$, $^{3}J_{HH}$ = 6.1 Hz), 7.09 (s, 2 H, $H_{IMes,1}$), 6.71 (s, 4 H, $H_{IMes,3}$), 6.48 ($H_{L,cis,3}$), 6.35 (d, 2 H, $H_{L,trans,3}$, $^{3}\mathrm{J}_{HH}$ = 6.1 Hz), 2.23 (s, $H_{IMes,4}$), 2.05 (s, $H_{IMes,2}$), -22.95 (s, $H_{Hydride}$)

^{13}C {*d$_4$*-methanol, 125.8 MHz, 243 K } δ: 164.3 ($C_{L,trans,4}$), 163.9 ($C_{L,cis,4}$), 156.0 ($C_{L,trans,2}$), 155.1 ($C_{L,cis,2}$), 153.5 ($C_{IMes,1}$), 140.0 ($C_{IMes,6}$), 137.8 ($C_{IMes,3}$), 135.0 ($C_{IMes,4}$), 128.2 ($C_{IMes,5}$), 122.1 ($C_{IMes,2}$), 112.3 ($C_{L,cis,3}$ and $C_{L,trans,3}$), 19.8 ($C_{IMes,8}$), 2.05 ($C_{IMes,7}$)

^{15}N {*d$_4$*-methanol, 50.7 MHz, 243 K} δ: 228.8 ($N_{L,cis}$), 212.1 ($N_{L,trans}$), 193.9 (N_{IMes})

6.5.6 [Ir(IMes)(H)$_2$(κ-O-4-pyridone)(κ-N-4-hydroxypyridine)]Cl

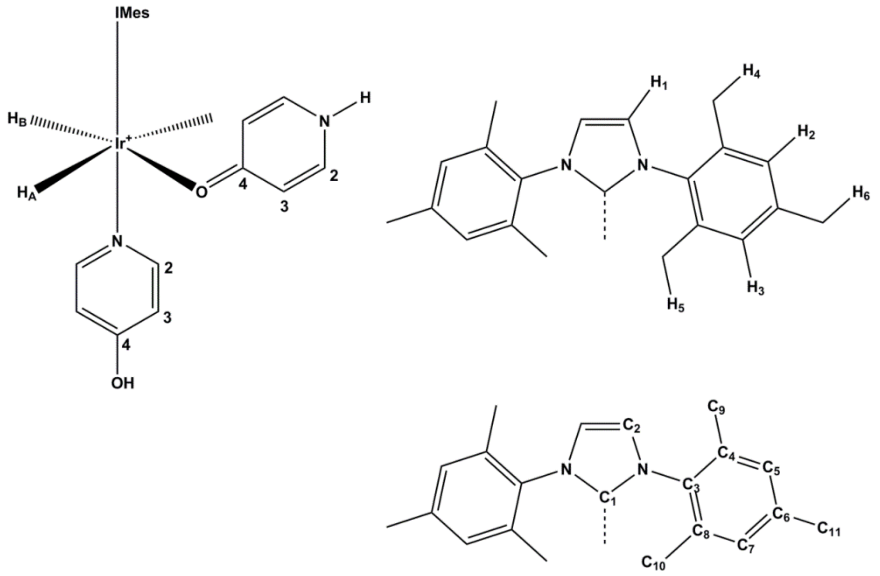

Figure 110: Labelled schematic of [Ir(IMes)(H)$_2$(κ-O-4-pyridone)(κ-N-4-hydroxypyridine)]$^+$

^{1}H {d_4-methanol, 500.1 MHz, 243 K} δ: 7.78 (d, 2 H, H$_{L,trans,2}$, $^3J_{HH}$ = 6.7 Hz), 7.39 (d, 2 H, H$_{L,cis,2}$, $^3J_{HH}$ = 6.7 Hz), 6.96 (s, 2 H, H$_{IMes,1}$), 6.74 (s, 2 H, H$_{IMes,2}$), 6.67 (s, 2 H, H$_{IMes,3}$), 6.47 (d, H$_{L,cis,3}$, $^3J_{HH}$ = 6.7 Hz), 6.27 (d, 2 H, H$_{L,trans,3}$, $^3J_{HH}$ = 6.7 Hz), 2.22 (s, 6 H, H$_{IMes,4}$), 2.19 (s, 6 H, H$_{IMes,6}$), 1.89 (s, 6 H, H$_{IMes,5}$), -22.09 (d, H$_{Hydride,A}$, $^2J_{HH}$ = 9 Hz), -27.43 (H$_{Hydride,B}$, $^2J_{HH}$ = 9 Hz)

^{13}C {d_4-methanol, 125.8 MHz, 243 K} δ: 180.1 (C$_{L,cis,4}$), 163.8 (C$_{L,trans,4}$), 155.0 (C$_{L,trans,2}$), 153.3 (C$_{IMes,1}$), 137.7 (C$_{IMes,3}$), 137.2 (C$_{IMes,6}$), 136.4 (C$_{L,cis,2}$), 135.7 (C$_{IMes,4}$), 135.4 (C$_{IMes,8}$), 128.3 (C$_{IMes,5}$), 128.1 (C$_{IMes,7}$), 121.5 (C$_{IMes,2}$), 118.0 (C$_{L,cis,3}$), 111.8 (C$_{L,trans,3}$), 19.8 (C$_{IMes,11}$), 17.4 (C$_{IMes,9}$), 17.2 (C$_{IMes,10}$)

^{15}N {d_4-methanol, 50.7 MHz, 243 K} δ: 212.2 (N$_{L,trans}$), 192.8 (N$_{IMes}$), 148.9 (N$_{L,cis}$)

6.5.7 [Ir(IMes)(H)$_2$(3-methoxypyridine)$_3$]Cl (1-3OMePy)

Labelled according to Figure 107.

^{1}H {d_4-methanol, 400.1 MHz, 298 K} δ: 8.04 (br s, 2 H, H$_{L,cis,6}$), 7.87 (br s, 2 H, H$_{L,cis,2}$), 7.74 (br d, 1 H, H$_{L,trans,6,}$ $^3J_{HH}$ = 5.4 Hz), 7.62 (br s, 1 H, H$_{L,trans,2}$), 7.38 (H$_{L,cis,4}$), 7.29 (dd, 1 H, H$_{L,trans,4}$, $^3J_{HH}$ = 8.5 Hz, J = 2.6 Hz), 7.13 (br m, 2 H, H$_{L,cis,5}$), 7.11 (s, 2 H, H$_{IMes,1}$), 6.93

(dd, 1 H, $H_{L, trans,5}$), $^3J_{HH}$ = 8.5, 5.4 Hz), 6.69 (s, 4 H, $H_{IMes,3}$), 3.72 (s, 6 H, $H_{L,cis,7}$), 3.60 (s, 3 H, $H_{L,trans,7}$), 2.21 (s, 6 H, $H_{IMes,4}$), 2.06 (s, 12 H, $H_{IMes,2}$), -22.99 (s, $H_{Hydride}$)

^{13}C {*d₄*-methanol, 100.6 MHz, 298 K} δ: 156.7 ($C_{L,trans,3}$), 156.6 ($C_{L,cis,3}$), 153.7 ($C_{IMes,1}$), 147.6 ($C_{L,trans,6}$), 145.0 ($C_{L,cis,6}$), 143.5 ($C_{L,cis,2}$), 143.3 ($C_{L,trans,2}$), 138.1 ($C_{IMes,6}$), 137.3 ($C_{IMes,4}$), 135.0 ($C_{IMes,3}$), 128.3 ($C_{IMes,5}$), 125.1 ($C_{L,trans,5}$), 124.9 ($C_{L,cis,5}$), 122.4 ($C_{IMes,2}$), 120.2 ($C_{L,trans,4}$), 119.8 ($C_{L,cis,4}$), 54.6 ($C_{L,cis,7}$ + $C_{L,trans,7}$), 19.6 ($C_{IMes,8}$), 17.5 ($C_{IMes,7}$)

6.5.8 [Ir(IMes)(H)$_2$(4-OMe)$_3$]Cl (1-4OMePy)

Labelled according to Figure 107.

^{1}H {*d₄*-methanol, 500.1 MHz, 298 K} δ: 8.1 (d, 4 H, $H_{L,cis,2}$, *J* = 3.9 Hz), 7.8 (d, 2 H, $H_{L,trans,2}$, $^3J_{HH}$ = 5.4 Hz), 7.05 (s, 2 H, $H_{IMes,1}$), 6.70 (s, 4 H, $H_{IMes, 3}$), 6.66 (br s, 4 H, $H_{L,cis,3}$), 6.54 (d, 2 H, $H_{L,trans,3}$, $^3J_{HH}$ = 5.4 Hz), 3.88 (s, 6 H, $H_{L,cis,5}$), 3.74 (s, 3 H, $H_{L,trans,6}$), 2.22 (s, 6 H, $H_{IMes, 4}$), 2.06 (s, 12 H, $H_{IMes,2}$)

^{13}C {*d₄*-methanol, 125.8 MHz, 298 K} δ: 165.6 ($C_{L,trans,4}$), 165.5 ($C_{L,cis,4}$), 155.8 ($C_{L,trasn,2}$), 155.0 ($C_{L,cis,2}$), 152.7 ($C_{IMes, 1}$), 137.9 ($C_{IMes,6}$), 137.8 ($C_{IMes,4}$), 135.1($C_{IMes,3}$), 128.2(C_{IMes5}), 122.3($C_{IMes,2}$), 110.9 ($C_{L,trans,3}$ and $C_{L,cis,3}$), 54.8 ($C_{L,cis,5}$ and $C_{L,trans,5}$), 19.1 ($C_{IMes,8}$), 17.4 ($C_{IMes,7}$)

^{15}N {*d₄*-methanol, 50.7 MHz, 298 K} δ: 233.0 ($N_{L,cis,Ar}$), 215.5 ($N_{L,trans,Ar}$), 194.3 (N_{IMes})

7. Appendices

7.1 Appendix 1 - Calculation of thermodynamic activation parameters

7.1.1 Collection of NMR data for the calculation of exchange rates

A series of ^{1}H EXSY NMR spectra were collected by selectively exciting the bound substrate and, after a short mixing time, collecting the resulting NMR spectrum. The mixing time allows for exchange and therefore the relative integrals of the bound and free substrate resonances can be used to monitor the exchange process. The absolute integrals are then plotted as a percentage of the total population as a function of mixing time as shown in Figure 111.

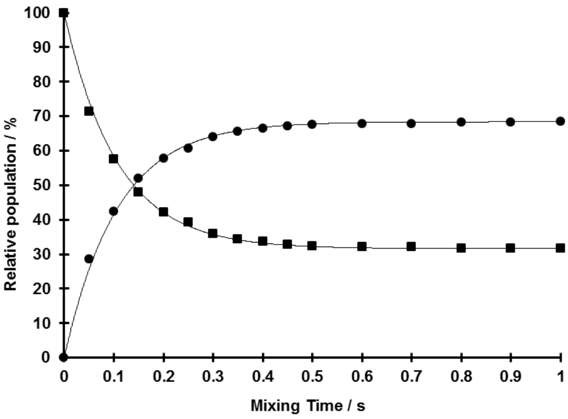

Figure 111: Relative population of **1-3OHPy** and **3OHPy** as a function of mixing time at 298 K. Sample contains 25 mM **3OHPy**, 5 mM **1-cod-Cl** in *d₄*-methanol and has been activated with H_2. ▪ represents experimental data for **1-3OHPy**, ● represents experimental data for **3OHPy**. Lines represent the model data.

A simplified mechanism of the ligand exchange process is given in Figure 112:

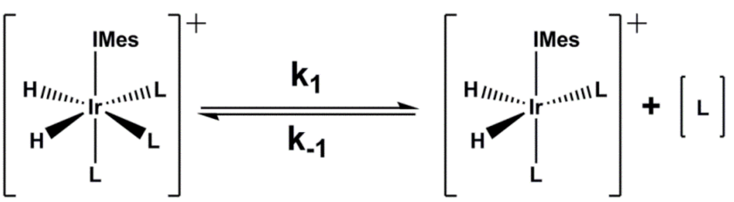

A **B**

Figure 112: Simplified mechanism of ligand exchange in solution

The rate, k_1, can be calculated using an Excel solver fit, assuming a first order rate. The model data is calculated from equations derived from the first order rate law given in Equation 7. Differentiating Equation 7 gives Equation 8.

$$[A] = [A]_0 e^{-k_1 T} \qquad \text{(Equation 7)}$$

Equation 7: First order rate equation for the concentration of a species A. [A] is the concentration of species A, $[A]_0$ is the concentration of species A at time $t = 0$, k_1 is the rate of exchange and T is the temperature

$$\frac{d[A]}{dt} = -k_1 [A]_t \qquad \text{(Equation 8)}$$

Equation 8: Change in concentration of A over time

Thus, the concentrations of A and B at time = t are given by Equation 9 and Equation 10.

$$[A]_{t+\delta t} = [A]_t - k_1 [A]_t \delta t \qquad \text{(Equation 9)}$$

Equation 9: Concentration of A at time = t

$$[B]_{t+\delta t} = [B]_t + k_1 [A]_t \delta t \qquad \text{(Equation 10)}$$

Equation 10: Concentration of B at time = t

k_1 is varied by the solver until the difference between the model data, based on these equations, and the experimental data is minimised.

7.1.2 Calculation of thermodynamic activation parameters

The thermodynamic activation parameters were calculated through the Eyring method. Plotting a graph of (1/T) against ln (2k/T), where T is the temperature in Kelvin and k is the experimentally measured rate constant in s^{-1}, produces a straight line which can be used to derive the parameters of interest as shown in Equation 11.

$$y = \quad mx \quad + c$$

$$\ln\left(\frac{k}{T}\right) = -\frac{\Delta H^{\ddagger}}{R}\frac{1}{T} + \ln\left(\frac{k_B}{h}\right) + \left(\frac{\Delta S^{\ddagger}}{R}\right) \qquad \text{(Equation 11)}$$

Equation 11: Determining thermodynamic activation parameters from an Eyring plot. R is the gas constant, k_B is the Boltzmann constant, h is the Planck constant. ΔH‡ is the enthalpy of activation, ΔS‡ is the entropy of activation

7.1.3 Collected rate constants and thermodynamic activation parameters for a sample of 1-cod-Cl hydrogenated in the presence of 3OHPy

The data in Table 6 was used to produce the Eyring plots shown in Figure 113. Figure 113 displays the equations which can be used to calculate the thermodynamic parameters presented in

Table 7.

Table 6: Rate constants (quoted to 3 d.p.) for the loss of **3OHPy** and hydride ligands from **1-3OHPy** in the presence of **3OHPy** in *d₄*-methanol at the indicated temperatures, with corresponding error values calculated using the Jackknife[125] method

T / K	Observed rate constant / s^{-1}	
	Loss of substrate ligands	Loss of hydride ligands
268	0.209 ± 0.0011	0.061 ± 0.00007
276	0.613 ± 0.002	0.219 ± 0.0005
283	1.447 ± 0.004	0.669 ± 0.002
288	2.445 ± 0.006	1.242 ± 0.004
293	4.211 ± 0.009	2.261 ± 0.007
298	6.369 ± 0.017	4.083 ± 0.5

Table 7: The thermodynamic parameters of activation for hydride and substrate exchange for **1-3OHPy** in *d₄*-methanol

Thermodynamic parameter	Ligand Loss	
	Substrate	Hydride
$\Delta H^{\ddagger}$ / kJ mol^{-1}	73.8 ± 0.7	85.5 ± 0.6
$\Delta S^{\ddagger}$ / J K^{-1} mol $^{-1}$	19 ± 2	59 ± 2
$\Delta G^{\ddagger}_{298}$ / kJ mol^{-1}	68.39 ± 0.01	69.5 ± 0.3

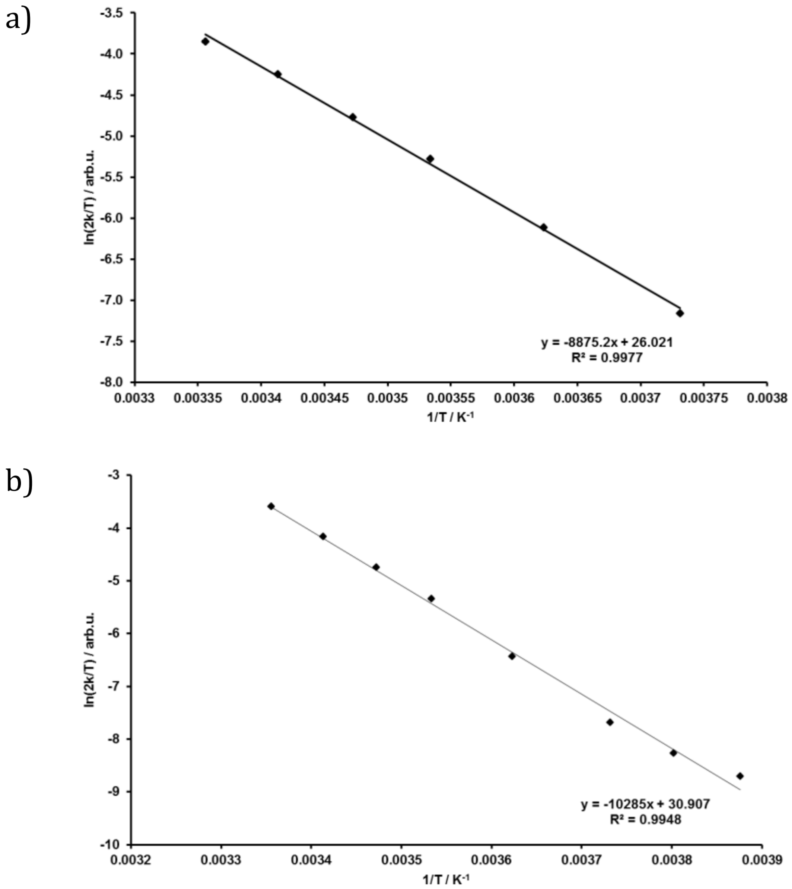

Figure 113: Eyring plots of a) substrate and b) hydride dissociation from **1-3OHPy** in *d₄*-methanol

7.2 X-ray crystallography data for [Ir(IMes)(H)$_2$(3-hydroxypyridine)$_3$]Cl

Single crystals of $C_{36}H_{39}ClIrN_5O_3$ (sbd1411) were grown from d$_4$-methanol. A suitable crystal was selected and extracted using oil on loop and interrogated on an Oxford Diffraction SuperNova diffractometer. The crystal was kept at 110.05(10) K during data collection. Using Olex2,[126] the structure was solved with the Superflip[127-129] structure solution program using Charge Flipping and refined with the ShelXL[130] refinement package using Least Squares minimisation.

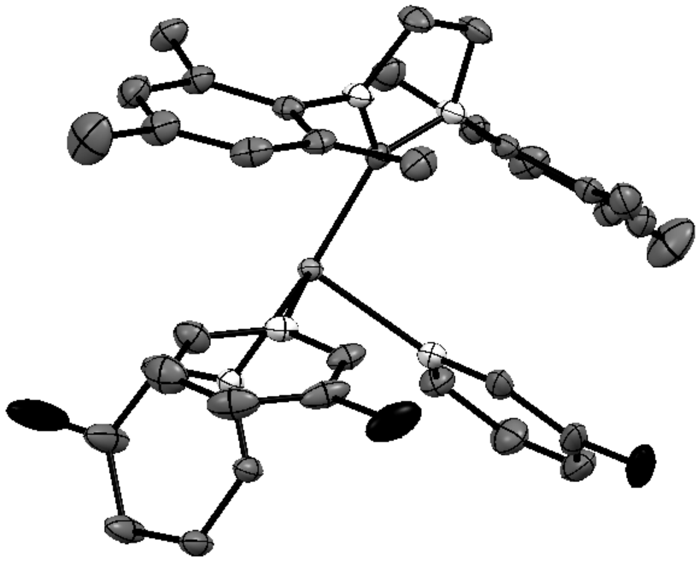

Figure 114: ORTREP diagram of crystal structure obtained for sample sbd1411, [Ir(IMes)(H)$_2$(3-hydroxypyridine)$_3$]Cl. Grey indicates carbon atoms, white indicates nitrogen atoms, black indicates oxygen atoms. The central iridium atom is shown in light grey. Hydrogen atoms are not displayed.

Table 8: Crystal data and structure refinement for sbd1411

Identification code	sbd1411
Empirical formula	$C_{36}H_{39}ClIrN_5O_3$
Formula weight	817.37
Temperature/K	110.05(10)
Crystal system	monoclinic
Space group	$P2_1/m$
a/Å	8.76747(17)
b/Å	16.6259(3)
c/Å	11.9624(2)
α/°	90

β/°	95.7053(18)
γ/°	90
Volume/Å^3	1735.09(6)
Z	2
ρ_{calc}g/cm^3	1.565
μ/mm^{-1}	3.967
F(000)	816.0
Crystal size/mm^3	0.1131 × 0.0663 × 0.0366
Radiation	MoKα (λ = 0.7107)
2Θ range for data collection/°	5.972 to 64.22
Index ranges	$-13 \leq h \leq 8$, $-20 \leq k \leq 23$, $-17 \leq l \leq 16$
Reflections collected	10272
Independent reflections	5647 [R_{int} = 0.0317, R_{sigma} = 0.0553]
Data/restraints/parameters	5647/0/230
Goodness-of-fit on F^2	1.039
Final R indexes [I>=2σ (I)]	R_1 = 0.0299, wR_2 = 0.0584
Final R indexes [all data]	R_1 = 0.0363, wR_2 = 0.0605
Largest diff. peak/hole / e Å^{-3}	1.78/-1.74

Table 9: Fractional Atomic Coordinates (×10^4) and Equivalent Isotropic Displacement Parameters (Å^2×10^3) for sbd1411. U_{eq} is defined as 1/3 of of the trace of the orthogonalised U_{IJ} tensor.

Atom	***x***	***y***	***z***	**U(eq)**
C1	4616(4)	7500	2563(3)	15.6(7)
C2	6447(3)	7905.8(17)	1435(2)	24.0(6)
C3	4993(3)	8989.2(15)	2252(2)	17.7(5)
C4	4065(3)	9360.8(16)	1387(2)	20.6(6)
C5	3753(3)	10177.8(16)	1517(3)	25.8(6)
C6	4363(4)	10604.7(16)	2443(3)	28.5(7)
C7	5320(3)	10218.0(16)	3267(3)	27.5(7)
C8	5672(3)	9400.8(15)	3184(2)	20.7(6)
C9	3451(4)	8923.7(18)	336(3)	28.4(7)
C10	4026(5)	11494.1(18)	2542(4)	48.7(11)
C11	6791(3)	9003.9(18)	4053(3)	27.8(7)
C12	830(3)	8553.2(17)	1984(2)	22.6(6)
C13	-64(3)	9209.0(19)	1598(3)	30.1(7)
C14	-142(4)	9871.1(19)	2283(3)	35.4(8)
C15	676(4)	9857.6(18)	3320(3)	33.7(8)
C16	1563(3)	9185.3(17)	3659(3)	26.5(6)
C17	73(4)	7500	4757(3)	19.1(8)
C18	-890(5)	7500	5602(3)	23.4(9)
C19	-300(5)	7500	6707(4)	34.8(11)
C20	1298(5)	7500	6938(4)	40.8(13)
C21	2209(5)	7500	6057(3)	29(1)
Ir1	3070.0(2)	7500	3676.4(2)	13.81(4)
N1	5343(3)	8142.2(13)	2119(2)	18.7(5)

N2	1637(3)	8537.2(13)	2995(2)	19.5(5)
N3	1621(4)	7500	4977(3)	16.7(6)
O1	-855(3)	9200.5(17)	557(2)	41.4(7)
O2	2027(4)	7500	7993(3)	77.8(16)
Cl1	-557.2(13)	7500	-463.6(9)	39.9(3)

Table 10: Anisotropic Displacement Parameters ($Å^2 \times 10^3$) for sbd1411. The Anisotropic displacement factor exponent takes the form: $-2\pi^2[h^2a^{*2}U_{11}+2hka^*b^*U_{12}+\ldots]$.

Atom	**U_{11}**	**U_{22}**	**U_{33}**	**U_{23}**	**U_{13}**	**U_{12}**
C1	14.5(17)	18.4(17)	13.6(17)	0	-0.1(14)	0
C2	21.2(14)	23.6(14)	29.3(17)	1.6(11)	12.8(12)	-3.5(11)
C3	14.3(12)	14.5(12)	25.2(15)	2.4(10)	5.7(10)	-0.7(10)
C4	16.5(13)	22.5(13)	23.1(15)	3.5(11)	4.0(11)	-4.3(11)
C5	18.7(14)	24.0(14)	34.3(18)	10.3(12)	0.9(12)	-0.3(12)
C6	24.8(15)	18.1(13)	42(2)	3.1(12)	0.6(14)	1.0(12)
C7	22.9(15)	22.7(14)	35.9(18)	-5.1(12)	-2.1(13)	-2.2(12)
C8	16.4(13)	19.7(13)	25.5(15)	1.9(11)	0.2(11)	-0.4(11)
C9	28.1(16)	33.1(16)	23.7(16)	3.8(12)	1.1(13)	-6.0(13)
C10	51(2)	24.3(16)	68(3)	-3.0(17)	-9(2)	10.9(16)
C11	20.1(14)	30.0(15)	31.8(17)	1.5(13)	-5.2(12)	-1.0(12)
C12	16.8(13)	26.1(14)	24.2(15)	8.8(11)	-0.7(11)	-5.6(11)
C13	16.3(14)	36.4(17)	36.0(18)	20.2(14)	-5.8(13)	-5.1(13)
C14	20.7(15)	29.6(16)	56(2)	15.8(15)	2.6(15)	5.4(13)
C15	31.9(18)	26.0(15)	44(2)	3.4(14)	7.3(15)	6.9(14)
C16	23.8(15)	26.9(14)	28.9(16)	1.6(12)	3.4(12)	6.2(12)
C17	13.9(17)	29(2)	14.4(18)	0	2.1(14)	0
C18	13.4(18)	38(2)	19(2)	0	2.1(15)	0
C19	18(2)	72(3)	15(2)	0	4.6(16)	0
C20	18(2)	88(4)	17(2)	0	1.8(17)	0
C21	10.9(18)	59(3)	17(2)	0	-1.7(15)	0
Ir1	10.74(7)	17.59(7)	13.08(7)	0	1.13(5)	0
N1	15.0(11)	18.8(10)	23.3(12)	0.4(9)	7.3(9)	-0.7(9)
N2	14.7(11)	23.5(11)	20.6(12)	3.8(9)	3.4(9)	-0.2(9)
N3	13.3(15)	23.1(16)	13.9(16)	0	2.5(12)	0
O1	30.8(14)	48.5(16)	41.1(16)	25.2(13)	-14.8(12)	-8.3(12)
O2	19.2(17)	202(5)	12.0(17)	0	1.3(14)	0
Cl1	24.6(5)	80.7(9)	14.5(5)	0	2.7(4)	0

Table 11: bond lengths for sbd1411

Atom	**Atom**	**Length/Å**
C1	Ir1	1.993(4)

C1	N1^1	1.377(3)
C1	N1	1.377(3)
C2	C2^1	1.349(6)
C2	N1	1.385(4)
C3	C4	1.395(4)
C3	C8	1.390(4)
C3	N1	1.453(3)
C4	C5	1.397(4)
C4	C9	1.505(4)
C5	C6	1.378(4)
C6	C7	1.387(4)
C6	C10	1.515(4)
C7	C8	1.399(4)
C8	C11	1.509(4)
C12	C13	1.394(4)
C12	N2	1.340(4)
C13	C14	1.378(5)
C13	O1	1.364(4)
C14	C15	1.370(5)
C15	C16	1.399(4)
C16	N2	1.344(4)
C17	C18	1.380(5)
C17	N3	1.357(5)
C18	C19	1.371(6)
C19	C20	1.401(6)
C20	C21	1.383(6)
C20	O2	1.357(5)
C21	N3	1.343(5)
Ir1	N2	2.239(2)
Ir1	N2^1	2.239(2)
Ir1	N3	2.104(3)

Table 12: Bond angles for sbd1411

Atom	Atom	Atom	Angle/°
N1	C1	Ir1	129.03(16)
N1^1	C1	Ir1	129.03(16)
N1^1	C1	N1	101.7(3)
C2^1	C2	N1	106.49(15)
C4	C3	N1	117.5(2)
C8	C3	C4	123.2(2)
C8	C3	N1	119.1(2)
C3	C4	C5	117.0(3)
C3	C4	C9	122.6(2)
C5	C4	C9	120.3(3)
C6	C5	C4	121.7(3)
C5	C6	C7	119.4(3)
C5	C6	C10	120.2(3)

C7	C6	C10	120.4(3)
C6	C7	C8	121.4(3)
C3	C8	C7	117.1(3)
C3	C8	C11	122.3(2)
C7	C8	C11	120.6(3)
N2	C12	C13	122.9(3)
C14	C13	C12	119.2(3)
O1	C13	C12	120.8(3)
O1	C13	C14	120.0(3)
C15	C14	C13	118.2(3)
C14	C15	C16	120.1(3)
N2	C16	C15	121.9(3)
N3	C17	C18	122.1(4)
C19	C18	C17	120.5(4)
C18	C19	C20	117.6(4)
C21	C20	C19	119.5(4)
O2	C20	C19	123.5(4)
O2	C20	C21	117.0(4)
N3	C21	C20	122.5(4)
C1	Ir1	N2[1]	98.68(9)
C1	Ir1	N2	98.68(9)
C1	Ir1	N3	174.33(13)
N2	Ir1	N2[1]	100.75(12)
N3	Ir1	N2[1]	84.89(8)
N3	Ir1	N2	84.89(8)
C1	N1	C2	112.7(2)
C1	N1	C3	126.7(2)
C2	N1	C3	120.5(2)
C12	N2	C16	117.7(2)
C12	N2	Ir1	124.82(19)
C16	N2	Ir1	117.45(19)
C17	N3	Ir1	121.5(2)
C21	N3	C17	117.8(3)
C21	N3	Ir1	120.6(3)

Table 13: Torsion angles for sbd1411

A	**B**	**C**	**D**	**Angle/°**
C2[1]	C2	N1	C1	-0.3(3)
C2[1]	C2	N1	C3	-176.63(19)
C3	C4	C5	C6	1.5(4)
C4	C3	C8	C7	3.6(4)
C4	C3	C8	C11	-174.0(3)
C4	C3	N1	C1	-97.6(4)
C4	C3	N1	C2	78.2(3)
C4	C5	C6	C7	0.4(5)
C4	C5	C6	C10	178.7(3)
C5	C6	C7	C8	-0.5(5)

C6	C7	C8	C3	-1.4(5)
C6	C7	C8	C11	176.2(3)
C8	C3	C4	C5	-3.7(4)
C8	C3	C4	C9	174.5(3)
C8	C3	N1	C1	86.7(4)
C8	C3	N1	C2	-97.5(3)
C9	C4	C5	C6	-176.6(3)
C10	C6	C7	C8	-178.8(3)
C12	C13	C14	C15	0.3(5)
C13	C12	N2	C16	0.3(4)
C13	C12	N2	Ir1	179.1(2)
C13	C14	C15	C16	0.2(5)
C14	C15	C16	N2	-0.5(5)
C15	C16	N2	C12	0.2(4)
C15	C16	N2	Ir1	-178.7(2)
C17	C18	C19	C20	0.000(1)
C18	C17	N3	C21	0.000(1)
C18	C17	N3	Ir1	180.000(1)
C18	C19	C20	C21	0.000(1)
C18	C19	C20	O2	180.000(1)
C19	C20	C21	N3	0.000(1)
C20	C21	N3	C17	0.000(1)
C20	C21	N3	Ir1	180.000(1)
Ir1	C1	N1	C2	174.9(2)
Ir1	C1	N1	C3	-9.0(5)
N1[1]	C1	N1	C2	0.4(4)
N1[1]	C1	N1	C3	176.50(17)
N1	C3	C4	C5	-179.1(2)
N1	C3	C4	C9	-1.0(4)
N1	C3	C8	C7	179.0(3)
N1	C3	C8	C11	1.4(4)
N2	C12	C13	C14	-0.6(5)
N2	C12	C13	O1	179.4(3)
N3	C17	C18	C19	0.000(1)
O1	C13	C14	C15	-179.6(3)
O2	C20	C21	N3	180.000(1)

Table 14: Hydrogen Atom Coordinates (Å×10^4) and Isotropic Displacement Parameters (Å^2×10^3) for sbd1411.

Atom	***x***	***y***	***z***	**U(eq)**
H2	7066	8240	1051	29
H5	3118	10440	964	31
H7	5737	10508	3888	33
H9A	4178	8959	-211	43
H9B	2500	9164	39	43
H9C	3283	8369	510	43

H10A	3049	11613	2142	73
H10B	4809	11800	2227	73
H10C	4008	11633	3319	73
H11A	6930	9337	4710	42
H11B	7757	8933	3752	42
H11C	6397	8489	4249	42
H12	868	8107	1518	27
H14	-734	10315	2047	42
H15	641	10296	3800	40
H16	2117	9187	4363	32
H17	-353	7500	4014	23
H18	-1946	7500	5420	28
H19	-939	7500	7284	42
H21	3268	7500	6220	35
H1	-610(50)	8790(20)	240(40)	49(15)
H2A	1392	7500	8452	117

8. Abbreviations

[A]	concentration of A
1-cod-Cl	[Ir(IMes)(cod)Cl]
1-cod-L	[Ir(IMes)(cod)(**L**)]Cl
1D	one-dimensional
1-L	[Ir(IMes)(H)$_2$(**L**)$_3$]$^+$
2D	2-dimensional
2F3OHPy	2-fluoro-3-hydroxypyridine
3AmPy	3-aminopyridine
3OHPy	3-hydroxypyridine
3OMePy	3-methoxypyridine
4OHPy	4-hydroxypyridine
4OMePy	4-methoxypyridine
Å	Angstrom
ALTADENA	adiabatic longitudinal transfer after dissociation engenders net alignment
arb.u.	Arbitrary Units
B	magnetic field
bar	unit of pressure

cod	1,5-cyclooctadiene
COSY	Correlated Spectroscopy
Cy	cyclohexyl
d.p.	decimal places
DCM	Dichloromethane
DFT	density functional theory
DME	dimethoxyethane
DMSO	dimethylsulfoxide
DNP	Dynamic Nuclear Polarisation
dppf	1,1'-Bis(diphenylphosphino)ferrocene
dppz	dipyrido phenazine
E	enhancement
EtOAc	ethyl acetate
EXSY	exchange spectroscopy
FcMeCN	Ferroceneacetonitrile
FcPy	(4-pyridyl)ferrocene
G	Gauss
GHz	gigahertz
h	Planck constant
ħ	reduced Planck constant
HMBC	Heteronuclear multiple bond correlation
HMQC	Heternouclear Multiple Quantum Correlation
I	spin quantum number
ICy	1,3-bis(cyclohexyl)-imidazole)
IMes	1,3-bis(2,4,6-trimethylphenyl)imidazole-2-ylidene
J	Joules
k	boltzmann constant
K	Kelvin
k_{Dissoc}	rate of substrate dissociation
$k_{Hydride}$	rate of hydride dissociation
kJ	kilojoules
L	2-electron donor substrate

MeCN	acetonitrile
MeOH	methanol
MHz	megahertz
mL	milliliter
mM	millimolar
mol	mole
MRI	Magnetic Resonance Imaging
n	population
NHC	N-heterocyclic Carbene
NMR	Nuclear Magnetic Resonance
nOe	Nuclear Overhauser Effect
NOESY	Nuclear Overhauser Effect Spectroscopy
$o\mathrm{H}_2$	orthohydrogen
PASADENA	Parahydrogen and synthesis allow dramatically enhanced nuclear alignment
Ph	phenyl
$p\mathrm{H}_2$	parahydrogen
phen	phenanthroline
PHIP	ParaHydrogen Induced Polarisation
PhMeCN	Benzylcyanide
PhPy	(4-phenyl)pyridine
PR_3	phosphine ligand
Py	pyridine
R	Gas constant
s	seconds
SABRE	Signal Amplification By Reversible Exchange
SIPr	1,3-bis(2,6-diisopropyl)-4,5-dihydroimidazol-2-ylidene
SNR	Signal to Noise Ratio
$\mathrm{S}_{\mathrm{pol}}$	Signal of polarised spectrum
$\mathrm{S}_{\mathrm{unpol}}$	Signal of unpolarised spectrum
T	Temperature
T	tesla

ν	frequency
γ	gyromagnetic ratio
$\Delta G^{\ddagger}_{300}$	Gibb's free energy of activation calculated at 300 K
$\Delta H^{\ddagger}$	Enthalpy of activation
$\Delta S^{\ddagger}$	Entropy of activation
μL	microliter
μM	micromolar
μ_{Sample}	mean signal of sample region
$\sigma_{background}$	standard deviation of background signal

9. References

1. Perrin, C.L. and R.E. Engler, *Weighted linear-least-squares analysis of EXSY data from multiple 1D selective inversion experiments.* Journal of Magnetic Resonance (1969), 1990. **90**(2): p. 363-369.
2. Abel, E.W., et al., *Two-dimensional NMR exchange spectroscopy. Quantitative treatment of multisite exchanging systems.* Journal of Magnetic Resonance (1969), 1986. **70**(1): p. 34-53.
3. Mogck, O., et al., *NMR Studies of the Reversible Dimerization and Guest Exchange Processes of Tetra Urea Calix[4]arenes Using a Derivative with Lower Symmetry.* Journal of the American Chemical Society, 1997. **119**(24): p. 5706-5712.
4. Owen, J.S., J.A. Labinger, and J.E. Bercaw, *Pyridinium-Derived N-Heterocyclic Carbene Complexes of Platinum: Synthesis, Structure and Ligand Substitution Kinetics.* Journal of the American Chemical Society, 2004. **126**(26): p. 8247-8255.
5. Takita, R., et al., *A New Entry in Catalytic Alkynylation of Aldehydes and Ketones: Dual Activation of Soft Nucleophiles and Hard Electrophiles by an Indium(III) Catalyst.* Organic Letters, 2005. **7**(7): p. 1363-1366.
6. Blacker, A.J., et al., *Synthesis and structure of "16-electron" rhodium(iii) catalysts for transfer hydrogenation of a cyclic imine: mechanistic implications.* Chemical Communications, 2009(44): p. 6801-6803.
7. Logothetis, N.K., *What we can do and what we cannot do with fMRI.* Nature, 2008. **453**(7197): p. 869-878.
8. Adams, R.W., et al., *Reversible Interactions with para-Hydrogen Enhance NMR Sensitivity by Polarization Transfer.* Science, 2009. **323**(5922): p. 1708-1711.
9. Gloggler, S., et al., *Para-hydrogen induced polarization of amino acids, peptides and deuterium-hydrogen gas.* Physical Chemistry Chemical Physics, 2011. **13**(30): p. 13759-13764.
10. Dücker, E.B., et al., *Similarity of SABRE field dependence in chemically different substrates.* Journal of Magnetic Resonance, 2012. **214**(0): p. 159-165.

11. Zhivonitko, V.V., I.V. Skovpin, and I.V. Koptyug, *Strong 31P nuclear spin hyperpolarization produced via reversible chemical interaction with parahydrogen.* Chemical Communications, 2015.
12. Cowley, M.J., et al., *Iridium N-Heterocyclic Carbene Complexes as Efficient Catalysts for Magnetization Transfer from para-Hydrogen.* Journal of the American Chemical Society, 2011. **133**(16): p. 6134-6137.
13. Eshuis, N., et al., *Toward Nanomolar Detection by NMR Through SABRE Hyperpolarization.* Journal of the American Chemical Society, 2014. **136**(7): p. 2695-2698.
14. Hövener, J.-B., et al., *Toward Biocompatible Nuclear Hyperpolarization Using Signal Amplification by Reversible Exchange: Quantitative in Situ Spectroscopy and High-Field Imaging.* Analytical Chemistry, 2014. **86**(3): p. 1767-1774.
15. Giernoth, R., et al., *PHIP Detection of a Transient Rhodium Dihydride Intermediate in the Homogeneous Hydrogenation of Dehydroamino Acids.* Journal of the American Chemical Society, 2000. **122**(49): p. 12381-12382.
16. Boutain, M., et al., *A parahydrogen based NMR study of Pt catalysed alkyne hydrogenation.* Dalton Transactions, 2010. **39**(14): p. 3495-3500.
17. Herrmann, T., P. Güntert, and K. Wüthrich, *Protein NMR Structure Determination with Automated NOE Assignment Using the New Software CANDID and the Torsion Angle Dynamics Algorithm DYANA.* Journal of Molecular Biology, 2002. **319**(1): p. 209-227.
18. Ardenkjær-Larsen, J.H., et al., *Increase in signal-to-noise ratio of > 10,000 times in liquid-state NMR.* Proceedings of the National Academy of Sciences of the United States of America, 2003. **100**(18): p. 10158-10163.
19. Kohler, S.J., et al., *In vivo 13carbon metabolic imaging at 3T with hyperpolarized 13C-1-pyruvate.* Magnetic Resonance in Medicine, 2007. **58**(1): p. 65-69.
20. Albert, M.S., et al., *Hyperpolarized129Xe MR Imaging of the Oral Cavity.* Journal of Magnetic Resonance, Series B, 1996. **111**(2): p. 204-207.
21. Kauczor, H.U., R. Surkau, and T. Roberts, *MRI using hyperpolarized noble gases.* European Radiology, 1998. **8**(5): p. 820-827.
22. Leawoods, J.C., et al., *Hyperpolarized 3He gas production and MR imaging of the lung.* Concepts in Magnetic Resonance, 2001. **13**(5): p. 277-293.
23. Natterer, J. and J. Bargon, *Parahydrogen induced polarization.* Progress in Nuclear Magnetic Resonance Spectroscopy, 1997. **31**: p. 293-315.
24. Duckett, S.B. and N.J. Wood, *Parahydrogen-based NMR methods as a mechanistic probe in inorganic chemistry.* Coordination Chemistry Reviews, 2008. **252**(21–22): p. 2278-2291.
25. Natterer, J. and J. Bargon, *Parahydrogen induced polarization.* Progress in Nuclear Magnetic Resonance Spectroscopy, 1997. **31**(4): p. 293-315.
26. Bowers, C.R. and D.P. Weitekamp, *Parahydrogen and synthesis allow dramatically enhanced nuclear alignment.* Journal of the American Chemical Society, 1987. **109**(18): p. 5541-5542.
27. Pravica, M.G. and D.P. Weitekamp, *Net NMR alignment by adiabatic transport of parahydrogen addition products to high magnetic field.* Chemical Physics Letters, 1988. **145**(4): p. 255-258.
28. Bargon, J., et al., *NMR-detection of intermediates during homogeneous hydrogenation of dienes using parahydrogen.* Tetrahedron Letters, 1990. **31**(40): p. 5721-5724.

29. Eisenschmid, T.C., et al., *Para hydrogen induced polarization in hydrogenation reactions.* Journal of the American Chemical Society, 1987. **109**(26): p. 8089-8091.
30. Kirss, R.U., T.C. Eisenschmid, and R. Eisenberg, *Para hydrogen induced polarization in hydrogenation reactions catalyzed by ruthenium phosphine complexes.* Journal of the American Chemical Society, 1988. **110**(25): p. 8564-8566.
31. Torres, O., et al., *Photochemical Pump and NMR Probe: Chemically Created NMR Coherence on a Microsecond Time Scale.* Journal of the American Chemical Society, 2014. **136**(28): p. 10124-10131.
32. Atkinson, K.D., et al., *Spontaneous Transfer of Parahydrogen Derived Spin Order to Pyridine at Low Magnetic Field.* Journal of the American Chemical Society, 2009. **131**(37): p. 13362-13368.
33. Herrmann, W.A., *N-Heterocyclic Carbenes: A New Concept in Organometallic Catalysis.* Angewandte Chemie International Edition, 2002. **41**(8): p. 1290-1309.
34. Hillier, A.C., et al., *Cationic Iridium Complexes Bearing Imidazol-2-ylidene Ligands as Transfer Hydrogenation Catalysts.* Organometallics, 2001. **20**(20): p. 4246-4252.
35. Lee, H.M., et al., *A Cationic Iridium Complex Bearing an Imidazol-2-ylidene Ligand as Alkene Hydrogenation Catalyst.* Organometallics, 2001. **20**(6): p. 1255-1258.
36. Lloyd, L.S., et al., *Hyperpolarisation through reversible interactions with parahydrogen.* Catalysis Science & Technology, 2014. **4**(10): p. 3544-3554.
37. van Weerdenburg, B.J.A., et al., *Ligand effects of NHC-iridium catalysts for signal amplification by reversible exchange (SABRE).* Chemical Communications, 2013. **49**(67): p. 7388-7390.
38. Truong, M.L., et al., *Irreversible Catalyst Activation Enables Hyperpolarization and Water Solubility for NMR Signal Amplification by Reversible Exchange.* The Journal of Physical Chemistry B, 2014.
39. Fekete, M., et al., *Iridium(III) Hydrido N-Heterocyclic Carbene–Phosphine Complexes as Catalysts in Magnetization Transfer Reactions.* Inorganic Chemistry, 2013. **52**(23): p. 13453-13461.
40. Mewis, R.E., et al., *Strategies for the hyperpolarization of acetonitrile and related ligands by SABRE.* 2015.
41. Holmes, A.J., et al., *The reaction of an iridium PNP complex with parahydrogen facilitates polarisation transfer without chemical change.* Dalton Transactions, 2015.
42. Lloyd, L.S., et al., *Utilization of SABRE-Derived Hyperpolarization To Detect Low-Concentration Analytes via 1D and 2D NMR Methods.* Journal of the American Chemical Society, 2012. **134**(31): p. 12904-12907.
43. Zeng, H., et al., *Optimization of SABRE for polarization of the tuberculosis drugs pyrazinamide and isoniazid.* Journal of Magnetic Resonance, 2013. **237**(0): p. 73-78.
44. Shi, F., et al., *Heterogeneous Solution NMR Signal Amplification by Reversible Exchange.* Angewandte Chemie International Edition, 2014. **53**(29): p. 7495-7498.

45. Zeng, H., et al., *Achieving 1% NMR polarization in water in less than 1 min using SABRE.* Journal of Magnetic Resonance, 2014. **246**(0): p. 119-121.
46. Albert, A., *210. Ionization constants of heterocyclic substances. Part IV. The effect of a tautomerizable [small alpha]-substituent on the ionization of a second substituent.* Journal of the Chemical Society (Resumed), 1960(0): p. 1020-1023.
47. Casalnuovo, A.L., J.C. Calabrese, and D. Milstein, *Nitrogen-hydrogen activation. 1. Oxidative addition of ammonia to iridium(I). Isolation, structural characterization and reactivity of amidoiridium hydrides.* Inorganic Chemistry, 1987. **26**(7): p. 971-973.
48. Kim, Y.O. and H.M. Goff, *Characterization of ammonia-ligated low-spin iron(III) porphyrin complexes.* Inorganic Chemistry, 1990. **29**(19): p. 3907-3908.
49. Sappa, E. and L. Milone, *Reactions of Ru3(CO)12 with nitrobenzene and aniline.* Journal of Organometallic Chemistry, 1973. **61**(0): p. 383-388.
50. Ozerov, O.V., et al., *Facile Oxidative Addition of N−C and N−H Bonds to Monovalent Rhodium and Iridium.* Journal of the American Chemical Society, 2004. **126**(15): p. 4792-4793.
51. Zhao, J., A.S. Goldman, and J.F. Hartwig, *Oxidative Addition of Ammonia to Form a Stable Monomeric Amido Hydride Complex.* Science, 2005. **307**(5712): p. 1080-1082.
52. Huang, Z., J. Zhou, and J.F. Hartwig, *N−H Activation of Hydrazines by Iridium(I). Double N−H Activation To Form Iridium Aminonitrene Complexes.* Journal of the American Chemical Society, 2010. **132**(33): p. 11458-11460.
53. Koleva, B., et al., *Spectral analysis and crystal structure of a new mononuclear copper(II) complex of 3-aminopyridine.* Transition Metal Chemistry, 2006. **31**(7): p. 866-873.
54. Xia, N. and M. Taillefer, *A Very Simple Copper-Catalyzed Synthesis of Anilines by Employing Aqueous Ammonia.* Angewandte Chemie International Edition, 2009. **48**(2): p. 337-339.
55. Neronov, Y.I. and S.G. Karshenboim, *NMR spectroscopy of hydrogen of deuteride and magnetic moments deuteron and triton.* Physics Letters A, 2003. **318**(1-2): p. 126-132.
56. Bowers, C.R. and D.P. Weitekamp, *Transformation of Symmetrization Order to Nuclear-Spin Magnetization by Chemical Reaction and Nuclear Magnetic Resonance.* Physical Review Letters, 1986. **57**(21): p. 2645-2648.
57. Balzani, V. and A. Juris, *Photochemistry and photophysics of Ru(II) · polypyridine complexes in the Bologna group. From early studies to recent developments.* Coordination Chemistry Reviews, 2001. **211**(1): p. 97-115.
58. Bitterwolf, T.E., *Photochemistry and reaction intermediates of the bimetallic Group VIII cyclopentadienyl metal carbonyl compounds, (η5-C5H5)2M2(CO)4 and their derivatives.* Coordination Chemistry Reviews, 2000. **206–207**(0): p. 419-450.
59. Kealy, T.J. and P.L. Pauson, *A New Type of Organo-Iron Compound.* Nature, 1951. **168**(4285): p. 1039-1040.
60. Kalenda, P., *Ferrocene and some of its derivatives used as accelerators of curing reactions in unsaturated polyester resins.* European Polymer Journal, 1995. **31**(11): p. 1099-1102.

61. Suzuma, Y., et al., *Asymmetric 1,4-addition of organoboronic acids to α,β-unsaturated ketones and 1,2-addition to aldehydes catalyzed by a palladium complex with a ferrocene-based phosphine ligand.* Tetrahedron: Asymmetry, 2009. **20**(23): p. 2751-2758.
62. Richards, C.J. and A.J. Locke, *Recent advances in the generation of non-racemic ferrocene derivatives and their application to asymmetric synthesis.* Tetrahedron: Asymmetry, 1998. **9**(14): p. 2377-2407.
63. Yamamoto, Y., et al., *γ-Selective Cross-Coupling Reactions of Potassium Allyltrifluoroborates with Haloarenes Catalyzed by a Pd(0)/D-t-BPF or Pd(0)/Josiphos ((R,S)-CyPF-t-Bu) Complex: Mechanistic Studies on Transmetalation and Enantioselection.* Organometallics, 2008. **28**(1): p. 152-160.
64. Saßmannshausen, J., et al., *Half-sandwich complexes of titanium and zirconium with pendant phenyl substituents. The influence of ansa-aryl coordination on the polymerisation activity of half-sandwich catalysts.* Journal of Organometallic Chemistry, 1999. **592**(1): p. 84-94.
65. Schwecke, C. and W. Kaminsky, *Syndiospecific polymerization of styrene with BzCpTiCl3 and methylaluminoxane as cocatalysts.* Journal of Polymer Science Part A: Polymer Chemistry, 2001. **39**(16): p. 2805-2812.
66. Fouda, M.F.R., et al., *On the medicinal chemistry of ferrocene.* Applied Organometallic Chemistry, 2007. **21**(8): p. 613-625.
67. Wilkinson, G., et al., *The structure of iron bis-cyclopentadienyl.* Journal of the American Chemical Society, 1952. **74**(8): p. 2125-2126.
68. Braga, D., et al., *Novel hetero-bimetallic metalla-macrocycles based on the bis-1-pyridyl ferrocene [Fe([small eta]5-C5H4-1-C5H4N)2] ligand. Design, synthesis and structural characterization of the complexes [Fe([small eta]5-C5H4-1-C5H4N)2](Ag)22+/(Cu)24+/(Zn)24+.* Chemical Communications, 2002(10): p. 1080-1081.
69. Braga, D., et al., *Novel Organometallic Building Blocks for Molecular Crystal Engineering. 2. Synthesis and Characterization of Pyridyl and Pyrimidyl Derivatives of Diboronic Acid, [Fe(η5-C5H4-B(OH)2)2], and of Pyridyl Boronic Acid, [Fe(η5-C5H4-4-C5H4N)(η5-C5H4-B(OH)2)].* Organometallics, 2003. **22**(10): p. 2142-2150.
70. Bhadbhade, M.M., et al., *Redox-responsive bi- and tri-nuclear iron/molybdenum complexes incorporating the ferrocenyl unit as a redox spectator.* Journal of the Chemical Society, Dalton Transactions, 1995(17): p. 2769-2777.
71. Ischay, M.A., et al., *Efficient Visible Light Photocatalysis of [2+2] Enone Cycloadditions.* Journal of the American Chemical Society, 2008. **130**(39): p. 12886-12887.
72. Tuite, E., P. Lincoln, and B. Nordén, *Photophysical Evidence That Δ- and Λ-[Ru(phen)2(dppz)]2+ Intercalate DNA from the Minor Groove.* Journal of the American Chemical Society, 1997. **119**(1): p. 239-240.
73. Lin, S., et al., *Radical Cation Diels–Alder Cycloadditions by Visible Light Photocatalysis.* Journal of the American Chemical Society, 2011. **133**(48): p. 19350-19353.
74. Kuss-Petermann, M. and O.S. Wenger, *Mechanistic Diversity in Proton-Coupled Electron Transfer between Thiophenols and Photoexcited [Ru(2,2′-Bipyrazine)3]2+.* The Journal of Physical Chemistry Letters, 2013. **4**(15): p. 2535-2539.

75. Maity, S., et al., *Intermolecular [3+2] Cycloaddition of Cyclopropylamines with Olefins by Visible-Light Photocatalysis.* Angewandte Chemie International Edition, 2012. **51**(1): p. 222-226.
76. Crutchley, R.J. and A.B.P. Lever, *Comparative chemistry of bipyrazyl and bipyridyl metal complexes: spectroscopy, electrochemistry and photoanation.* Inorganic Chemistry, 1982. **21**(6): p. 2276-2282.
77. Crutchley, R.J. and A.B.P. Lever, *Ruthenium(II) tris(bipyrazyl) dication - a new photocatalyst.* Journal of the American Chemical Society, 1980. **102**(23): p. 7128-7129.
78. Marklund, S. and G. Marklund, *Involvement of the Superoxide Anion Radical in the Autoxidation of Pyrogallol and a Convenient Assay for Superoxide Dismutase.* European Journal of Biochemistry, 1974. **47**(3): p. 469-474.
79. Wu, X., et al., *Insight into and Practical Application of pH-Controlled Asymmetric Transfer Hydrogenation of Aromatic Ketones in Water.* Angewandte Chemie International Edition, 2005. **44**(22): p. 3407-3411.
80. Prüsse, U. and K.-D. Vorlop, *Supported bimetallic palladium catalysts for water-phase nitrate reduction.* Journal of Molecular Catalysis A: Chemical, 2001. **173**(1–2): p. 313-328.
81. Laha, S. and R.G. Luthy, *Oxidation of aniline and other primary aromatic amines by manganese dioxide.* Environmental Science & Technology, 1990. **24**(3): p. 363-373.
82. Casey, J.R., S. Grinstein, and J. Orlowski, *Sensors and regulators of intracellular pH.* Nat Rev Mol Cell Biol, 2010. **11**(1): p. 50-61.
83. Smith, A.P., J.J.S. Lamba, and C.L. Fraser, *Efficient Synthesis of Halomethyl-2,2'-bipyridines: 4,4'-Bis(chloromethyl)-2,2'-bipyridine.* Organic Syntheses, 2002. **78**: p. 82.
84. W. Alder, R., et al., *Complexation of stable carbenes with alkali metals.* Chemical Communications, 1999(3): p. 241-242.
85. Canle L, M. and H. Maskill, *Acid-catalysed hydrolysis of trityl derivatives in strongly acidic aqueous media.* Journal of Physical Organic Chemistry, 2013. **26**(12): p. 1016-1022.
86. Tanokura, M., *1H-NMR study on the tautomerism of the imidazole ring of histidine residues: I. Microscopic pK values and molar ratios of tautomers in histidine-containing peptides.* Biochimica et Biophysica Acta (BBA) - Protein Structure and Molecular Enzymology, 1983. **742**(3): p. 576-585.
87. Costello, A.J.R., T. Glonek, and T.C. Myers, *31P Nuclear magnetic resonance ・pH titrations of myo-inositol hexaphosphate.* Carbohydrate Research, 1976. **46**(2): p. 159-171.
88. Adams, R.W., et al., *A theoretical basis for spontaneous polarization transfer in non-hydrogenative parahydrogen-induced polarization.* J. Chem. Phys, 2009. **131**.
89. Olaru, A.M., et al., *pH mapping using SABRE.* To be submitted to Nature.
90. Tarn, K.Y. and K. Takács-Novák, *Multiwavelength Spectrophotometric Determination of Acid Dissociation Constants: Part II. First Derivative vs. Target Factor Analysis.* Pharmaceutical Research, 1999. **16**(3): p. 374-381.
91. NMRNotes. *A Guide to NMR Reference Compounds*. 04/12/2014]; Available from: http://www.nmrnotes.org/NMRPages/refcomps.html.
92. Espinosa, S., E. Bosch, and M. Rosés, *Retention of Ionizable Compounds on HPLC. 12. The Properties of Liquid Chromatography Buffers in*

Acetonitrile–Water Mobile Phases That Influence HPLC Retention. Analytical Chemistry, 2002. **74**(15): p. 3809-3818.

93. Gao, J. and L. Shao, *Polarization Effects on the Tautomeric Equilibria of 2- and 4-Hydroxypyridine in Aqueous and Organic Solution.* The Journal of Physical Chemistry, 1994. **98**(51): p. 13772-13779.
94. Tsuchida, N. and S. Yamabe, *Reaction Paths of Tautomerization between Hydroxypyridines and Pyridones.* The Journal of Physical Chemistry A, 2005. **109**(9): p. 1974-1980.
95. Lu, Z.Z., et al., *Diaqua(nitrato-kappa O-2,O ')bis(4-pyridone-kappa O)cobalt(II) nitrate.* Acta Crystallographica Section E-Structure Reports Online, 2004. **60**: p. M811-M813.
96. Gao, S., et al., *Dichlorobis(4-pyridone-kappa O)cobalt(II).* Acta Crystallographica Section E-Structure Reports Online, 2004. **60**: p. M609-M610.
97. Kee, J.W. and W.Y. Fan, *Infrared studies of halide binding with CpMn(CO)(2)X complexes where X = ligands bearing the O-H or N-H group.* Journal of Organometallic Chemistry, 2013. **729**: p. 14-19.
98. Chen, C.-n., et al., *4- and 3-Hydroxypyridine complexes of pentacyanoferrate(II, III).* Inorganica Chimica Acta, 1998. **267**(1): p. 81-86.
99. Clarke, Z.E., et al., *A Family of Active Iridium Catalysts for Transfer Hydrogenation of Ketones.* Organometallics, 2006. **25**(17): p. 4113-4117.
100. Carmona, D., et al., *Chiral Octahedral Phosphano–Oxazoline Iridium(III) Complexes as Catalysts in Asymmetric Cycloaddition Reactions.* Organometallics, 2013. **32**(6): p. 1609-1619.
101. Nguyen, D.H., et al., *Unsaturated Iridium(III) Complexes Supported by a Quinolato–Carboxylato ONO Pincer-Type Ligand: Synthesis, Reactivity, and Catalytic C–H Functionalization.* Organometallics, 2013. **32**(23): p. 6918-6930.
102. Chianese, A.R., et al., *Iridium Complexes of CCC-Pincer N-Heterocyclic Carbene Ligands: Synthesis and Catalytic C–H Functionalization.* Organometallics, 2010. **29**(13): p. 3019-3026.
103. Zuo, W. and P. Braunstein, *N-Heterocyclic Dicarbene Iridium(III) Pincer Complexes Featuring Mixed NHC/Abnormal NHC Ligands and Their Applications in the Transfer Dehydrogenation of Cyclooctane.* Organometallics, 2011. **31**(7): p. 2606-2615.
104. Albert, A. and J.N. Phillips, *264. Ionization constants of heterocyclic substances. Part II. Hydroxy-derivatives of nitrogenous six-membered ring-compounds.* Journal of the Chemical Society (Resumed), 1956(0): p. 1294-1304.
105. Nonat, A., et al., *Structure, Stability, Dynamics, High-Field Relaxivity and Ternary-Complex Formation of a New Tris(aquo) Gadolinium Complex.* Chemistry – A European Journal, 2007. **13**(30): p. 8489-8506.
106. Aime, S., M. Fasano, and E. Terreno, *Lanthanide(III) chelates for NMR biomedical applications.* Chemical Society Reviews, 1998. **27**(1): p. 19-29.
107. Phelps, M.E., *Positron emission tomography provides molecular imaging of biological processes.* Proceedings of the National Academy of Sciences, 2000. **97**(16): p. 9226-9233.
108. Barskiy, D.A., et al., *In Situ and Ex Situ Low-Field NMR Spectroscopy and MRI Endowed by SABRE Hyperpolarization.* ChemPhysChem, 2014: p. n/a-n/a.
109. Greguric, I., et al., *Discovery of [18F]N-(2-(Diethylamino)ethyl)-6-fluoronicotinamide: A Melanoma Positron Emission Tomography Imaging*

Radiotracer with High Tumor to Body Contrast Ratio and Rapid Renal Clearance. Journal of Medicinal Chemistry, 2009. **52**(17): p. 5299-5302.

110. Liu, H., et al., *Development of 18F-Labeled Picolinamide Probes for PET Imaging of Malignant Melanoma.* Journal of Medicinal Chemistry, 2013. **56**(3): p. 895-901.
111. Gallagher, F.A., et al., *Magnetic resonance imaging of pH in vivo using hyperpolarized 13C-labelled bicarbonate.* Nature, 2008. **453**(7197): p. 940-943.
112. Webb, B.A., et al., *Dysregulated pH: a perfect storm for cancer progression.* Nat Rev Cancer, 2011. **11**(9): p. 671-677.
113. Gillies, R.J., et al., *pH imaging.* Engineering in Medicine and Biology Magazine, IEEE, 2004. **23**(5): p. 57-64.
114. Huang, X., et al., *Multi-Chromatic pH-Activatable 19F-MRI Nanoprobes with Binary ON/OFF pH Transitions and Chemical-Shift Barcodes.* Angewandte Chemie International Edition, 2013. **52**(31): p. 8074-8078.
115. Martinez, G.V., et al., *Imaging the extracellular pH of tumors by MRI after injection of a single cocktail of T1 and T2 contrast agents.* NMR in Biomedicine, 2011. **24**(10): p. 1380-1391.
116. Garlick, P.B., G.K. Radda, and P.J. Seeley, *Studies of acidosis in the ischaemic heart by phosphorus nuclear magnetic resonance.* Biochemical Journal, 1979. **184**(3): p. 547-554.
117. L., S., *13C-labeled bicarbonate (H13CO3-) for in vivo pH measurement with 13C magnetic resonance spectroscopy*, in *Molecular Imaging and Contrast Agent Database (MICAD)*. 2010, National Center for Biotechnology Information (US): http://www.ncbi.nlm.nih.gov/books/NBK32324.
118. Hillmer, A.T., et al., *Measuring [alpha]4[beta]2[ast] nicotinic acetylcholine receptor density in vivo with [lsqb]18F[rsqb]nifene PET in the nonhuman primate.* J Cereb Blood Flow Metab, 2013. **33**(11): p. 1806-1814.
119. Constantinescu, C.C., et al., *Evaluation of [18F]Nifene biodistribution and dosimetry based on whole-body PET imaging of mice.* Nuclear Medicine and Biology, 2013. **40**(2): p. 289-294.
120. Hennig, J., A. Nauerth, and H. Friedburg, *RARE imaging: A fast imaging method for clinical MR.* Magnetic Resonance in Medicine, 1986. **3**(6): p. 823-833.
121. Herde, J.L., et al., *Cyclooctene and 1,5-Cyclooctadiene Complexes of Iridium(I)*, in *Inorganic Syntheses*. 1974, John Wiley & Sons, Inc. p. 18-20.
122. Uson, R., et al., *Dinuclear Methoxy, Cyclooctadiene, And Barrelene Complexes Of Rhodium(I) And Iridium(I).* Inorganic Syntheses, 1985. **23**: p. 126-127.
123. Torres, O., M. Martín, and E. Sola, *Labile N-Heterocyclic Carbene Complexes of Iridium.* Organometallics, 2009. **28**(3): p. 863-870.
124. Dolle, F., et al., *Synthesis of 2-[18F]fluoro-3-[2(S)-2-azetidinylmethoxy]pyridine, a highly potent radioligand for in vivo imaging central nicotinic acetylcholine receptors.* Journal of Labelled Compounds and Radiopharmaceuticals, 1998. **41**(5): p. 451-463.
125. Harris, D.C., *Nonlinear Least-Squares Curve Fitting with Microsoft Excel Solver.* Journal of Chemical Education, 1998. **75**(1): p. 119.
126. Dolomanov, O.V., et al., *OLEX2: a complete structure solution, refinement and analysis program.* Journal of Applied Crystallography, 2009. **42**: p. 339-341.

127. Palatinus, L. and G. Chapuis, *SUPERFLIP - a computer program for the solution of crystal structures by charge flipping in arbitrary dimensions.* Journal of Applied Crystallography, 2007. **40**: p. 786-790.
128. Palatinus, L. and A. van der Lee, *Symmetry determination following structure solution in P1.* Journal of Applied Crystallography, 2008. **41**: p. 975-984.
129. Palatinus, L., S.J. Prathapa, and S. van Smaalen, *EDMA: a computer program for topological analysis of discrete electron densities.* Journal of Applied Crystallography, 2012. **45**: p. 575-580.
130. Sheldrick, G.M., *A short history of SHELX.* Acta Crystallographica Section A, 2008. **64**: p. 112-122.